



Zewail City for Science and Technology
University of Science and Technology

Nanotechnology and Nanoelectronics Engineering

**Design and Fabrication of 5G IOT Reconfigurable
Antenna Based on Low-Voltage RF MEMS
Switches**

A Graduation Project

Submitted in Partial Fulfillment of B.Sc. Degree
Requirements in Nanotechnology and Nanoelectronics

Prepared By

Muhammad Khalid Khalaf	201600562
Alaa Walid Elshazly	201600473
Mario Nagy Mounir	201600648
Muhammad Mahmoud Faris	201600657

Supervised By

Dr. Hassan Mostafa	Dr. Yasmine Elogail
--------------------	---------------------

Acknowledgements

First and foremost, praises and thanks Allah, the Almighty, for his showers of blessings and guidance throughout the entirety of our work.

This dissertation does not only hold the results of the year's work, but also reflects the relationships with many generous and stimulating people. We would like to take this opportunity to show our gratitude; because without them this work would not have been possible.

We would like to thank our supervisors, Dr Hassan Mostafa and Dr Yasmine Elogail, and to express our sincere gratitude and appreciation for their excellent guidance, caring, patience, and immense help in planning and executing this work. We are very grateful to all of ZC professors and NANENG program for this wonderful journey.

There are not enough words to express to our families how much their love and support meant for us. We would like to thank Dr Faycel and Dr Adham for their support and technical help throughout the project. We would also like to express our endless gratitude to Dr Raffat Mansour and Eng Edward Jin, from Waterloo University, for their generous guidance and help in the fabrication process.

Abstract

With technology advancing day after day, new trends in technology appear rapidly. In this decade, 5G technologies is one of the most important trends all over the world with the IOT applications. These applications are mostly small in size to be mobile, hence the need for smaller antennas to be used. These applications may require multiple frequencies of operation such as Wi-Fi, Bluetooth, and cellular data, so reconfigurable antennas can help reduce the number of antennas used as well as be small in size. On the other hand, the switching mechanism used in the reconfigurable antenna to change frequency should be compatible with mobile applications such as consuming low power and operating on low voltage. In this work, an RF MEMS switch frequency reconfigurable antenna is designed. The antenna design targets the midband 5G, with frequencies of 1-2 GHz, and 3-4 GHz with bandwidths of less than 300 MHz. This work presents the design, simulation and fabrication of novel RF MEMS switches. The aim is achieving low-voltage RF MEMS switches compatible with reconfigurable microstrip antennas for Fifth Generation (5G) networks. The switches should have low insertion loss, high isolation, low actuation voltage and high reliability. The complete system of the reconfigurable antenna is to be implemented into IOT 5G systems for communication applications

Keywords: RF MEMS; MEMS switch; Reconfigurable antenna; 5G antenna; IOT band

Acknowledgements	2
Abstract	3
Chapter 1	1
1.1 General Introduction and overview of the topic	2
1.2 Problem Definition	2
1.3 Objectives	3
1.4 Functional Requirements/product specification	4
1.5 Report Organization	4
Chapter 2	6
Market	6
&	6
Literature Review	6
2.1 Background on Antennas:	8
2.1.1 Microstrip (Patch) antenna	9
2.1.2 Antenna reconfiguration :	10
2.1.3 Bandwidth Reconfigurable Antenna :	11
2.1.4 Beam steering - pattern re-configuration :	11

2.1.5	Frequency Reconfigurable Antenna :	11
2.2	Background on RF MEMS Switches	14
2.2.1	RF MEMS Switches	16
A.	Definition of RF Switches:	16
B.	Characterization of RF Switches:	17
2.2.2	Types of RF MEMS Switches	19
A.	Actuation Mechanism	20
B.	Circuit Configuration	24
C.	Contact Type	25
2.3	Switch library	27
2.3.1	low-voltage shunt capacitive RF MEMS switch	27
2.3.2	RF MEMS capacitive switches using meanders	29
2.3.4	Metal-contact Cantilever-based Series RF MEMS Switch	32
Chapter 3		35
Project Design		35
3.1	Project purpose and constraints	36
3.1.1	RF Performance	36

3.1.2	Actuation Voltage	39
3.1.3	Reliability	40
3.1.4	Switching Time	41
3.1.5	Fabrication	43
3.2	Project technical specifications	43
3.3	Design alternatives and justification	46
3.4	Description of the selected design	47
3.4.1	Antenna design:	47
3.4.2	RF MEMS Switches:	47
3.5	Block diagram and functions of the subsystems	47
Chapter 4		49
Project Execution		49
4.1	Project Tasks and Gantt chart	50
4.2	Description of each subsystem	51
4.2.1	Antenna	52
4.2.2	RF MEMS Switches	64
4.2.3	Control:	69

4.3 Testing and Evaluation	71
4.3.1 Reconfigurable Antenna Testing and Evaluation	71
A. First design	72
B. Second design:	85
4.3.2 RF MEMS Switches	93
A. First Design	93
Other Designs	98
B. Second Design	100
C. Third Design	101
D. Fourth Design	102
E. Fifth Design	103
F. Fabrication	104
G. Masks Layout	109
4.3.2.3 Discussion	110
4.3.2.4 RF MEMS Switches Simulation	111
A. First Design	111
B. Second Design	115

C. Third Design	117
D. Fourth Design	119
E. Fifth Design	121
Chapter 5	124
Cost Analysis	124
Chapter 6	126
Conclusion and Future work	126
References	128

List of Tables

Table 1: Comparison between switching mechanisms	17
Table 2. Performance comparison of FETs, PIN Diode, and RF MEMS electrostatic switches	22
Table 3. Performance Comparison between the different types of actuation	26
Table 4. The technical specifications for the antenna	46
Table 5. The technical specifications for the MEMS switch	47
Table 6. demonstrates the design parameters after conducting parametric analysis and optimization	61
Table 7. Materials we have used in our design	63
Table 8. Patches parameter values before optimization	64
Table 9. shows the bandwidth based on the switches' state	75
Table 10. Bandwidth values with using RLC model from the novel MEMS switch design	86
Table 11. The bandwidth based on the switches' state	88
Table 12: device structure specifications	97
Table 13. Layers thickness for fabrication	101
Table 14: Specifications of the Fabrication Layers	107

List of Acronyms

RF	Radio Frequency
MEMS	Micro-Electro-Mechanical Systems
5G	Fifth Generation
IOT	Internet of Things
CPW	CoPlanar Waveguide
WBS	Work Breakdown Structure

Chapter 1

Introduction

&

Overview

1.1 General Introduction and overview of the topic

The global market witnesses major advances in high speed communications and increasing complexities in multiple devices connectivity especially with the deployment of 5G network communications. Today's applications are inherently dependent on real time multiple device connectivity, i.e., automobiles, smart cities, digital health...etc. There are a major number of devices that have to be connected in real time to deliver the best performance and functionality. Each device works on a specific frequency and bandwidth to meet the system requirements. Therefore, an acute problem arises from these different specifications which complicates the compatibility among these numerous connected devices.

As the 5G frequency ranges are various, and different applications may require different frequency bands, the problem of standardization becomes harder, especially because of the national telecommunications regulations of each country, and this leads to the addition of more hardware in the same device just to compensate for the different applications required. In other words, different antennas with different frequencies and bandwidths are being used within the same device to hit the compatibility standards. Hence, this increases the cost of manufacturing as well as using a large part of the available space in the device.

1.2 Problem Definition

Due to the increasing need for high internet and communication speed, the technology pioneers do their best to make all applications such as mobile phones and IoT connections compatible with

the 5G network. Moreover, there is an irresistible urge to obviate the need for multiple antennas in order to limit the physical space occupied providing less jammed signals at the same time. In summary, the development of a low voltage RF MEMS based reconfigurable antenna helps improve the functionality and performance of devices communications in most of 4.0 trending industries. It provides all IoT based applications with outstanding abilities of operating in different frequencies with different bandwidths while at the same time minimizing the size and the cost of the system.

1.3 Objectives

The goal of this project is to develop a fully integrated system that consists of :

- I. A frequency reconfigurable antenna that has a capability of changing its resonant frequency while being matched to 50 ohms. The chosen frequency bands are determined based on 5G IoT systems, and the antenna resonant frequencies are 3.4 GHz and 1.45 GHz.
- II. Design and fabrication of an RF MEMS switch that has a capability of operating at the pre identified resonant frequencies.
- III. Performing a system integration of the RA and RF MEMS switches on a single functioning PCB board.

1.4 Functional Requirements/product specification

Referring to **Figure 1**, The system consists of two varying sized patches. Patch 1 operates at 3.4 GHz while the two patches combined operate at resonant frequency of 1.45 GHz. RF MEMS switches will be used to connect between Patch 1 and Patch 2. Those switches provide high isolation at the system operation frequencies to maintain the reconfigurability feature of the system. Patches will be matched to 50 ohms via inset feed matching or two matching networks for each patch feedline. Switching mechanism will be controlled by an MCU.

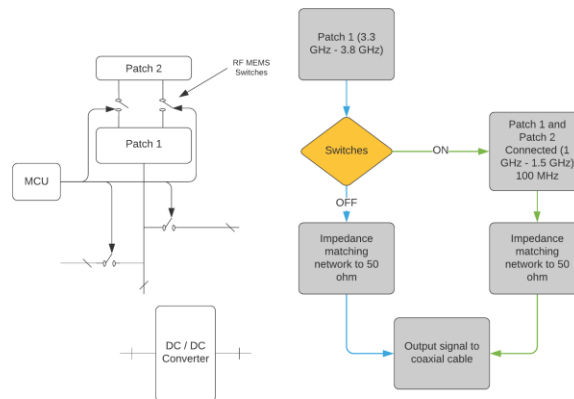


Figure 1. The full system components.

1.5 Report Organization

This report is written to thoroughly state what has been done in this project from its very beginnings till its end results. Therefore, the information flow will start with a general overview on the project and the driving motives towards this topic, then literature review is written to shed the light on the state-of-the-art works regarding the same topic, then a comprehensive design description is illustrated, then simulation results and design modifications is investigated, then

fabrication processes of every system components is pointed out, then system physical measurement is declared and compared to results obtained from simulations, finally, a conclusion to all the work is written to conclude what has been done through all the project phases and to shed the light on different possibilities for future work and to recommend different strategies for further improvements.

Chapter 2

Market

&

Literature Review

This chapter covers the market conditions related to our project, and how they pushed us to take on this project. Moreover, it gives highlights on the knowledge conditions and provides fundamental information about the works related to antenna technology and RF MEMS technologies, as we had to invest much time and efforts to deepen our knowledge in such vital tracks, specifically the antenna theory as this part is not covered in our major study plan.

According to data disclosed from market research- attached in the appendix- on IIoT, it is expected to grow 76.7 billion in 2021 to USD 106.1 billion by 2026. Such tremendous growth results from technological advancements in electronic devices and semiconductors, growing utilization of cloud computing, governmental support to R&D centres, and standardization of IPV6. Furthermore, in recent years, 5G networks have become the main interest in the communication industry, as it empowers and dramatically increases the communication speed. 5G is the key of the 4.0 industrial revolution that the world is impatiently waiting for. According to Polaris market research, it is estimated that 5G private networks will hit \$ 13.19 billion by 2028 with a CAGR anticipated to be 40.9% 2020 to 2028. Accordingly, there is a peak demand for ultra low latency networks in industrial applications, including the robotics industry and industrial sensors which strongly drive the market growth.

On a sub system level, the market size of both antenna and RF MEMS is expected to grow rapidly in the wake of the 4.0 industrial revolution.

As per the above-mentioned market status and the vitality of IIoT empowered by the 5G network, we decided to utilize our knowledge and experience gained from the interdisciplinary based curriculum covered in our department. By combining our expertise

in MEMS design and basic communication knowledge, we could capitalize on such diverse fields and work on designing a RF MEMS switched based reconfigurable antenna. Such a journey has been full of challenges and rewarding experiences. In the below paragraphs, a comprehensive literature review is conducted on both fields of antenna reconfigurability and RF MEMS.

2.1 Background on Antennas:

Antenna simply is a structure that produces radiation by supporting a suitable current distribution [1].

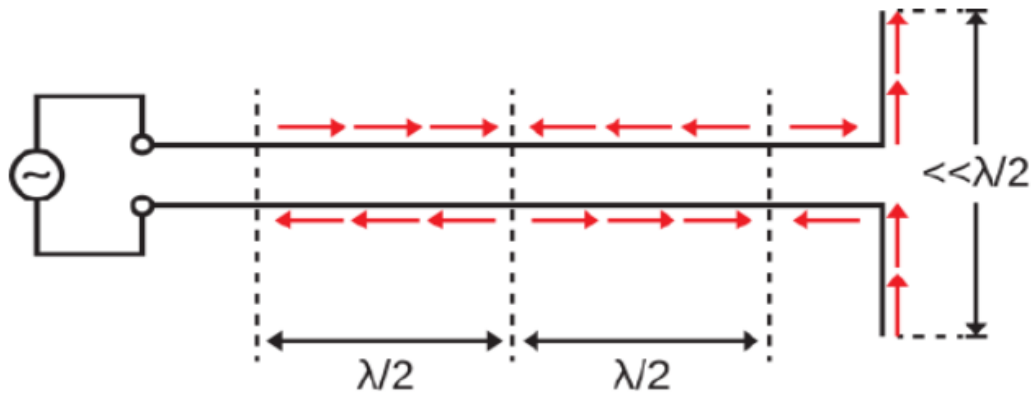


Figure 2: a simple circuit connected to a short dipole antenna [1]

In figure 2, the circuit is composed of three parts; a source (at the left), a transmission line (at the middle), and finally an antenna (the vertical lines at the right). This antenna part is similar to the electrical dipole, in which there are two electrical charges equal in magnitude and opposite in direction and have a distance between them. However, this dipole antenna is like several dipoles connected together. The process of radiation in this antenna works

as follows. When the AC source is connected to the circuit, however the circuit is open ended, hence the current at the tip of the free ends is exactly zero. However, the current at different points in the antenna part or the transmission line part is not not particularly zero, but the current value varies with changing the position along the transmission lines or the dipole. To simplify more, in figure 2, the length of the transmission line is λ (one wavelength), so at distance zero the current is zero, at distance $\lambda/2$ the current is maximum, and at distance λ the current is zero again, and so on. So there is a current distribution present although the circuit is open. The AC source makes the current in this distribution change as well, this change in current makes an electromagnetic wave that is the radiation itself, but the transmission lines do not radiate because there are two lines carrying current equal in magnitude and opposite in direction, so they cancel each other. On the other hand, the wires in the dipole antenna part are configured so that they do not cancel each other, but they produce a radiation with half wavelength equivalent to length of the whole dipole antenna.

2.1.1 Microstrip (Patch) antenna

In this work, a patch antenna is used in our design, so a quick introduction for the patch antenna is provided. Microstrip or patch antennas are very useful as they can be easily printed directly onto a circuit board. Microstrip antennas are becoming very common in mobile phone technologies. Patch antennas are low cost, have a low profile and are easily fabricated [2].

For a rectangular patch antenna, the width of the patch is calculated as follows

$$W = \frac{c}{2f_0 \sqrt{\frac{\epsilon + 1}{2}}}$$

While the length of the patch is calculated as follows

$$L = \frac{c}{2f_0 \sqrt{\epsilon_r}} - 2\Delta L$$

Where ΔL is defined as

$$\Delta L = 0.412h * \frac{(\epsilon_{eff} + 0.3) \left(\frac{W}{L} + 0.264\right)}{(\epsilon_{eff} - 0.258) \left(\frac{W}{L} + 0.8\right)}$$

2.1.2 Antenna reconfiguration :

The reason behind the promising performance of reconfigurable antennas is its ability to change the operating frequency, bandwidth, radiation pattern, and polarization. All the aforementioned reconfigure features are obtained by the change in the size of an antenna and the radiators shape while utilizing active switching elements integrated to the antenna system, i.e., RF MEMS switches, PIN diodes, Varactors, or Optical switches. In the following subsections, the different reconfiguration types are going to be comprehensively discussed.

2.1.3 Bandwidth Reconfigurable Antenna :

The next reconfigure feature is about the operational bandwidth change. For a communication system to function both in narrowband and wideband communication. Literature shows numerous applications for the bandwidth reconfigurable antenna specially in WLAN and WiMAX applications. There are two main approaches to change between wideband and narrowband. First, utilizing a matching network or reconfigurable filter structure in the feed line of the antenna. Second, utilizing a modified ground plane particularly for patch antennas.

2.1.4 Beam steering - pattern re-configuration :

Pattern re-configuration has different attractive applications. For example it is required in beam steering and surveillance applications. Also, it is a good candidate for implementing MIMO antennas for mobile, hand-held, or small form factor devices[3].

Pattern reconfiguration can be realized by; Changing the structure using impedance/parasitic arrays and metal surfaces as reflectors. In this technique, parasitic arrays are switched ON to act as reflectors with a certain dimension, and switched OFF to stop acting as a reflector. Hence, changing the pattern shape according to the switching state [4].

2.1.5 Frequency Reconfigurable Antenna :

Modern communication systems have much complex interoperability in terms of signal frequency bands. The connectivity of different devices has been increasing over the years. Smart phones, IoT systems, ...etc. require flexibility and ability to get connected to different devices with different frequencies simultaneously. As a result it is imperative to integrate a lot of antennas within each device to span as much as of frequency bands which contradicts with size and cost reduction

paradigms. Hereby, the significance of frequency reconfigurable antennas comes to resolve these issues by allowing the same antenna system to operate at different frequency bands for better functioning wireless systems.

This type of reconfiguration is the one chosen for design in this work. The idea simply is to change the dimensions of the antenna by using switches whether the switches are diodes, MEMS, or varactors. This change in the dimensions will cause a change in the radiated frequency. In case of the patch antenna, this change in dimensions changes the current distribution in the patch and hence changes the radiation frequency. Mainly, as the antenna size increases, in case of patch antenna, the radiation frequency decreases and vice versa. This is because the radiation wavelength is comparable to the antenna size, so as the antenna patch increases the radiation wavelength increases as well causing the decrease in the radiation frequency.

The process of changing the dimensions is made easily by connecting two or more patch antennas together using switches, and according to the switches on/off state, different connection between patches is obtained hence obtaining an overall patch antenna with different dimensions. For example, figure 2a shows a patch antenna consisting of three patches. However, in figure 2a, only the middle patch is connected, hence the resulting radiation is due the middle patch only. In case of figure 2b, the side patches are connected to the middle patch, resulting in decreasing the produced radiation frequency as the patch size increases.

This is simply the frequency reconfiguration concept. However, it is not as simple as just connecting different patches together and getting a linear change in the radiation frequency. There are different factors and interactions that should be taken into consideration such as the patch size,

the separating distance between the patches, the direction of the feedline, the impedance of the switch used to connect patches together, ...etc. Hence, a simulating software is required to compute the resulting radiation frequency, and make it easier for trying different configurations.

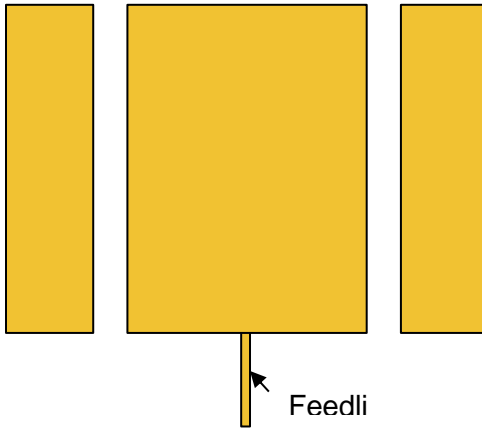


Figure 2a: Frequency reconfigurable antenna with switches in OFF state

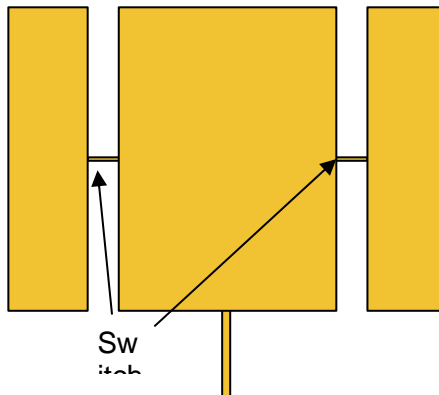


Figure 2b: Frequency reconfigurable antenna with switches in ON state

2.2 Background on RF MEMS Switches

There are multiple types of switches used to connect between antenna patches in order to different antenna configurations as mentioned previously. Of course, each type of switch has different advantages and disadvantages that affect the overall performance of the antenna. Different types of switches include electrical switches such as; PIN diodes, varactors, and RF MEMS switches. Moreover, there are optical switches that use photoconductive configurations to act as a switching mechanism. Different types of switches have different mechanisms to work. For example, PIN diodes operate in two stages, the ON state where the diode is forward biased, and the OFF state where the diode is reverse biased. On the other hand, varactors can give a spectrum of states, not just ON and OFF, according to the capacitance value. RF MEMS switches, as the one used in this work, used mechanical motion to physically close or open the circuit [5]. A comparison between different types of switches is given in table 1.

Properties	PIN Diode	Varactor	RF MEMS	Photoconductive
Speed (μs)	$1-100 \times 10^{-6}$	0.1	1-200	3-9
Quality Factor	50-85	25-55	86-165	-

Voltage (V)	3-5	0.1-15	20-100	1.8-1.9
Current (mA)	3-20	1-25	0	0-87
Power (mW)	5-100	10-200	0.05-0.1	0-50
Temperature sensitivity	medium	High	Low	Low
Cost	Low	Low	Medium	High
Loss of 1 GHz (dB)	0.3-1.2	0.5-3	0.05-0.2	0.5-1.5
Fabrication complexity	Commercially available	Commercially available	Low fabrication complexity	Complex

Table 1: Comparison between switching mechanisms [5]

2.2.1 RF MEMS Switches

A. Definition of RF Switches:

An RF switch is a device used for routing and controlling high frequency electric signals through transmission lines. RF switches can be implemented into arrays for routing signals from multiple inputs to multiple outputs using the same setup.

RF switches can be subdivided into two main categories (fig. 3):

- Electromechanical switches, such as MEMS switches.
- Solid state switches, such as MOSFET and PIN diodes.

Electromechanically operated switches mainly use electromagnetic induction with mechanical moving parts. On the other hand, solid state switches rely on electronic switching of semiconductors with no moving parts. We will dive into the characteristics of each type in the following sections.

RF switches are usually implemented into reconfigurable antennas. Since the switching process can be automated, RF switches give faster performance and reduce the footprint of the antenna on the chip

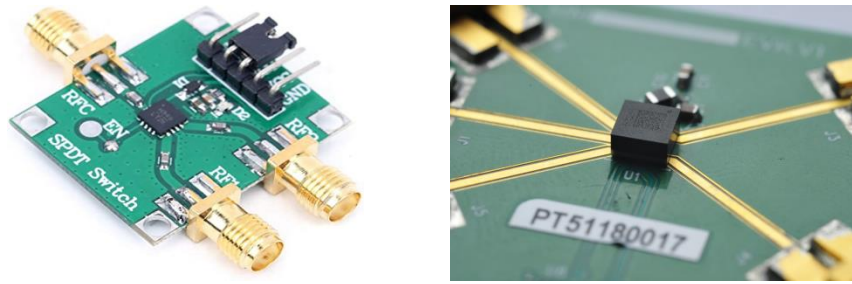


Figure 3. Commercial RF switches:SPDT RF Solid State switch (left) [1],
SP4T RF MEMS switch (right)[2]

B. Characterization of RF Switches:

A lot of parameters are to be optimized in an RF switch to achieve the required specifications. The main characteristics of an RF switch are:

- Frequency Range

Each RF switch has a frequency range where it gives the best performance. RF applications vary from a few hundreds of MHz to several tens of GHz. Semiconductor applications, for example, can require frequencies as low as 100 MHz, while satellite communications range around 60 GHz.

- Operating Voltage

The supply voltage needed for the switch to operate in the expected behavior achieving the required performance.

- Insertion Loss

It is the loss in the signal, or power, passing from one terminal to another in a two-port RF network, in the switch-on state. In other words, It represents how much the passing signal was affected by the addition of the RF switch into its path. An ideal RF switch should give a zero insertion loss, in its on-state. Its value can be calculated by the formula,

$$\textit{Insertion Loss} = -10 \log \frac{P_{L_b}}{P_{L_a}}$$

Insertion loss formula (in dB), where P_{L_b} is the incident power and P_{L_a} is the transmitted power

- Isolation

It is the loss in the signal, or power, transferred from one terminal to another in the off-state of the switch. An Ideal RF switch should give an infinity isolation, when the switch is off.

- Power Consumption

It is the power that the switch needs or consumes during its operation. This depends on the switch's design, materials and operation mechanism. An Ideal RF switch is to have zero power consumption.

- Durability

The lifetime of the switch in successful operation, usually represented as the number of cycles before failure.

- Power Handling

The maximum power the RF switch can handle and operate at without being damaged.

- Switching Time

The time the switch needs to complete one full cycle, from ON to OFF state then back to ON state again.

2.2.2 Types of RF MEMS Switches

Micro-Electro-Mechanical Systems or MEMS is the field of tiny devices, in microns, that can be fabricated using semiconductor technologies. These devices can be varactors, inductors or switches among many other things.

A typical RF MEMS switch is used to open or close an RF circuit in order to pass or block the RF signal. RF MEMS switches showed a lot of advantages over traditional semiconductor switches. Here is a comparison between RF MEMS switches and semiconductor switches.

Parameter	RF MEMS	PIN	FET
Voltage (V)	20–80	± 3 –5	3–5
Current (mA)	0	3–20	0
Power consumption ^a (mW)	0.05–0.1	5–100	0.05–0.1
Switching time	1–300 μ s	1–100 ns	1–100 ns
C_{up} (series) (fF)	1–6	40–80	70–140
R_s (series) (Ω)	0.5–2	2–4	4–6
Capacitance ratio ^b	40–500 ^b	10	n/a
Cutoff frequency (THz)	20–80	1–4	0.5–2
Isolation (1–10 GHz)	Very high	High	Medium
Isolation (10–40 GHz)	Very high	Medium	Low
Isolation (60–100 GHz)	High	Medium	None
Loss (1–100 GHz) (dB)	0.05–0.2	0.3–1.2	0.4–2.5
Power handling (W)	<1	<10	<10
Third-order intercept point (dBm)	+66–80	+27–45	+27–45

^aIncludes voltage upconverter or drive circuitry.

^bCapacitive switch only. A ratio of 500 is achieved with high- ϵ_r dielectrics.

Table 2. Performance comparison of FETs, PIN Diode, and RF MEMS electrostatic switches [6]

It is evident that MEMS switches, with their extremely low up-state capacitance and their very high capacitance ratio, offer a superior performance compared to solid-state switches for low to medium power applications. RF MEMS switches can be a lot of different types, which we will explore in detail.

A. Actuation Mechanism

- Electrostatic Actuation

It uses the electrostatic attraction between charged objects to cause deformation or displacement (fig. 4). This is widely used in MEMS switches, despite its reliability issues. The lifetime of the capacitive switch is exponentially dependent on actuation voltage. Reducing actuation voltage not only extends switch lifetime, but also facilitates its use in wireless devices. [4]

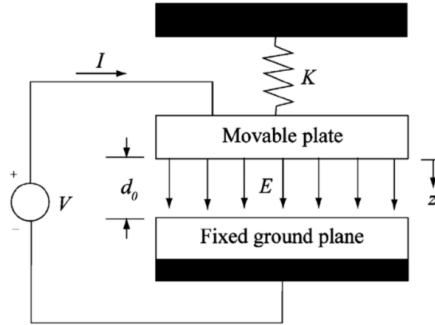


Figure 4. Schematic diagram explaining Electrostatic Actuation

[8]

- *Electromagnetic Actuation*

It uses the concept of Lorentz force. When an electric current flows through a conductive element within an external magnetic field, an electromagnetic force is generated. The force is perpendicular to the magnetic field and the current (fig. 5). It depends on the flowing current, dimensions of the element and the magnetic flux density. Although it has a low operating voltage and can cover large displacements, magnetic actuation consumes a lot of power and chip area.

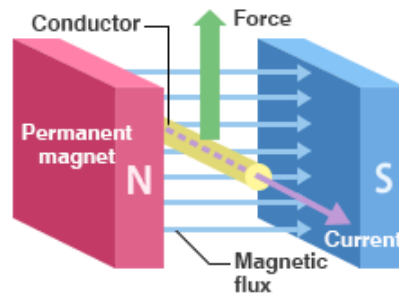


Figure 5. Schematic diagram explaining Electromagnetic Actuation [9]

- Piezoelectric Actuation

It relies on the piezoelectric property of certain crystals. When these materials are introduced to a voltage signal, it results in expansion or contraction resulting in certain stress or motion (fig. 6). Piezoelectric drive gives fast response time and requires a relatively low voltage, however, piezoelectric materials are expensive and not compatible with the normal semiconductor fabrication technologies.

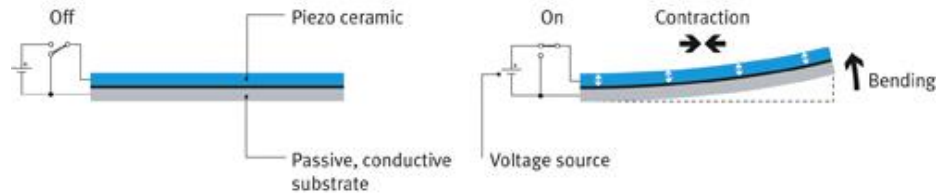


Figure 6. Schematic diagram explaining Piezoelectric Actuation [7]

- *Electrothermal Actuation*

A thermal bimorph actuator uses the difference in the thermal expansion coefficient between two heated materials that results in a mechanical bending in the direction of the material with lower coefficient (fig. 8). Another common method is using two branches of the same material with different dimensions, hence different thermal resistance (fig. 7). When an electric current passes through, the two branches expand differently resulting in a bending and thus force in a certain

direction. Although it can give large displacement, electrothermal actuation consumes a lot of power and space.

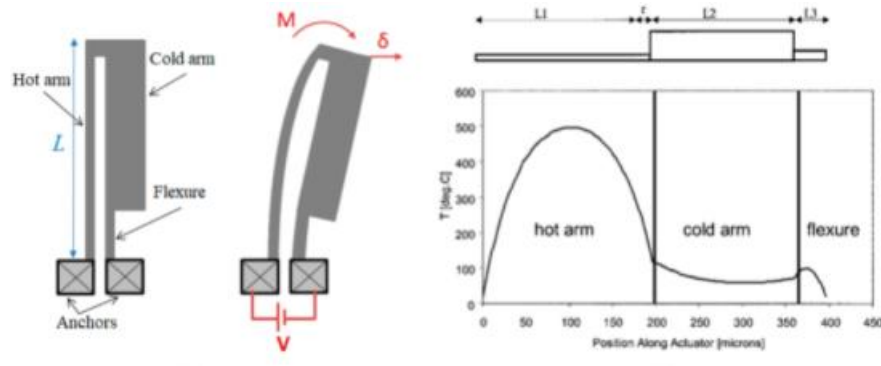


Figure 7. The principle of the U-shaped hot-and-cold-arm actuator

[10]

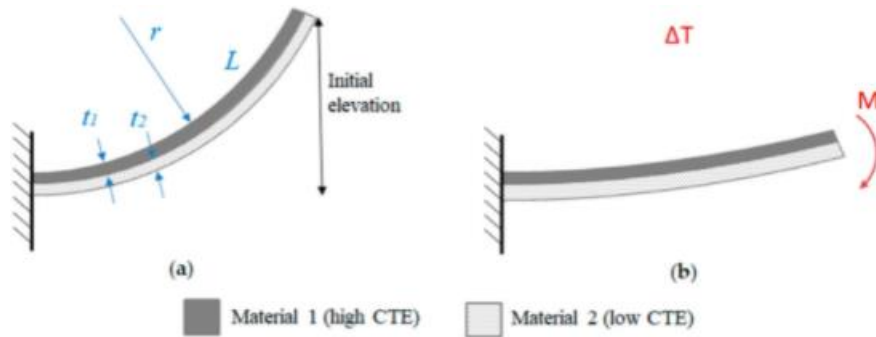


Figure 8. The principle of the Bimorph actuator

[10]

- In RF MEMS switches vertical motion is the most common as the gap is normally a few micrometres. In table 3, there is a summarizing comparison between the four mentioned actuation types.

	Voltage (V)	Current (mA)	Power (mW)	Size	Switching Time (μ s)	Contact Force (μ N)
Electrostatic	20–80 ^a	0	0	Small	1–200	50–1000
Thermal	3–5	5–100	0–200 ^b	Large ^c	300–10,000	500–4000
Magnetostatic	3–5	20–150	0–100 ^b	Medium	300–1,000	50–200
Piezoelectric	3–20	0	0	Medium	50–500	50–200

- Table 3. Performance Comparison between the different types of actuation [6]

B. Circuit Configuration

There are two basic switches used in RF to millimeter-wave circuit design: the shunt switch and the series switch.

- Series Switch

An ideal series switch results in an open circuit in the transmission line (or t-line) when no bias voltage is applied (up-state position), and it achieves a short circuit in the t-line when a bias voltage is applied (down-state position). Ideal series switches have infinite isolation in the up-state position and have zero insertion loss in the down-state position.

RF MEMS series switches are commonly used for 0.1- to 40-GHz applications and offer high isolation at RF frequencies (> 30 dB). In the down-state position, they result in very low insertion loss (< -0.2 dB).

- Shunt Switch

The shunt switch is placed in shunt between the t-line and ground. Depending on the applied bias voltage, it either leaves the t-line undisturbed or connects it to

ground. Therefore, the ideal shunt switch results in zero insertion loss when no bias is applied (up-state position) and infinite isolation when bias is applied (down-state position).

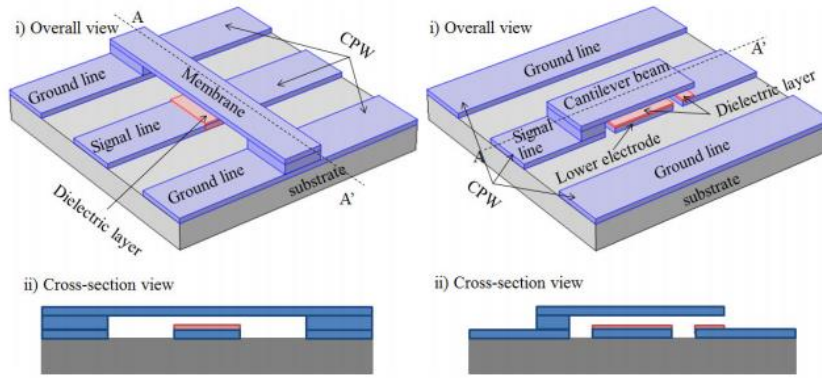


Figure 10. Typical structures of Capacitive RF-MEMS switch [7], Shunt Type (left) and Series Type (right) [7]

Shunt capacitive switches are more suited for higher frequencies (5–100 GHz). A typical shunt capacitive switch results in acceptable isolation (> 20 dB) in the down-state position and low insertion loss (< -0.1 dB) in the up-state position.

C. Contact Type

RF-MEMS switches, in general, can be realized by two different contact mechanisms, either metal-contact type (namely metal-to-metal contact) or capacitive type (namely metal insulator-metal contact).

- Metal-contact RF MEMS Switch

For electrostatic switches, by applying voltage between the cantilever beam (or membrane) and the bottom electrode, the switch can be actuated via the induced electrostatic force between two electrodes and the suspended part will be in direct contact to the signal line.

For the series metal-contact RF-MEMS switch, as shown in (fig. 9) , the RF signal can be passed through the CPW (coplanar waveguide) transmission line, namely switch-on state, when the switch is actuated. For the shunt-type switch, as shown in (fig. 9) , the RF signal would be bypassed to the ground line, namely switch-off state, when the switch is actuated; and vice versa.

These switches use metal-to-metal contact (or ohmic contact) between the signal line and suspended electrode. There have been many metal-contact RF-MEMS switches developed and reported so far, with different design structures and fabrication methods.

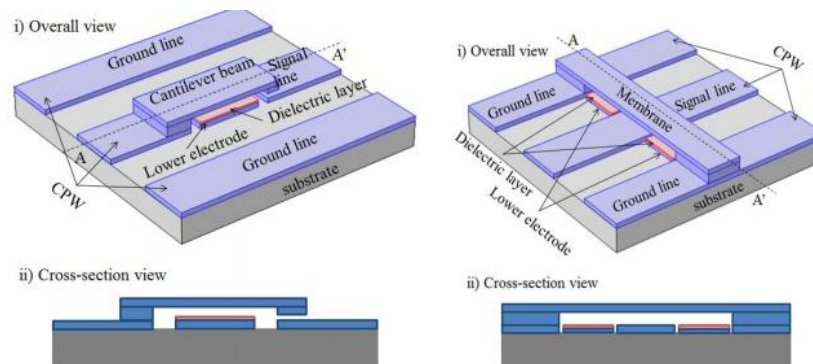


Figure 9. Typical structures of metal-contact RF-MEMS switch [7],

Series Type (left) and Shunt Type (right)

- Capacitive RF MEMS Switch

Capacitive RF-MEMS switches, actuated by electrostatic force, are suitable for high-frequency applications. In switch-on state, the bridge is suspended in its original position and there is an air gap existing between the two electrode plates. Hence, the up-state capacitance is small which results in a high impedance between input and ground. In switch-off state, the membrane is pulled down to the signal line and there is only a very thin dielectric layer between the two electrode plates, resulting in a large down state capacitance (fig. 10).

The RF-MEMS capacitive switch is more likely to employ the shunt-type structure since it has less parasitic effect when the switch is actuated. The basic principle of a capacitive RF-MEMS switch is a function of “state-off/state on” capacitance ratio, which is considered to be a crucial figure-of-merit (FOM) and should be as high as possible.

Generally, most capacitive RF-MEMS switches are operated in a wider and higher frequency range, compared to metal-contact RF-MEMS switches.

2.3 Switch library

In this section, we will present some of the earlier novel work that showed promising performance and inspired us along the way.

2.3.1 low-voltage shunt capacitive RF MEMS switch

Li-Ya Ma et al. presented a novel shunt capacitive RF MEMS switch with very low operating voltage and CMOS-compatible fabrication process (fig. 11). The structure consists of an electrostatically actuated membrane suspended over a coplanar waveguide,

four folded beams to support the membrane and four straight beams to provide the bias voltage. The switch is designed in standard $0.35\ \mu\text{m}$ complementary metal oxide semiconductor process and has a very low pull-in voltage of $3.04\ \text{V}$ fig 12. For optimizing the dimensions, They implemented Taguchi method and weighted principal component analysis to optimize the geometric parameters of the beams, in order to obtain a low spring constant, low pull-in voltage, and a robust design.

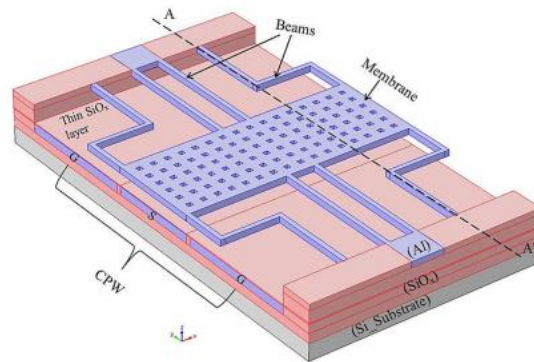


Figure 11. RF MEMS switch overall design [4]

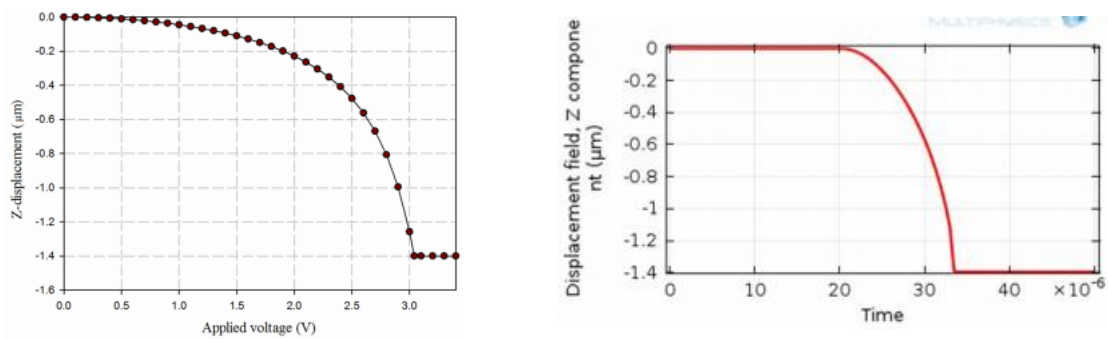


Figure 12. Simulation of the optimized RF-MEMS switch: (left) Operating Voltage, (right) Switching time.

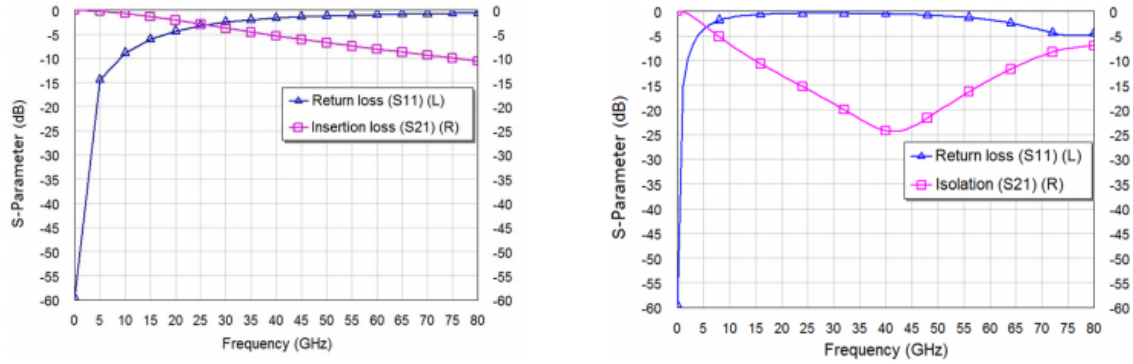


Figure 13. Simulation of the RF Performance: (left) Insertion Loss, (right) Isolation.

The simulated actuation time of the optimized switch is 13.5 μs (fig. 12) and the capacitance ratio is 52. The insertion loss and isolation is -5.65 dB and -24.38 dB at the frequency of 40 GHz, respectively (fig. 13).

The RF performance of the switch may not be optimal but this is compensated with the ultra-low pull-in voltage and CMOS compatibility, which enables the design to be implemented in portable and mobile devices.

2.3.2 RF MEMS capacitive switches using meanders

Kaur et al. presented the design and simulation of low voltage capacitive shunt MEMS switches together with its RF performance for high frequency applications. The low voltage switches are realized by lowering the spring constant of the beam using serpentine spring designs together with a large capacitive area so as to achieve the good RF performance as well.

The paper compares between two meander designs, switch A and switch B; one with 2 arms and the other with 4 arms, respectively. Each arm consists of three meanders.

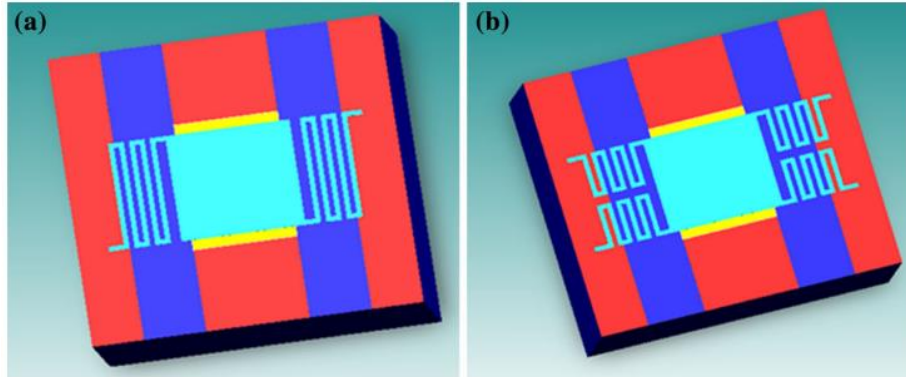


Figure 14. 3-D Layout of RF MEMS switches with different meander types,

a) switch A. b) switch B

The pull-in voltage is analyzed with commercial CAD finite element analysis software CoventorWare. The actuation voltage was obtained to be for switch A 1.5 V and for switch B is 4.75 V (fig. 15). The results showed that a lower voltage can be obtained using the serpentine spring which lowers the spring constant and the pull-in voltage.

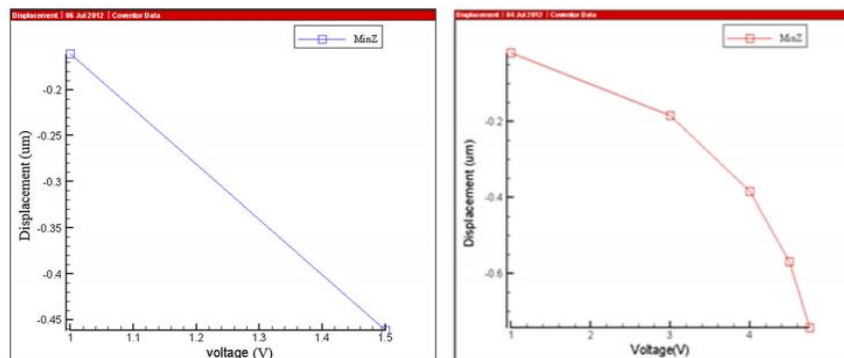


Figure 15. Simulated pull-in voltage for both designs. **(left)** switch A,

(right) switch B

The electromagnetic performance in terms of scattering parameters, insertion loss, and isolation are analyzed with software Ansoft HFSS10 (fig. 16).

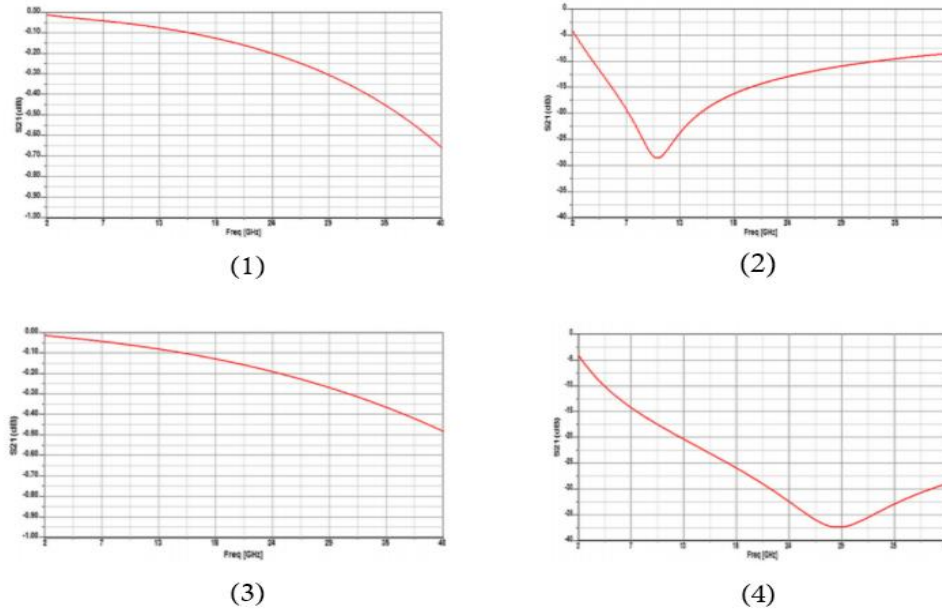


Figure 16. S-parameters (S21): for Switch A 1) Insertion loss, 2) Isolation; Switch E 3) Insertion loss, 4) Isolation

Switch A showed an insertion loss of -0.15 dB at 20 GHz and isolation of -15 dB at 20 GHz. Switch B achieved an insertion loss of -0.15 dB at 20 GHz and isolation of -37 dB at 30 GHz.

The results show that switch B introduced better isolation at higher frequencies. However, switch A has the advantage of lower actuation voltage and comparable excellent insertion loss. Overall, the paper shows the significant reduction in actuation voltage when adding meander beams as supports.

2.3.4 Metal-contact Cantilever-based Series RF MEMS Switch

Rao et al. presented in this paper a micro level electrostatically actuated cantilever and metal contact based series RF MEMS Switch (fig. 17). The designed switch is simulated and the performance is verified over the frequency range 0.8–20 GHz. Using Comsol Multiphysics FEM tools, the paper presents the RF performance and the actuation voltage of the switch.

The paper concentrated on achieving very low actuation voltage, by using less weight polymer material like Poly Tetra Fluoro Ethylene (PTFE). The series switching is implemented in the microstrip Transmission line using cantilever structure associated with gold contact material.

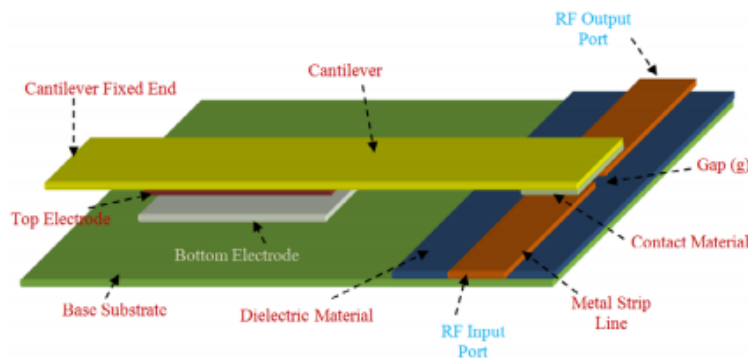


Figure 17. Series RF MEMS switch

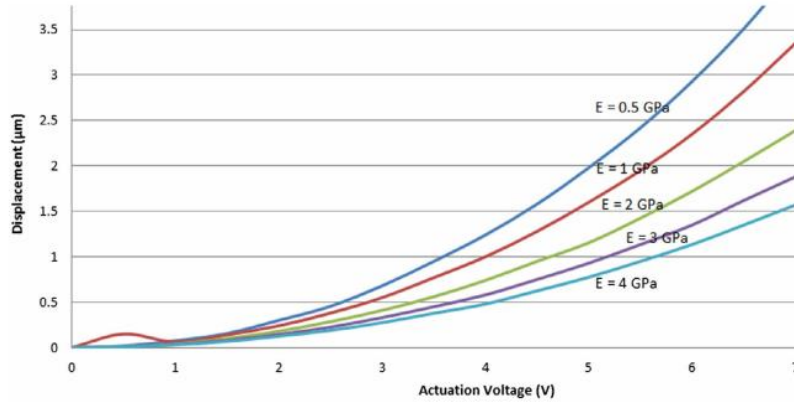


Figure 18. Displacement vs. actuation voltage with respect to Young's Modulus (E)

The paper shows the change in the actuation voltage with the structure's young modulus (fig. 18). The proposed cantilever can achieve a voltage of 3.55 V. For insertion losses, when the voltage applied is zero, the switch results in an isolation loss in the range -58 to -20 dB over the frequency 0.8 – 20 GHz respectively as shown (fig. 19).

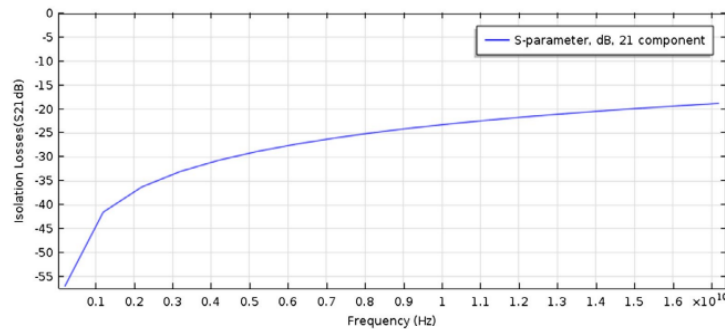


Figure 19. Isolation losses (S21), when the cantilever is in Up state.

For the insertion losses, when applying a voltage of 3.55 V, the structure will start to deform, and cover the gap in the transmission line (fig. 20). That results in a constant insertion loss of -0.08 to -0.14 dB over the frequency range 0.8–20 GHz.

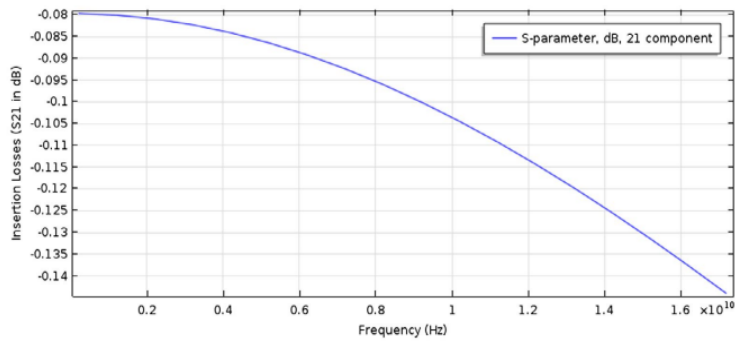


Figure 20. Insertion losses (S21), when the cantilever is in Down state.

This design managed to achieve an excellent operating voltage, using a special polymer, and very good RF performance. However, the cantilever is very long and uses uncommon materials resulting in issues with fabrication. The switch is recommended to work within the reconfigurable communication frequency range.

Chapter 3

Project Design

3.1 Project purpose and constraints

This project aims to design a frequency reconfigurable antenna in the midband 5G for IOT applications, targeting the 1-2 GHz and 3.3-3.8 GHz with bandwidth less than 100 MHz. Also, the switch is required to consume low power and to operate on low voltage to be compatible with the mobile 5G IOT applications. Hence, RF MEMS switches are designed for this purpose as MEMS switches consume much less power. However, MEMS switches require relatively high voltage of operation, so it is a goal in this project to design a MEMS switch operating on low voltage as well.

After designing the antenna, and the MEMS switch, they should be fabricated, then integrated together on a PCB using an electronic control circuit. However, the fabrication step takes a lot of time, hence the system integration step did not have time as the fabrication step is still in progress.

RF MEMS switches have several parameters and variables that are usually in need of optimization and tuning in order to achieve the required specifications. These parameters are in tradeoffs with each other resulting in numerous challenges in designing an efficient RF MEMS switch. In this section, we will explore various techniques to optimize and improve RF MEMS switches.

3.1.1 RF Performance

For an RF MEMS switch, the most important parameters for its RF performance are insertion loss and isolation. Scattering parameters generally can be used to estimate the

RF performance. When the RF-MEMS switch is turned on (fig. 21), S_{21} indicates the insertion loss; and when the RF-MEMS switch is turned off, S_{21} represents isolation.

S_{21} can be estimated theoretically by the following equation.

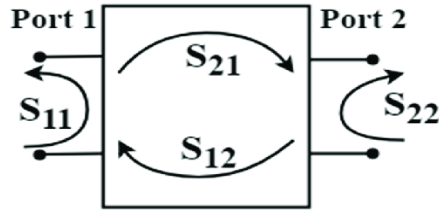


Figure 21. Scattering parameters in a typical two-port network [9]

$$S_{21} = \frac{2}{2 + \omega C Z_0} (1)$$

Where, Z_0 is the switch's characteristic impedance, ω is the resonant frequency, C is the up-state or down-state capacitance.

As shown from equation (1), the insertion loss and isolation of the RF-MEMS switch are directly proportional with its up-state and down-state capacitance. More precisely, a small up-state capacitance results in a low insertion loss and a large down-state capacitance leads to a high isolation. Therefore, it can be concluded that a large capacitance ratio improves the RF performance for RF-MEMS capacitive switches. The capacitance ratio can be estimated through the following equation.

$$C_{ratio} = \frac{C_d}{C_u} \approx \frac{g_0 \epsilon_r t_d}{(1+x) t_d} \quad (2)$$

where, g_0 is the air gap between two electrodes; ϵ_r and t_d is the permittivity and thickness of the dielectric layer, respectively; C_d and C_u is down-state and up-state capacitance, respectively and x is a coefficient of fringing field capacitance ($=0.3 \sim 0.4$). As indicated in equation (2), a large capacitance ratio can be realized through several methods.

Choosing a dielectric material with high permittivity is a simple technique for increasing the capacitance ratio. Materials such as aluminum nitride (AlN, $\epsilon_r=9.8$), hafnium dioxide (HfO₂, $\epsilon_r=20 \sim 25$) have promising results; However, they are usually not compatible with typical fabrication techniques. So, they are not easily fabricated and quite expensive.

Also, the dielectric thickness needs to be as small as possible to achieve a high capacitance ratio. However, it is usually limited by the limitations of the fabrication process. Also, very small thickness can lead to dielectric break down by the pull-in voltage.

Increasing the air gap is also a great way to enlarge the capacitance ratio. Nevertheless, it leads to very high actuation voltages, which is crucial for certain applications. Therefore, a trade-off between the operating voltage and the RF performance of the RF MEMS switch is always in play. Typically, the air gap is around 2-3 μm .

There are other unconventional methods that can be used in order to achieve the best RF performance possible, such as shunt-series configurations.

3.1.2 Actuation Voltage

Typically, RF MEMS switches require high actuation voltages (30~80 V). Hence, reducing this voltage is a major challenge in designing MEMS switches. Small operating voltage results in reduced interface circuit's complexity and improved switch's reliability. The switch also can be compatible with small and portable devices such as mobile phones and wireless devices.

For electrostatically-actuated RF-MEMS switches, the actuation (or pull-in) voltage can be obtained theoretically by the following equation.

$$V_{pull-in} = \sqrt{\frac{8kg_0^3}{27\epsilon_0 A}} \quad (3)$$

where, k is the total spring constant of the membrane and beams; g_0 is the initial air gap between the membrane and the signal line, ϵ_0 is the permittivity of air and A is the overlapping area of the actuation electrodes.

This equation implies the methods of reducing the actuation voltage, which are lowering the spring constant and air gap or increasing the overlapping area of the actuation electrodes.

- **Spring Constant**

Designing an RF MEMS switch with low spring constant can greatly reduce the actuation voltage. From a mechanical point of view, the low spring constant of a movable structure can be obtained by using folded beams, serpentine beams or reducing the beam thickness

fully or selectively. However, the beam with very small spring constant will provide weak restoring force to release the membrane up which results in down-state stiction. In addition, the whole structure may be very fragile, have low natural frequency and switching speed.

- **Design Dimensions**

Increasing the effective area of the electrostatic actuator leads to notable reduction in the RF-MEMS switch's actuation voltage. On the other hand, it leads to an increase in stiction problems; and it is limited by size and footprint considerations. The pull-in voltage is highly dependent on the air gap between the suspended structure and the bottom electrode. It is usually around 2~3 μm . However, reducing the air gap has a negative impact on insertion loss; because of the increase in the up-state capacitance. Also, a too small gap can lead to contact with the other electrode without any applied voltage.

3.1.3 Reliability

One of the main concerns and setbacks for RF MEMS switches is the reliability issue, which prevented many switches from being commercialized widely. For metal-contact switches, the reliability is mainly limited by micro welding and stiction problems.

Typically, the switches' failure mechanisms include fusing of contacts, increased contact resistance between the moveable contacts and the transmission line, as well as a micro welding problem after repeated actuations.

For capacitive type, the switches' reliability is generally restricted by the stiction between the dielectric layer and the metal, dielectric layer breakdown or mechanical shock due to high actuation voltage. Often, with high actuation voltage, charge injection and charge trapping in the dielectric layers cause the switch to stick in the downstate position or increase the pull-in voltage.

3.1.4 Switching Time

The switching time of an RF MEMS switch is highly dependent on the mechanical response of the structure. The frequency response of a fixed-fixed or cantilever beam is useful for determining the switching time, the mechanical bandwidth over which it can be used, and the impact of thermal noise.

Since only the central (or end) portion of the beam is moving, the effective mass of the resonant mode can be around 0.35–0.45 times the actual mass of the beam, depending on the size of the pull-down electrode and the thickness. Typically, the mechanical resonant frequency of electrostatic MEMS switches is 10–200 kHz.

The switching time depends strongly on the applied voltage since the larger the voltage, the stronger the electrostatic force (fig. 22). There is also a substantial improvement, shorter switching time, with increasing the quality factor. Above a quality factor of 2, there is no considerable change, as seen in figure.

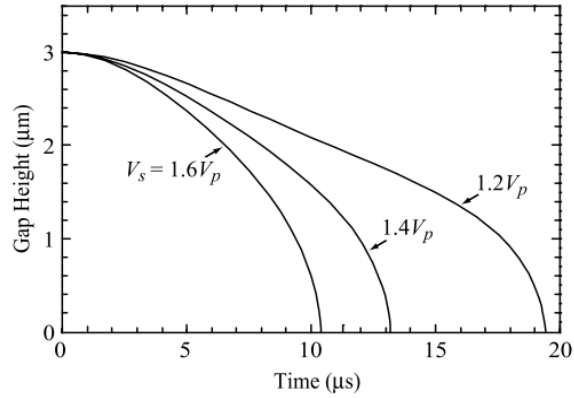


Figure 22. Pull-down simulations for the Au beam versus the applied voltage, at $Q = 1$ [6]

Squeezing the air under the membrane can negatively affect the switching time.

However, it becomes truly insignificant for structures with holes. A good approximation

of the switching time is obtained using the relation, $t_s \approx 3.67 \frac{V_p}{V_s \omega_0}$

Where, V_p is the pull-in voltage and V_s is the applied voltage, for $V_s > 1.4V_p$ and $Q > 2$.

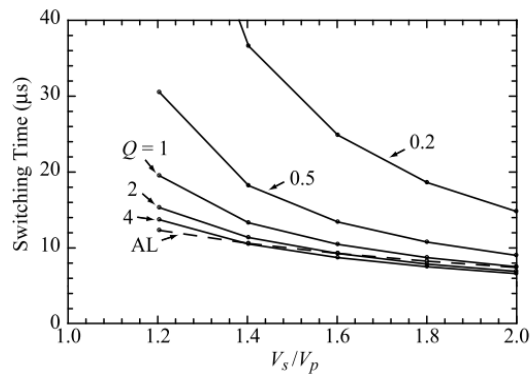


Figure 23. Switching time for the Au beam (“AL”, Acceleration-Limited) [6]

3.1.5 Fabrication

The fabrication of RF MEMS devices is a major setback in the development of mass-produced switches. Usually, it can have a relatively complex fabrication process. This is due to increasing the number of layers and masks, having very small dimensions and using unconventional materials.

Most MEMS switches are fabricated using low temperature processes and are post-CMOS and post-GaAs compatible. However, there are too many fabrication processes. However, many of the fabrication techniques are not compatible with each other.

The packaging of MEMS switches is a larger challenge than typical MEMS devices due to hermeticity, temperature, and outgassing constraints. Also, MEMS devices must be packaged in a nitrogen or dry-air atmosphere for high reliability.

Furthermore, monolithically integrated (e.g., CMOS based) RF-MEMS switches for have shown several advantages, such as i) easily integrated with integration circuits on a single chip, ii) reduced parasitic capacitance, ii) low insertion loss even in very high frequency range; iii) high isolation; and iv) low fabrication cost since most of them need mask or maskless post-CMOS process.

3.2 Project technical specifications

The technical specifications for the antenna is shown in the following table

Antenna	Design 1	Design 2
Patch 1 dimensions L*W*H	17*26.2*0.35	18*26.2*0.035
Patch 2 dimensions L*W*H	38*26.2*0.35	0.5*26.2*0.035
Frequency in OFF state	3.74 GHz	3.452 GHz
Frequency in ON state	1.056 GHz	3.164 GHz
Substrate name	FR-4 lossy	FR-4 lossy
Substrate dielectric constant	4.3	4.3
Substrate dimensions L*W*H	70*45*1.6 (mm)	40*35*1.6 (mm)
Separation between patches	3 mm	3 mm
Feedline thickness	3.06 mm	2.8 mm

Number of switches	2	2
---------------------------	---	---

Table 4. The technical specifications for the antenna

The technical specifications for the MEMS switch is shown in the following table

	Design 1 - Novel	Design 2 - Co	Design 3 - 2M	Design 4 - 1M	Design 5 - 4L
Operation voltage (V)	3.1	21	14	6	16
Power	Zero	Zero	Zero	Zero	Zero
Switching Time (μs)	70	30	45	100	22
Insertion loss (dB)	< 0.017	< 0.04	< 0.02	< 0.07	< 0.5
Isolation (dB)	> 25	> 23	> 30	> 23	> 30

Table 5. The technical specifications for the MEMS switch

3.3 Design alternatives and justification

Our design is RF MEMS switch reconfigurable antenna, so it is divided into two parts, the antenna part which is chosen to be a patch antenna, and the switching part which is chosen to be a MEMS switch. For the antenna part, the antenna is going to be used in mobile applications, which require miniaturizing the components sizes to make small mobile packages. Hence the antenna as well needs to be small in size, that is why the patch antenna is used.

The patch antenna is small in size, as well as having very small thickness compared to its area, so it is suitable for this kind of application. Furthermore, there is a variant of patch antennas called Planar Inverted F-Antenna or PIFA for short. It is called like this because it has the shape of an inverted F letter. Anyway, PIFA antenna is similar to patch antenna but it is half of its size, so this helps more in making smaller packages for small applications such as in IOT applications. Hence, patch antenna is a good choice for the antenna part due to sizing requirements as mentioned, it can be upgraded to a PIFA, and it has low cost fabrication as well.

For the switching part there are two choices to be made, the first is whether the switch used is a diode, varactor, MEMS, or photoconductive switch. RF MEMS switch is chosen in our design. Table 1 contains a clear comparison between different switch types.

In a nutshell, MEMS switch is used as it has lower power consumption, lower insertion losses, and high quality factor. This is suitable for mobile applications which is the goal of this project. However, it has higher operating voltages which is not good for our required

mobile applications. This is a main problem for the MEMS switch, so it is tackled in this project and a design with low working voltage is made. The second choice is for choosing the MEMS switch concept of operation, whether it is capacitive, magnetic, or piezoelectric.

3.4 Description of the selected design

3.4.1 Antenna design:

Refer to section 4.2.1

3.4.2 RF MEMS Switches:

In total, we designed five RF MEMS switches each with different design concepts and purposes. The first one is a series contact switch with two sides electrodes and meanders to operate at ultra low voltage. This design is suitable for the low frequency range antennas, < 5 GHz. This design is fabricatable as we used only compatible materials and processes. In addition, we designed four more designs to be fabricated at The University of Waterloo RF MEMS cleanroom. The first of them is a series contact meander based switch with low operating voltage and low frequency range. The second one is a capacitive shunt switch with a step down part for high operating voltage purposes. The fourth design is two side meanders-based capacitive and is also a shunt switch for high frequency applications. The last design is a series contact cantilever-like switch. The five designs are simulated using Multiphysics COMSOL and HFSS, and the Layouts are drawn using KLayout.

3.5 Block diagram and functions of the subsystems

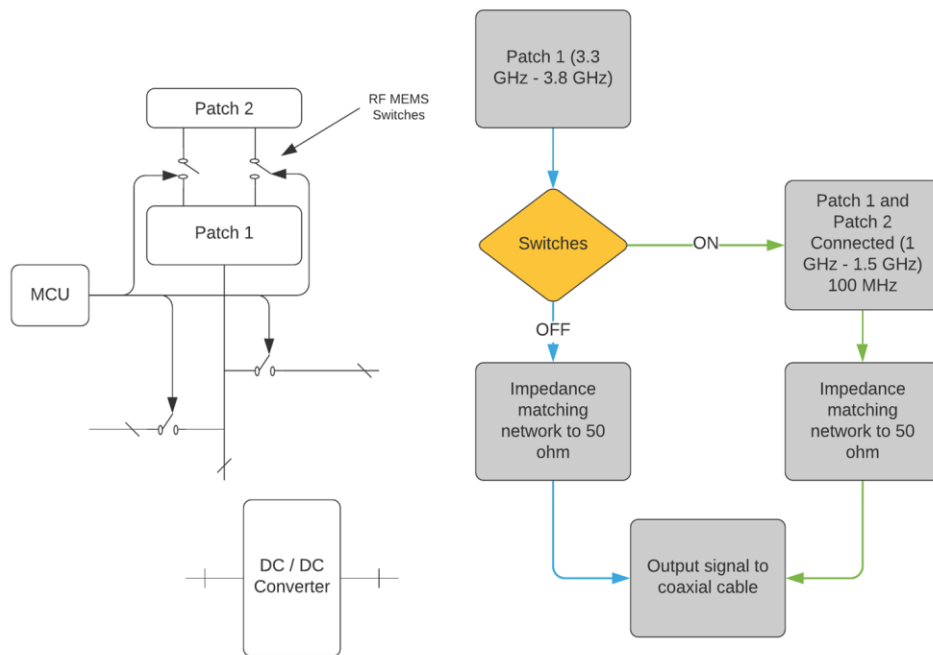


Figure 24. The block diagram of the system

Referring to the block diagram (fig. 24), the system consists of two varying sized patches. In the example shown in the block diagram, patch 1 operates at 3.4 GHz while the two patches combined operate at resonant frequency of 1.45 GHz. RF MEMS switches will be used to connect between Patch 1 and Patch 2. Those switches provide high isolation at the system operation frequencies to maintain the reconfigurability feature of the system. According to the switches state, different antenna configuration is obtained, and hence different frequency is obtained. The block diagram example changes frequency from 3.4 to 1.5 GHz. However, this project has two antenna designs. A design is changing frequency from 3.3 to 3.49 GHz, and another design changing frequency in 1-2 GHz range. Patches will be matched to 50 ohms via inset feed matching or two matching networks for each patch feedline. Finally, the switching mechanism will be controlled by a Microcontroller Unit (MCU).

Chapter 4

Project Execution

4.1 Project Tasks and Gantt chart

According to the nature of our project, we subdivided the whole project into three core parts:

1. Reconfigurable antenna design, optimization, testing, and fabrication.
2. RF MEMS switch design, optimization, testing, and fabrication.
3. Fabrication and physical system integration and implementation of a controlling circuitry to control the whole system reconfigurability on demand.

After the project initiation, we found out that we lack some knowledge in the different parts of the project, specially the antenna design. Therefore, we focused our resources, time and effort, on understanding the fundamentals of antenna theory and getting deep into both fields of knowledge, Antenna design and RF MEMS. Our four member team was divided into two sub teams each working on separate fields, yet on a strong communications channel. The plan was set to clarify the operation frequency which is allocated in the 5G medium band, 1 - 5 GHz. After that, one team was to design the antenna and the other to design RF MEMS switches. The following WBS, figure 25, shows clearly the planned team dynamics and the feedback loops between the team members.

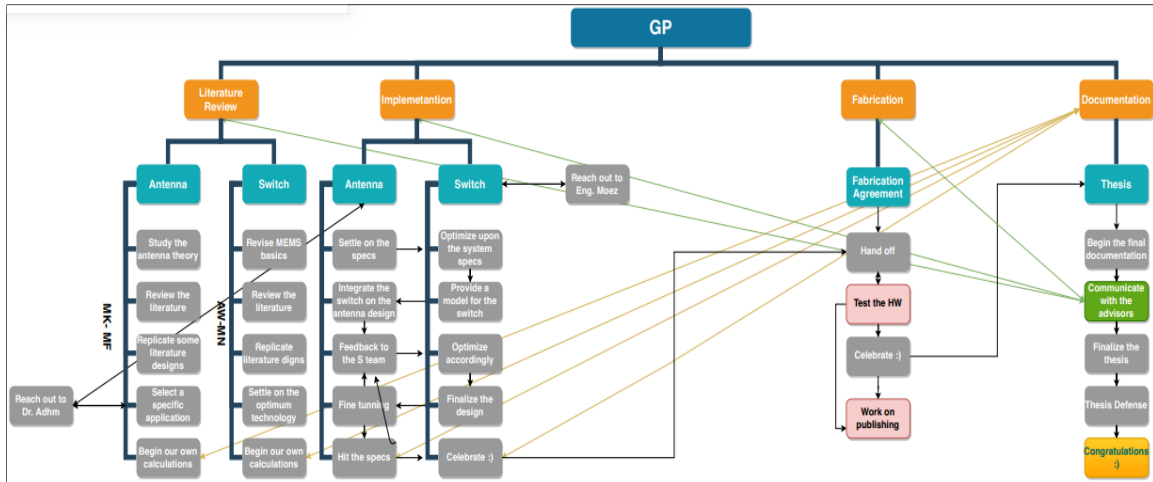


Figure 25. The Work Breakdown Structure (WPS) for the project

4.2 Description of each subsystem

As mentioned earlier, the project is divided into two major parts. In this section, each subsystem is discussed thoroughly including each subsystem's components, schematics, material selection, and manufacturing processes. Starting with the antenna part, and to be focused on a coherent sequence of execution steps, reader should know that in this part we start with identifying the targeted frequencies of operation and international standards, then the initial design for two micro strip patches, then integrating idealized switches between the two patches, then a generalized model for RF MEMS switches, then the RLC models designed by our team, and finally the optimization is demonstrated through the whole phases.

4.2.1 Antenna

Frequency of operations and standards inspired by the 4.0 industrial revolution onsets, our choice of operating frequencies is following the 5G standards issued by GSMA titled ‘5G Spectrum GSMA Public Policy Position’ in March 2021. The figure 26 demonstrates different bands allowed for 5G communications.

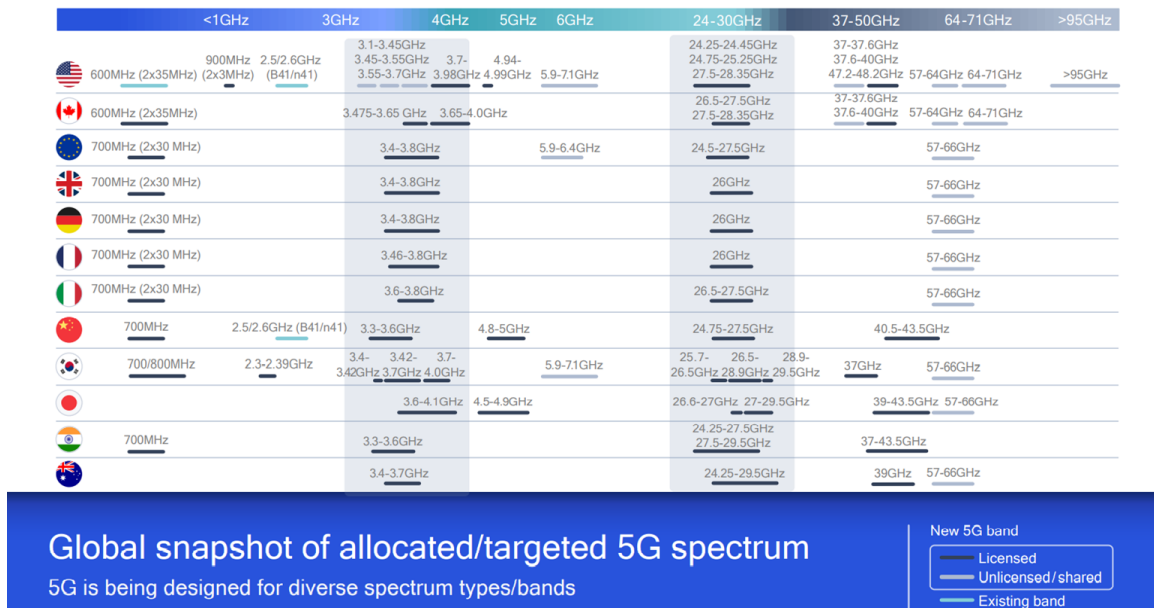


Figure 26. The global snapshot of allocated 5G spectrum

As mentioned above, the working range of the antenna is from 1-5 GHz, and in that range some bandwidths are chosen for the antenna to work in. The general workflow is described, then each design will be addressed specifically. For a given bandwidth, the workflow is as follows:

- According to the bandwidth, the patch dimensions (length and width) is calculated using the following equations. For a rectangular patch antenna, the width of the patch is calculated as follows:

$$W = \frac{c}{2f_0 \sqrt{\frac{\epsilon_r + 1}{2}}}$$

Where f_0 is the required frequency, c is the speed of light in vacuum, and ϵ_r is the relative electrical permittivity. While the length of the patch is calculated as follows

$$L = \frac{c}{2f_0 \sqrt{\epsilon_r}} - 2\Delta L$$

Where ΔL is defined as

$$\Delta L = 0.412h * \frac{(\epsilon_{eff} + 0.3) \left(\frac{W}{L} + 0.264\right)}{(\epsilon_{eff} - 0.258) \left(\frac{W}{L} + 0.8\right)}$$

Where ϵ_{eff} is the effective electric permittivity, and it is equal to $\epsilon_r * \epsilon_0$

- The thickness of the copper is 0.035 mm, which is a standard.
- The obtained dimensions are used to make a model for the antenna on CST software.
- Material for the substrate is chosen FR-4 lossy with dielectric constant $\epsilon_r =$

4.3

- A ground plane with area equal to that of the substrate is placed on the other side of the substrate (one side is the patch, the other is the ground plane).

Figure 27 shows an example for the antenna shape

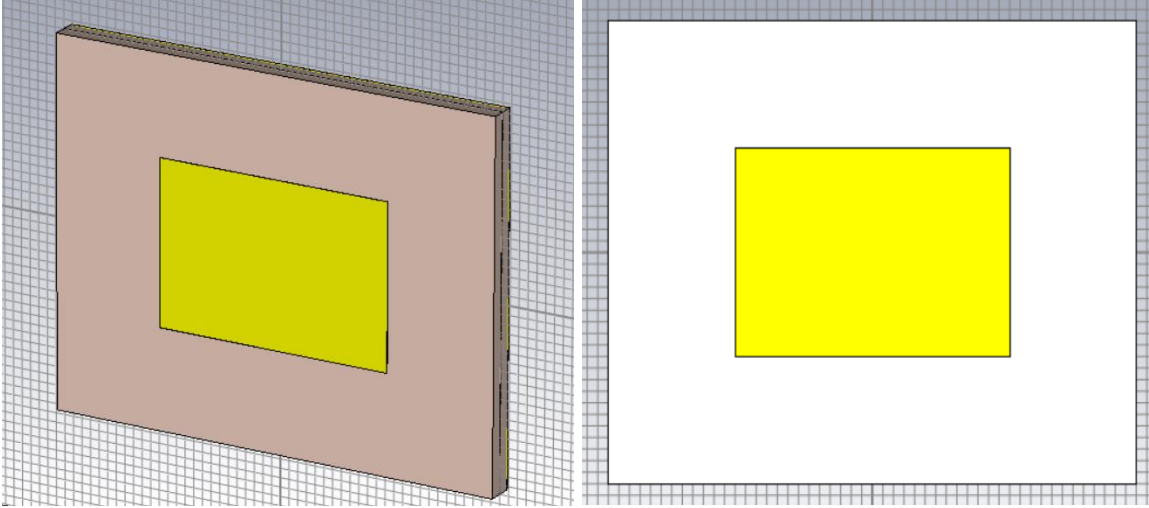


Figure 27. The shape of a patch antenna showing the patch (yellow) and the substrate

- The feed-line is placed as a thin copper wire connected to the patch, and from CST a waveguide port is added at the feed-line surface as shown in figure 28.

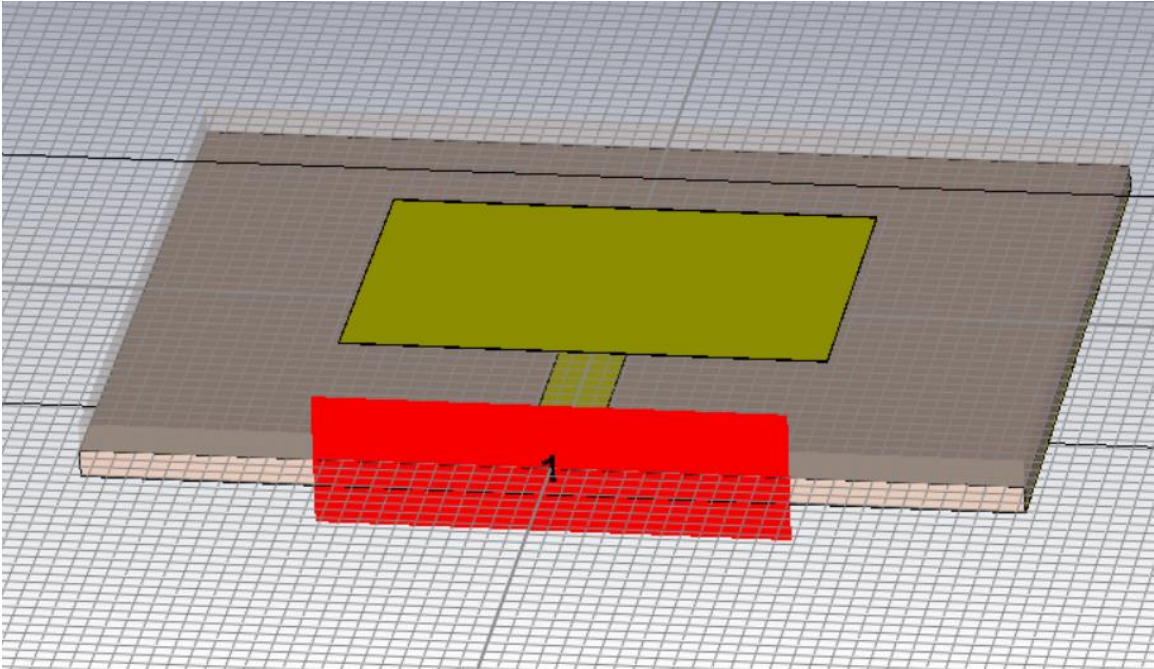


Figure 28. Image showing the patch antenna with the feed-line (thin yellow line) and waveguide port (red)

- It is a convention for the waveguide port setup to be 5-6 times wider than the feed-line itself. The waveguide port is for simulating the signal entrance to the feedline.
- Now the CST simulation is ready to start. The equations used to calculate the antenna dimensions act as an approximation to get the initial dimensions. Then using simulations, iterations can be made to fine tune the antenna to the required bandwidth.
- The results obtained from the simulations are given as graphs in CST. The results include the S-parameter (S11), the Voltage Stand-Wave Ratio (VSWR), the fairfield field which describes the magnitude and direction

of the radiation, and it can be viewed in 1D, polar coordinates, or in 3D view.

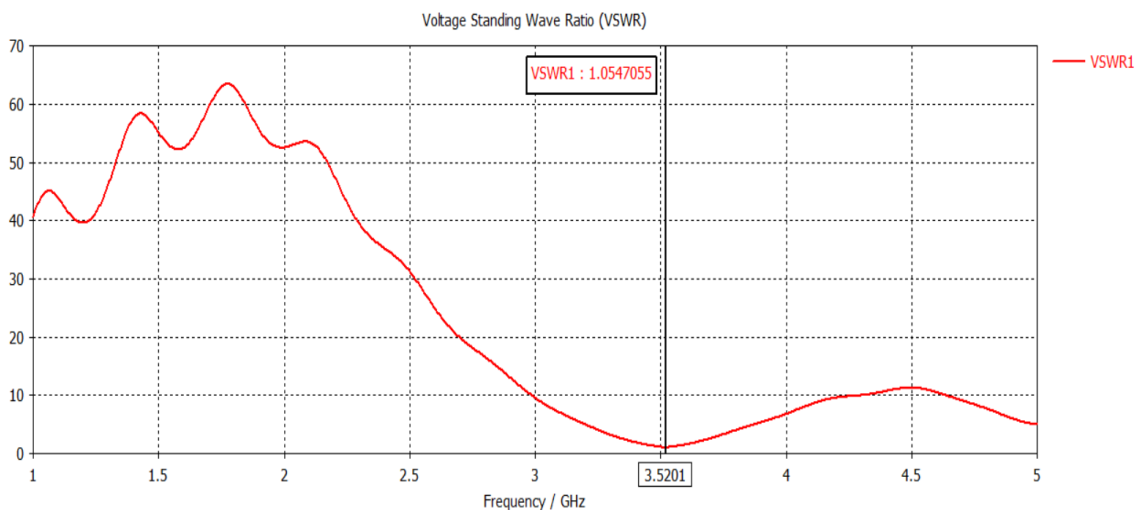


Figure 29. Showing the VSWR to be minimum at the frequency of operation which is 3.52 GHz

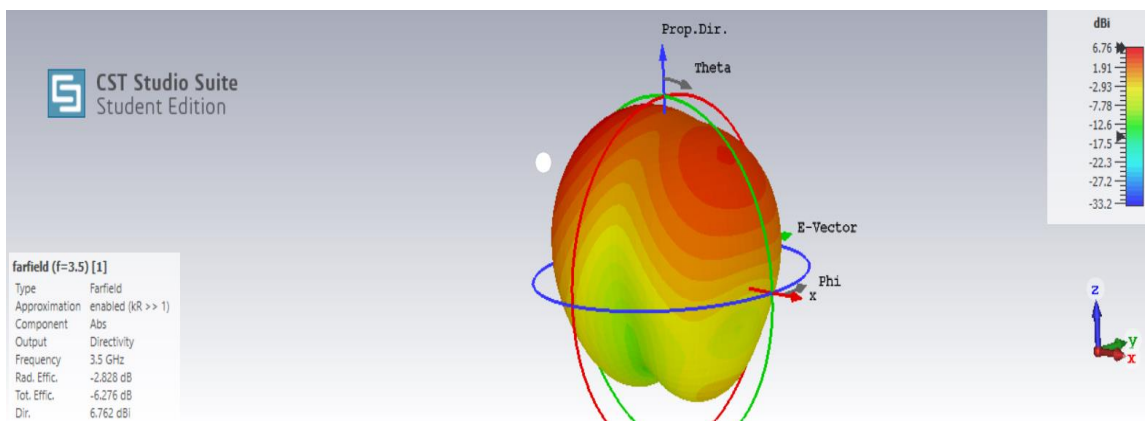


Figure 30. The Farfield in 3D view

This figure shows that most radiation is in the direction perpendicular to the antenna surface and above the antenna, while below the antenna the radiation is nearly zero, and that is expected due to the presence of the ground plane at the bottom.

Two different designs for our RA have been designed. First is set to work for 5G IoT applications, and the second is set to work within 3-4GHz as it is regarded as the hot band for commercial 5G applications.

- First design

This design is to operate within a band set by Huawei, [see the appendix](#), to be utilized in its 5G IoT deployment. The band is set between 3 GHz - 4 GHz and 1 GHz - 2 GHz. One of the challenges we faced with this design, besides impedance matching and other parameter optimization, was the frequency drop from the higher frequency to the lower frequency. In other words, this antenna centre frequency is 3.752 GHz with two patches not connected (idealized insulation) as in figure 31 while in case of idealized switches connecting between both patches as in figure 32, it is designed to operate on 1.096 GHz.

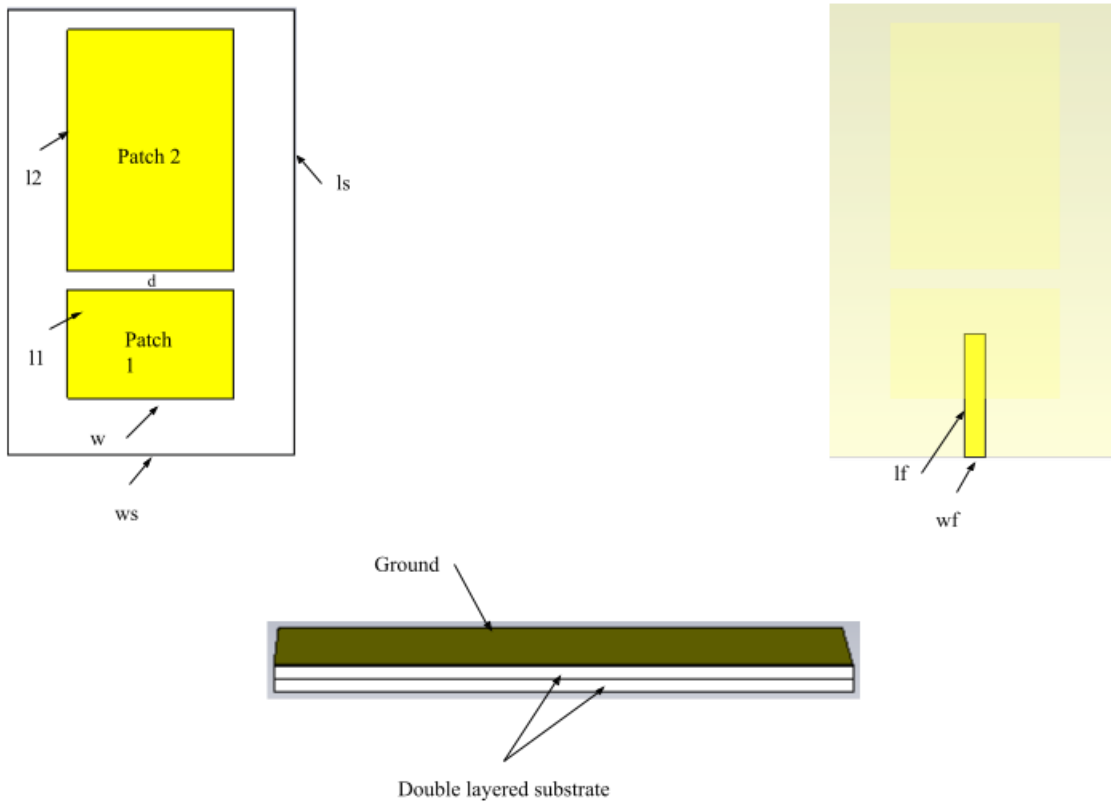


Figure 31. Design 1 structure with no switches connected

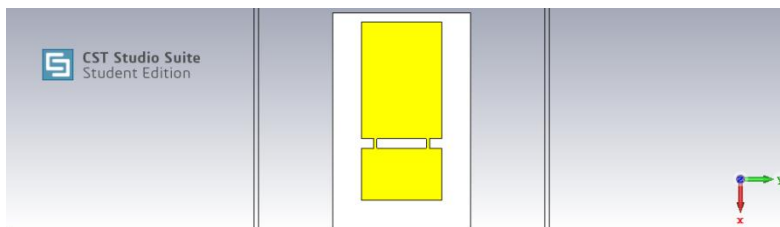


Figure #x3

Figure 32. Design 1 structure with idealized switches connected

Parameter	Value (mm)
-----------	------------

Substrate width (w_s)	45
Substrate length (l_s)	70
Patch1 length (l_1)	17
Patch 1 width (w)	26.2
Patch 2 length (l_2)	45
Patch 2 width (w)	26.5
Feed line length (l_f)	19
Fed line width (w_f)	3.06
Separation (d)	3

Table 6. demonstrates the design parameters after conducting parametric analysis and optimization.

In an attempt to achieve optimization, figure 33 shows the parametric analysis of I1, I2, I3, I4, I5, I6, I7, I8, I9, I10, I11, I12, I13, I14, I15, I16, I17, I18, I19, I20, I21, I22, I23, I24, I25, I26, I27, I28, I29, I30, I31, I32, I33, I34, I35, I36, I37, I38, I39, I40, I41, I42, I43, I44, I45, I46, I47, I48, I49, I50, I51, I52, I53, I54, I55, I56, I57, I58, I59, I60, I61, I62, I63, I64, I65, I66, I67, I68, I69, I70, I71, I72, I73, I74, I75, I76, I77, I78, I79, I80, I81, I82, I83, I84, I85, I86, I87, I88, I89, I90, I91, I92, I93, I94, I95, I96, I97, I98, I99, I100, I101, I102, I103, I104, I105, I106, I107, I108, I109, I110, I111, I112, I113, I114, I115, I116, I117, I118, I119, I120, I121, I122, I123, I124, I125, I126, I127, I128, I129, I130, I131, I132, I133, I134, I135, I136, I137, I138, I139, I140, I141, I142, I143, I144, I145, I146, I147, I148, I149, I150, I151, I152, I153, I154, I155, I156, I157, I158, I159, I160, I161, I162, I163, I164, I165, I166, I167, I168, I169, I170, I171, I172, I173, I174, I175, I176, I177, I178, I179, I180, I181, I182, I183, I184, I185, I186, I187, I188, I189, I190, I191, I192, I193, I194, I195, I196, I197, I198, I199, I200, I201, I202, I203, I204, I205, I206, I207, I208, I209, I210, I211, I212, I213, I214, I215, I216, I217, I218, I219, I220, I221, I222, I223, I224, I225, I226, I227, I228, I229, I230, I231, I232, I233, I234, I235, I236, I237, I238, I239, I240, I241, I242, I243, I244, I245, I246, I247, I248, I249, I250, I251, I252, I253, I254, I255, I256, I257, I258, I259, I260, I261, I262, I263, I264, I265, I266, I267, I268, I269, I270, I271, I272, I273, I274, I275, I276, I277, I278, I279, I280, I281, I282, I283, I284, I285, I286, I287, I288, I289, I290, I291, I292, I293, I294, I295, I296, I297, I298, I299, I300, I301, I302, I303, I304, I305, I306, I307, I308, I309, I310, I311, I312, I313, I314, I315, I316, I317, I318, I319, I320, I321, I322, I323, I324, I325, I326, I327, I328, I329, I330, I331, I332, I333, I334, I335, I336, I337, I338, I339, I340, I341, I342, I343, I344, I345, I346, I347, I348, I349, I350, I351, I352, I353, I354, I355, I356, I357, I358, I359, I360, I361, I362, I363, I364, I365, I366, I367, I368, I369, I370, I371, I372, I373, I374, I375, I376, I377, I378, I379, I380, I381, I382, I383, I384, I385, I386, I387, I388, I389, I390, I391, I392, I393, I394, I395, I396, I397, I398, I399, I400, I401, I402, I403, I404, I405, I406, I407, I408, I409, I410, I411, I412, I413, I414, I415, I416, I417, I418, I419, I420, I421, I422, I423, I424, I425, I426, I427, I428, I429, I430, I431, I432, I433, I434, I435, I436, I437, I438, I439, I440, I441, I442, I443, I444, I445, I446, I447, I448, I449, I450, I451, I452, I453, I454, I455, I456, I457, I458, I459, I460, I461, I462, I463, I464, I465, I466, I467, I468, I469, I470, I471, I472, I473, I474, I475, I476, I477, I478, I479, I480, I481, I482, I483, I484, I485, I486, I487, I488, I489, I490, I491, I492, I493, I494, I495, I496, I497, I498, I499, I500, I501, I502, I503, I504, I505, I506, I507, I508, I509, I510, I511, I512, I513, I514, I515, I516, I517, I518, I519, I520, I521, I522, I523, I524, I525, I526, I527, I528, I529, I530, I531, I532, I533, I534, I535, I536, I537, I538, I539, I540, I541, I542, I543, I544, I545, I546, I547, I548, I549, I550, I551, I552, I553, I554, I555, I556, I557, I558, I559, I560, I561, I562, I563, I564, I565, I566, I567, I568, I569, I570, I571, I572, I573, I574, I575, I576, I577, I578, I579, I580, I581, I582, I583, I584, I585, I586, I587, I588, I589, I590, I591, I592, I593, I594, I595, I596, I597, I598, I599, I600, I601, I602, I603, I604, I605, I606, I607, I608, I609, I610, I611, I612, I613, I614, I615, I616, I617, I618, I619, I620, I621, I622, I623, I624, I625, I626, I627, I628, I629, I630, I631, I632, I633, I634, I635, I636, I637, I638, I639, I640, I641, I642, I643, I644, I645, I646, I647, I648, I649, I650, I651, I652, I653, I654, I655, I656, I657, I658, I659, I660, I661, I662, I663, I664, I665, I666, I667, I668, I669, I670, I671, I672, I673, I674, I675, I676, I677, I678, I679, I680, I681, I682, I683, I684, I685, I686, I687, I688, I689, I690, I691, I692, I693, I694, I695, I696, I697, I698, I699, I700, I701, I702, I703, I704, I705, I706, I707, I708, I709, I710, I711, I712, I713, I714, I715, I716, I717, I718, I719, I720, I721, I722, I723, I724, I725, I726, I727, I728, I729, I730, I731, I732, I733, I734, I735, I736, I737, I738, I739, I740, I741, I742, I743, I744, I745, I746, I747, I748, I749, I750, I751, I752, I753, I754, I755, I756, I757, I758, I759, I760, I761, I762, I763, I764, I765, I766, I767, I768, I769, I770, I771, I772, I773, I774, I775, I776, I777, I778, I779, I780, I781, I782, I783, I784, I785, I786, I787, I788, I789, I790, I791, I792, I793, I794, I795, I796, I797, I798, I799, I800, I801, I802, I803, I804, I805, I806, I807, I808, I809, I810, I811, I812, I813, I814, I815, I816, I817, I818, I819, I820, I821, I822, I823, I824, I825, I826, I827, I828, I829, I830, I831, I832, I833, I834, I835, I836, I837, I838, I839, I840, I841, I842, I843, I844, I845, I846, I847, I848, I849, I850, I851, I852, I853, I854, I855, I856, I857, I858, I859, I860, I861, I862, I863, I864, I865, I866, I867, I868, I869, I870, I871, I872, I873, I874, I875, I876, I877, I878, I879, I880, I881, I882, I883, I884, I885, I886, I887, I888, I889, I890, I891, I892, I893, I894, I895, I896, I897, I898, I899, I900, I901, I902, I903, I904, I905, I906, I907, I908, I909, I910, I911, I912, I913, I914, I915, I916, I917, I918, I919, I920, I921, I922, I923, I924, I925, I926, I927, I928, I929, I930, I931, I932, I933, I934, I935, I936, I937, I938, I939, I940, I941, I942, I943, I944, I945, I946, I947, I948, I949, I950, I951, I952, I953, I954, I955, I956, I957, I958, I959, I960, I961, I962, I963, I964, I965, I966, I967, I968, I969, I970, I971, I972, I973, I974, I975, I976, I977, I978, I979, I980, I981, I982, I983, I984, I985, I986, I987, I988, I989, I990, I991, I992, I993, I994, I995, I996, I997, I998, I999, I1000.

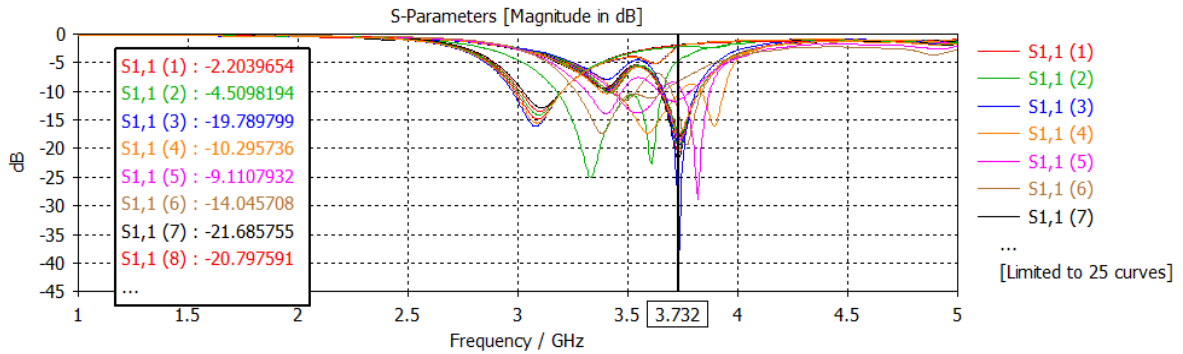


Figure 33. Parametric sweep on some parameters

Moreover, the separation distance was an effective parameter in the optimization process as it affects the frequency of operation for the first patch in case of unconnected patches as shown in figure 34. It shows that a d of value 3 mm presents most impedance matching and most importantly shows no accompanying frequencies as we decrease the separation distance it results in a neighbouring frequency for the centre frequency and , hereby, there are two frequencies of operation in this case.

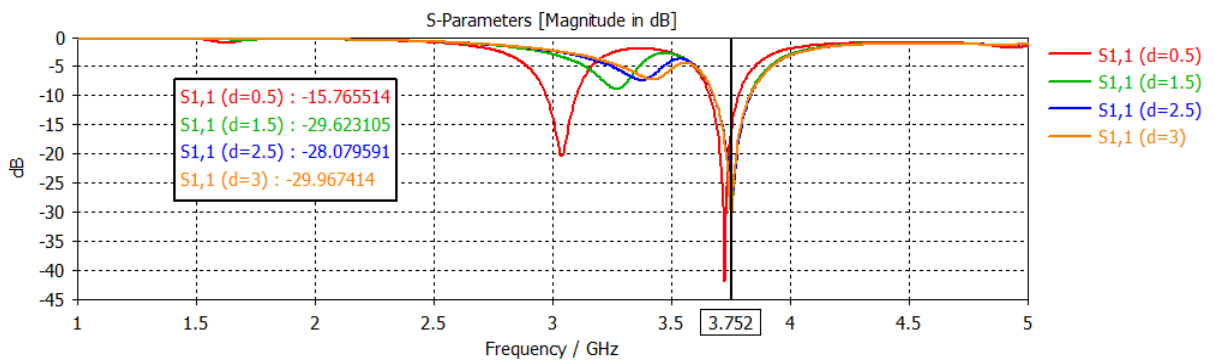


Figure 34. Parametric sweep on separation distance between patches

- Materials selection

Following the standards and specifications set at the project initiation, the materials we have used in our design are mentioned in table 7.

Component	Material
Patches	Copper (annealed)
Ground	Copper (annealed)
Substrates	FR-4 (lossy) (Epsilon = 4.3)

Table 7. Materials we have used in our design

The use of FR-4 material for the substrate is based on a design requirement as we wanted a material of epsilon close to 4 besides its abundance at the targeted fabrication facility.

In spite of the frequency shift occurring with this design, we believe that this can be useful and an advantage for this design, as the user of our product now has four possible channels to switch instead of only two. This feature may be perfectly deployed in military applications where communication is to be most secured and anti-jamming.

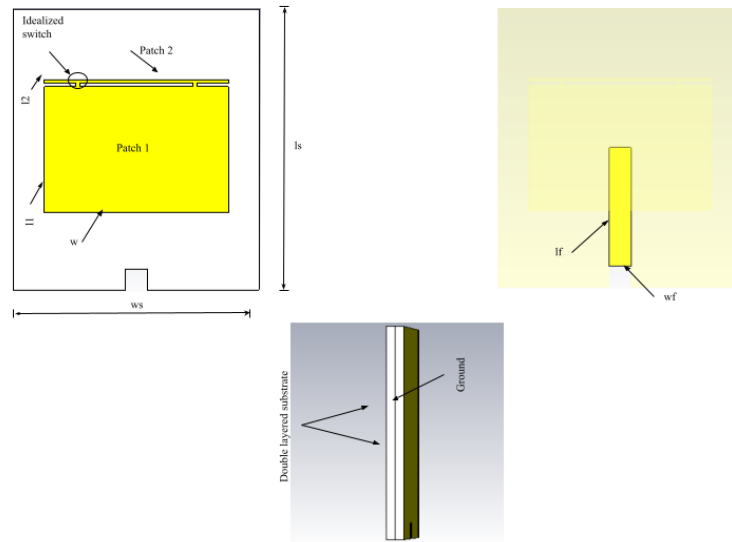


Figure 35. Second design structure with idealized switches connected

- Second design

In this design, we worked to prove our assumption about the first antenna which says that ‘smaller the ratio between the lengths of the two patches, more unexpected results frequency shifts occur in the case of connection between the two patches’. Same design procedure and material selection criteria were adopted in this design as the first one. However, we designed this design to operate on two neighbouring frequencies, 3.5 GHz - 3.3 GHz, unlike the first design as mentioned above. Figure 35 shows the design schematic from different views in case of connected patches. Moreover, table 8 shows the patches parameter values before optimization.

Parameter	Value (mm)
Substrate width (w_s)	35
Substrate length (l_s)	40
Patch1 length (l_1)	18
Patch 1 width (w)	26.2
Patch 2 length (l_2)	0.5
Patch 2 width (w)	26.5
Feed line length (l_f)	17
Fed line width (w_f)	2.8
Separation (d)	0.5

Table 8. Patches parameter values before optimization

It is worth mentioning here that a smaller separation distance is likely perfect and no need to increase it, as the second patch is much relatively small in dimensions compared to the second patch of the first design.

In the optimization process, it has been found that the miniaturization, to a threshold value, of the feed line width (wf) improves the impedance matching of the antenna.

Figure 36 shows different S11 parameters for different values of feed line widths in case of connected patches with idealized switches.

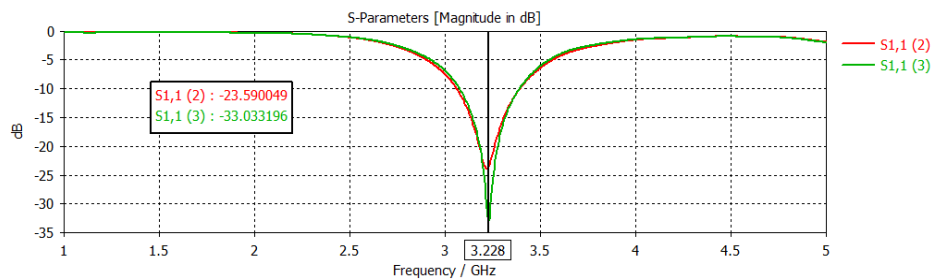


Figure 36. Different S11 parameters for different values of feed line widths in case of connected patches with idealized switches

4.2.2 RF MEMS Switches

- **Optimization**

A lot of parameters affect the RF performance, namely insertion loss and isolation, resulting in a system of interchanged variables, in need of constant optimization. In this section, we will show these changes using the HFSS simulator.

- **Transmission Line**

There are two types of transmission lines that are commonly used in RF MEMS switches, Microstrip line and Coplanar Waveguide (CPW). In the microstrip line, a conductor is separated from a ground plane by a dielectric layer, the substrate.

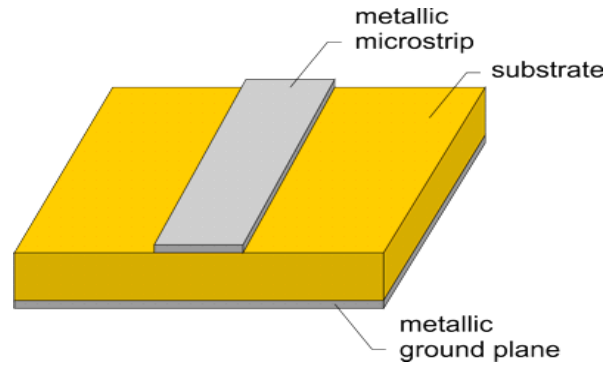


Figure 37. Typical Microstrip transmission line

Here, we show how varying the dimensions of a transmission line can substantially change the RF performance of the wave traveling in the line.

As shown in figures 38 and 39, increasing the width or the length of the line results in significant increase in the insertion loss; it also gives a worse isolation.

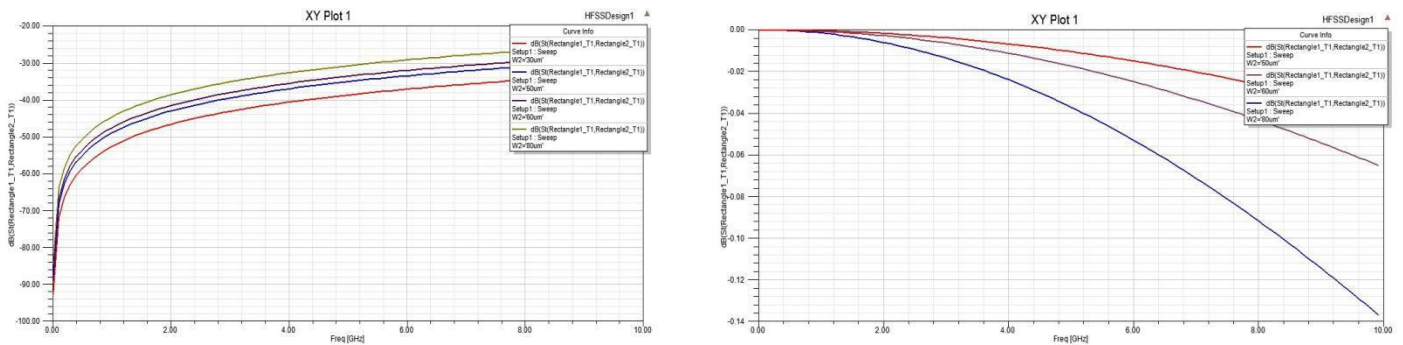


Figure 38. Isolation and Insertion loss at different widths of the transmission line

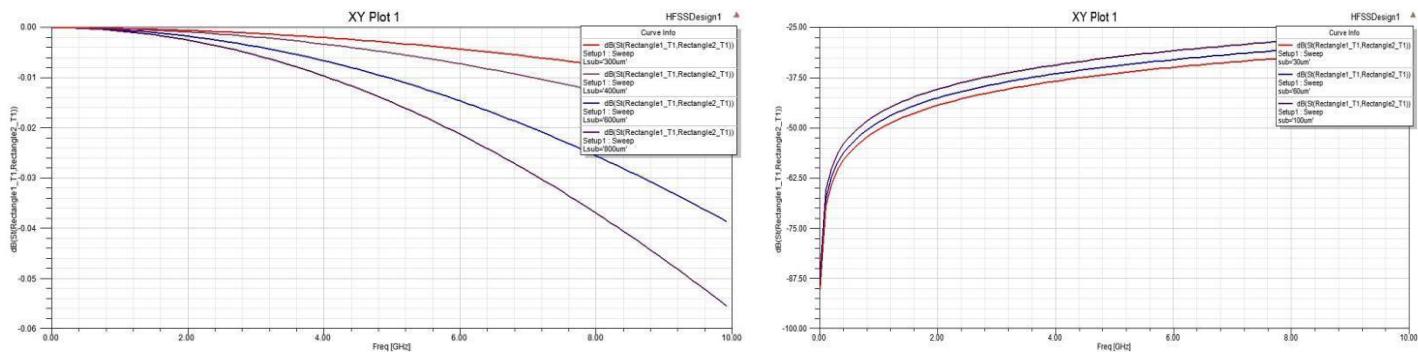


Figure 39. Insertion loss at different lengths of the transmission line, Isolation at different Substrate thickness

In the microstrip line, because of the ground plane, the thickness of the substrate greatly affects the RF performance.

For the CPW transmission line, a single conducting track is printed onto a dielectric substrate, together with a pair of return conductors, one to either side of the track.

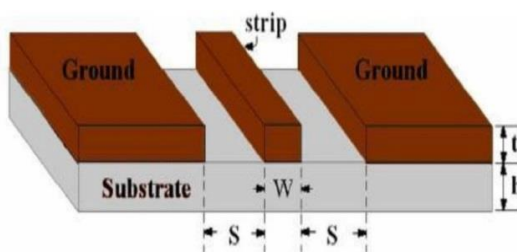


Figure 40. Typical CPW transmission line

A crucial factor in CPW is the gap between the signal line and the ground on each side (S). As shown in figures 41, and 42, since it changes the impedance of the line, by

varying the gap we can control the resonance frequency, hence the isolation, of the switch. However, a large gap increases the insertion loss.

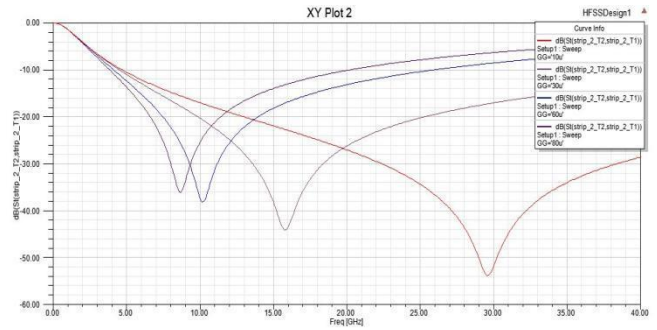
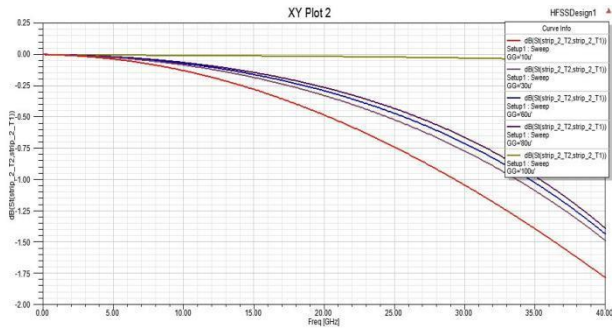


Figure 41. Insertion loss and Isolation at different CPW gap

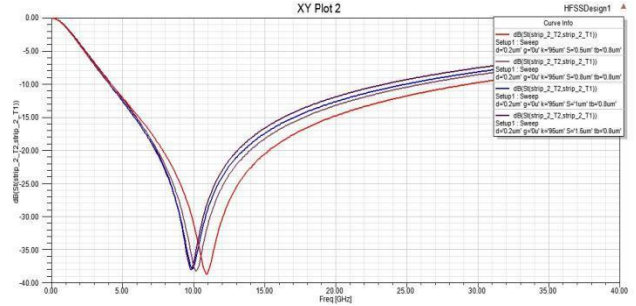
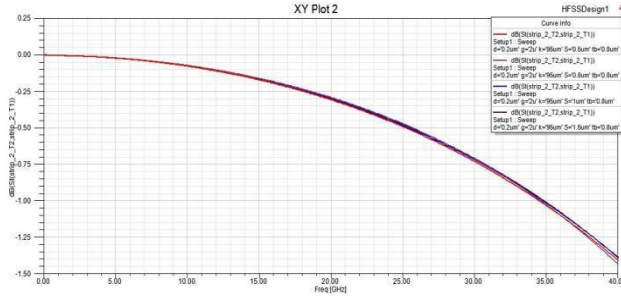


Figure 42. Insertion loss and isolation at different thicknesses of the transmission line

As shown in 43, changing the thickness of the line has negligible effect on the RF performance. The substrate thickness has almost no effect on the RF performance (fig).

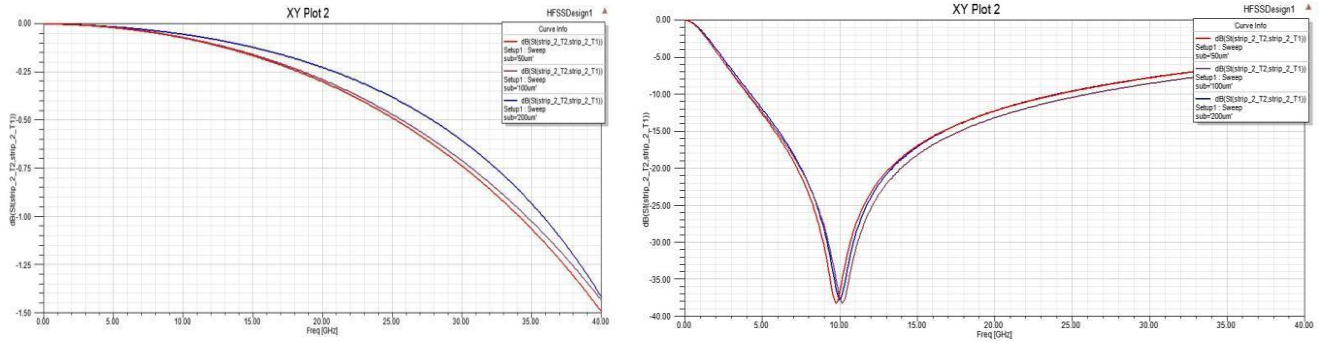


Figure 43. Insertion loss and Isolation at different Substrate thickness

- **Other Parameters**

Several other parameters play a significant role in the RF performance of the RF MEMS switch, such as the dielectric and switch dimensions. In a capacitive switch, the dielectric thickness has a huge effect on the isolation of the switch as shown in figure 44.

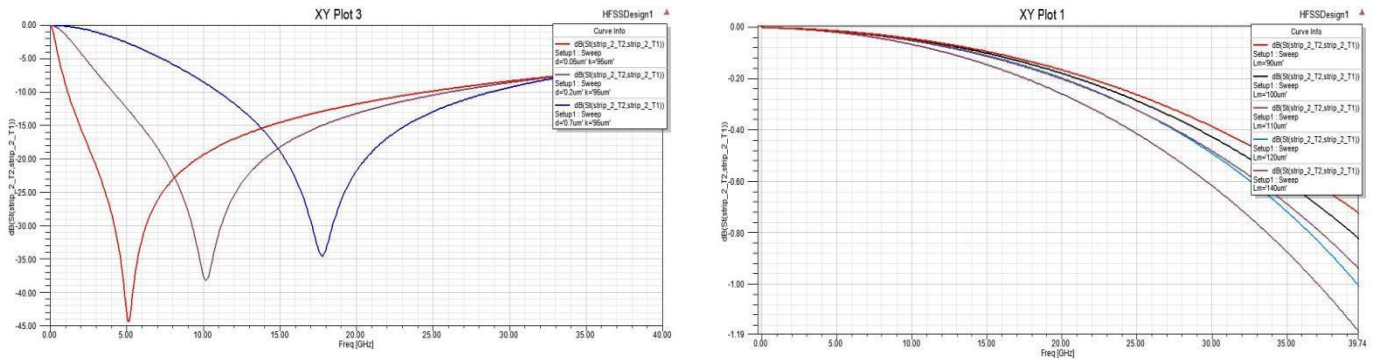


Figure 44. Isolation and Insertion loss at different Dielectric thicknesses for a capacitive switch

As shown in figure 45, by optimizing the dimensions of the bridge, much control on the isolation can be achieved, with minimal change in the insertion loss.

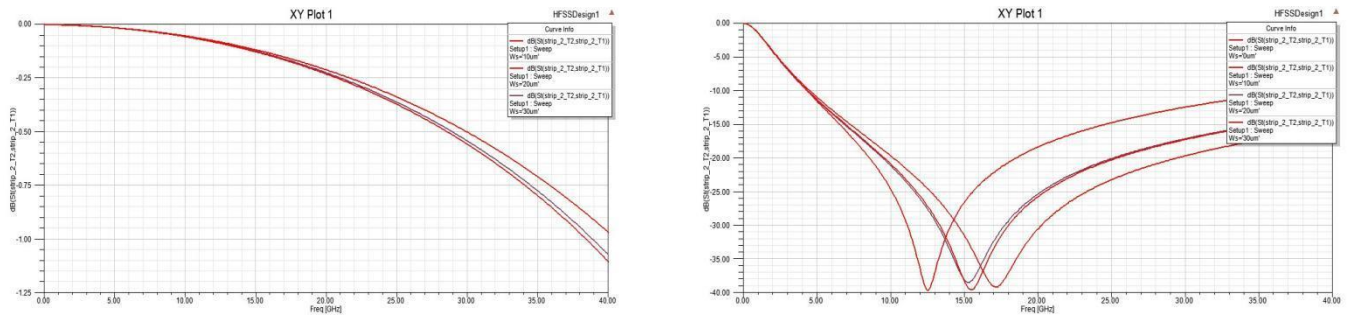


Figure 45. Insertion loss and Isolation at different membrane widths for a capacitive switch

4.2.3 Control:

This part is supposed to be made after both antenna and the MEMS switch fabrication. However, the fabrication is still in progress, so this part is mentioned in the project description only and has not reached execution yet. The control of the antenna and switches is pretty simple, and it will be as follows. The antenna patches will be connected together via the MEMS switches. Each switch has a terminal to control its switching, so this terminal is connected to a microcontroller to control it. When the microcontroller sends high signals to the switch terminal, the MEMS is switched ON, and then switched OFF when the control signal is set low by the microcontroller. The microcontroller will have multiple configurations for the switch states. For example, if two switches are used, then the microcontroller will have four configurations; the two switches are ON, first switch is ON and the second is OFF, first is OFF and the second is ON, and finally both are OFF. The switching between different configurations can be controlled by us through using a push button. The push button is connected to the microcontroller as well, and when the push button is pressed, the microcontroller changes the configuration of the switches. This is mainly the control circuit, for more clarification, a model for the system is shown in the following figure.

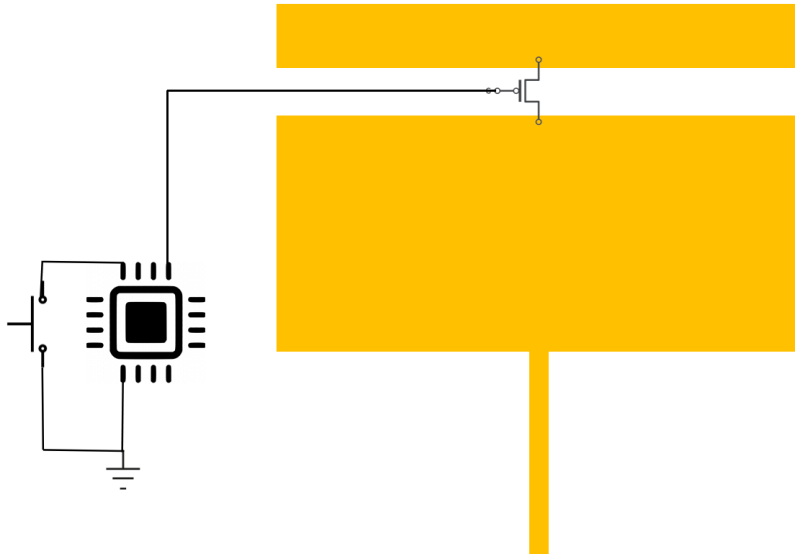


Figure 46. Model for the switching control circuit

As shown in figure 46, the two patches are connected together via a switch. The switch control terminal is connected to the microcontroller (the big black square), and the push button (at left of the microcontroller) is connected separately to the microcontroller as well. In this figure, only one switch is used, so two configurations only exist. When the button is pushed once, the microcontroller turns the switch ON, and when the button is pushed again, the microcontroller turns the switch OFF, and so on.

4.3 Testing and Evaluation

This section contains the results of each sub system testing trials besides the results after the integration. First, we will begin by presenting the Reconfigurable Antenna simulation results, then the simulation results of RF MEMS switches are presented.

4.3.1 Reconfigurable Antenna Testing and Evaluation

The demonstration of the testing results will proceed on hierarchical bases. First, the RA is tested with idealized switching and idealized insulation, then a generic RLC Model for RF MEMS is implemented to replace the idealized switches, then three different RLC models of our own design are implemented in replacement of the generic RLC model respectively. It is worth noting that all following results are renormalized to 50 ohm source.

A. First design

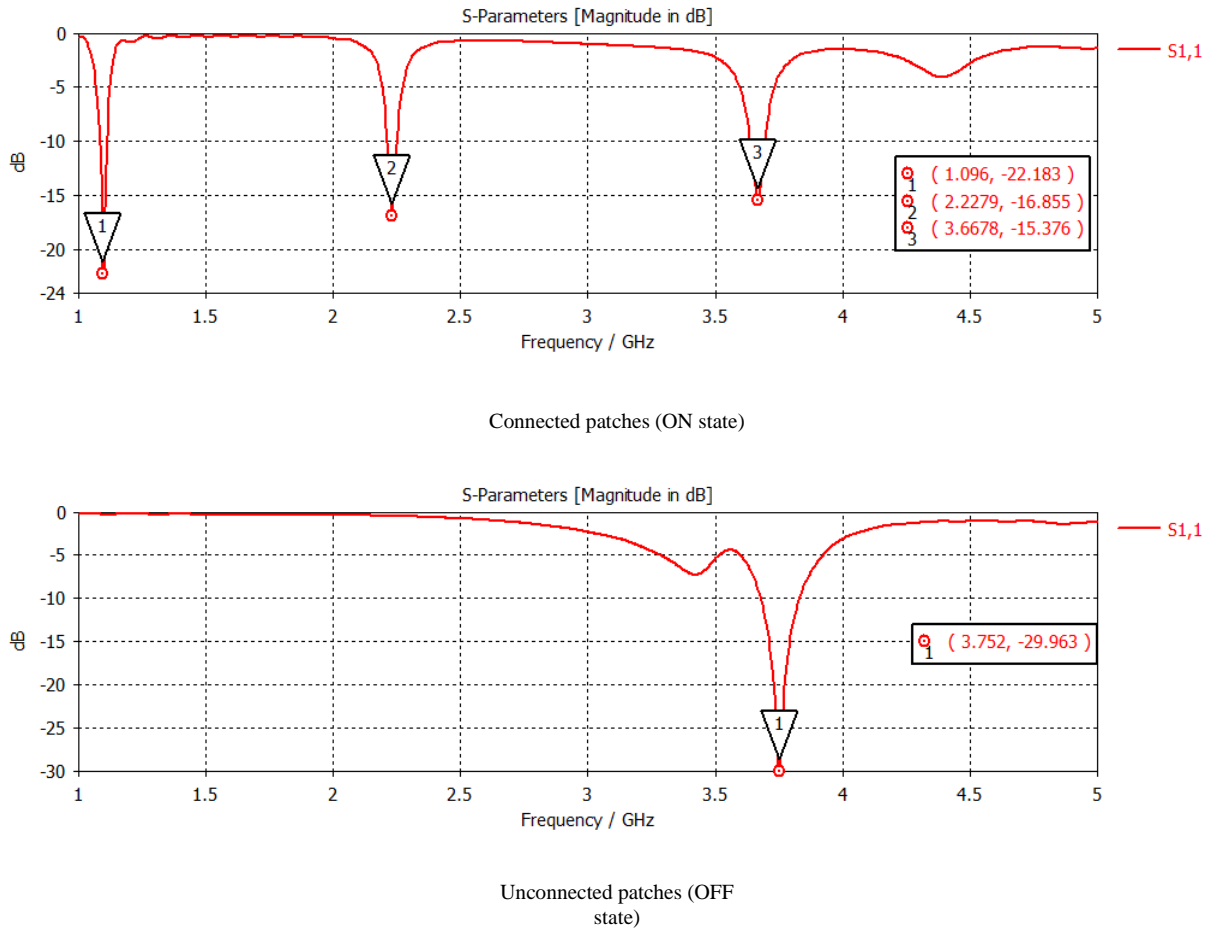


Figure 47. S₁₁ values in case of idealized switch

As a common standard between RF antenna designers, S₁₁ values greater than -20 dB are regarded as being not perfectly matched and, hereby, they become not reliable. Moreover, there is an undesirable expected shift in these values after the fabrication of the antenna. Therefore, the 2.2279 GHz and 3.6678 GHz could be neglected.

State	Bandwidth (MHz)
ON	30
OFF	160

Table 9. shows the bandwidth based on the switches' state.

Figure 48 shows the VSWR values for both states ON/OFF of the idealized switches.

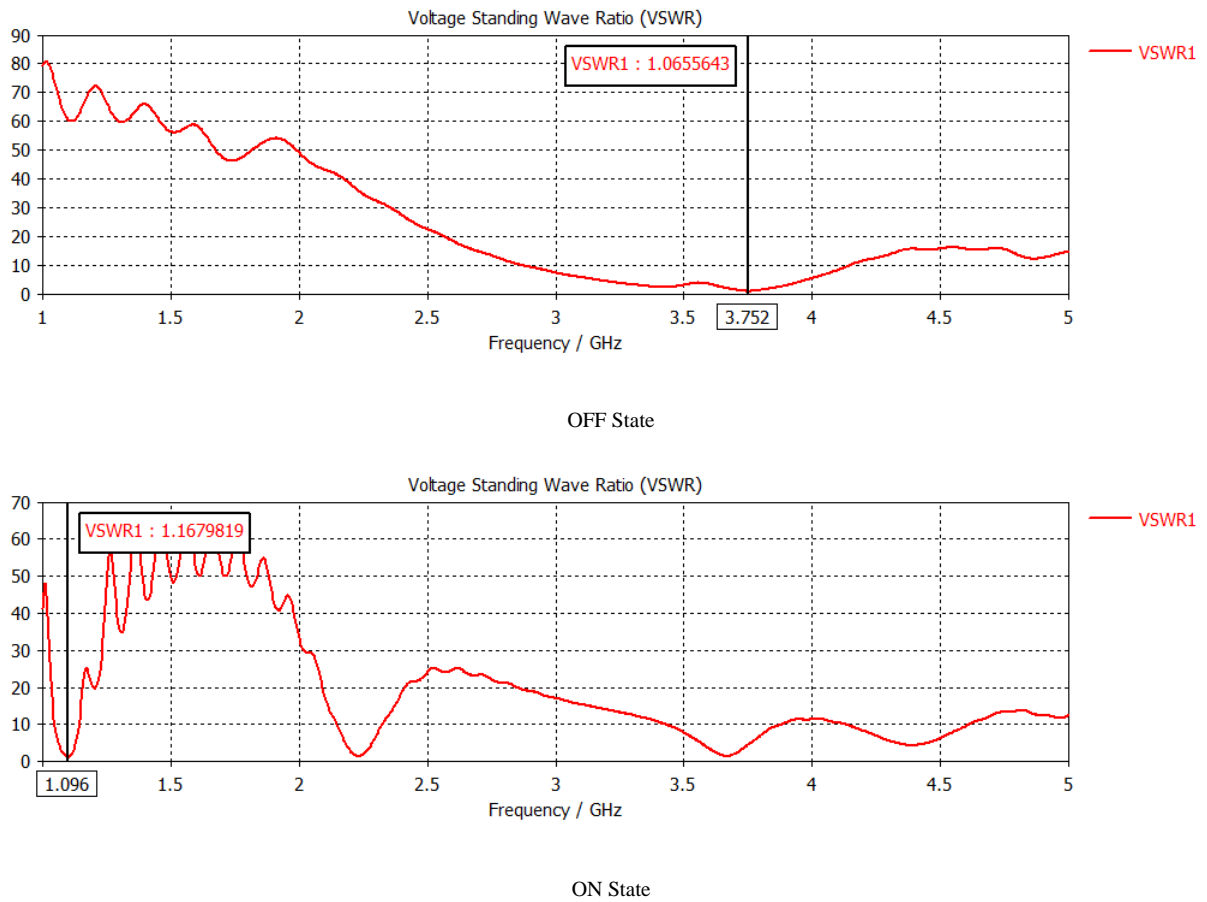


Figure 48.VSWR values for both states ON/OFF of the idealized switches

Now the results from using a switch modeled with a generic RLC model, in which when the switch is ON, the values for the RLC circuit are, $R = 0.9\Omega$, $L = 55\text{nH}$, $C = 0$. When the switch is OFF, the values are, $R = 0$, $L = 0$, $C = 2.2\text{ pF}$. These values are assumed to be constant with changing the frequency of the antenna. This assumption is made at first for simply testing the antenna. The results are shown in the following figures.

In the first test, one switch is used, and placed at the center between the two patches as in the following figure 49.

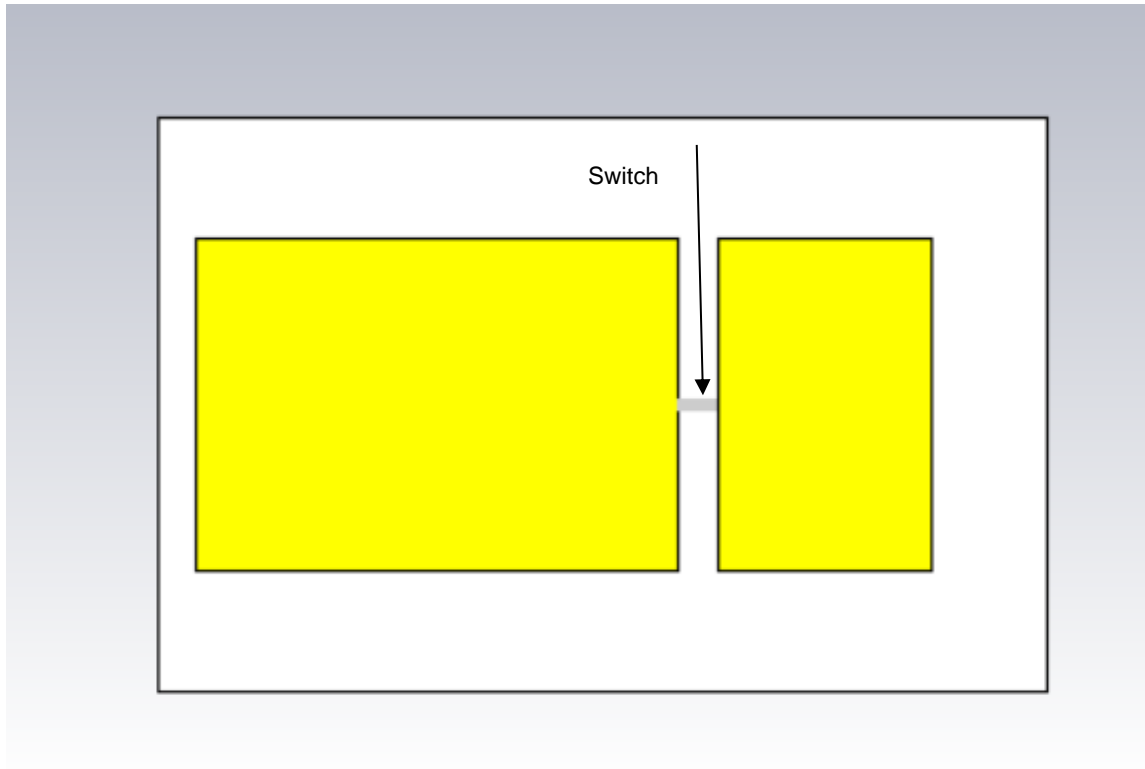


Figure 49: The antenna with the switch placed at middle

The S_{11} value when the switch is ON are shown as follows in figures 50, and 51.

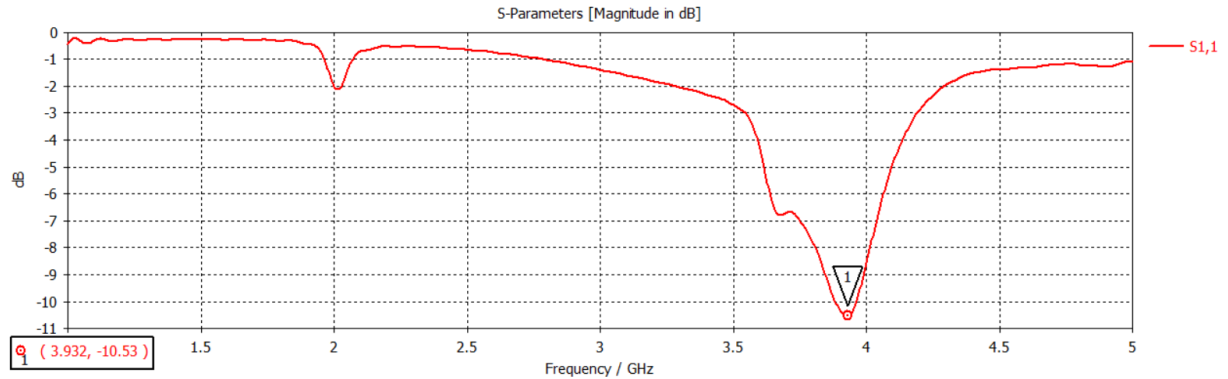


Figure 50. The S₁₁ parameter for the switch ON

As shown in figure 50, the value of the S₁₁ is not good, showing that the impedance matching is very low. Hence, the performance of this configuration is not acceptable.

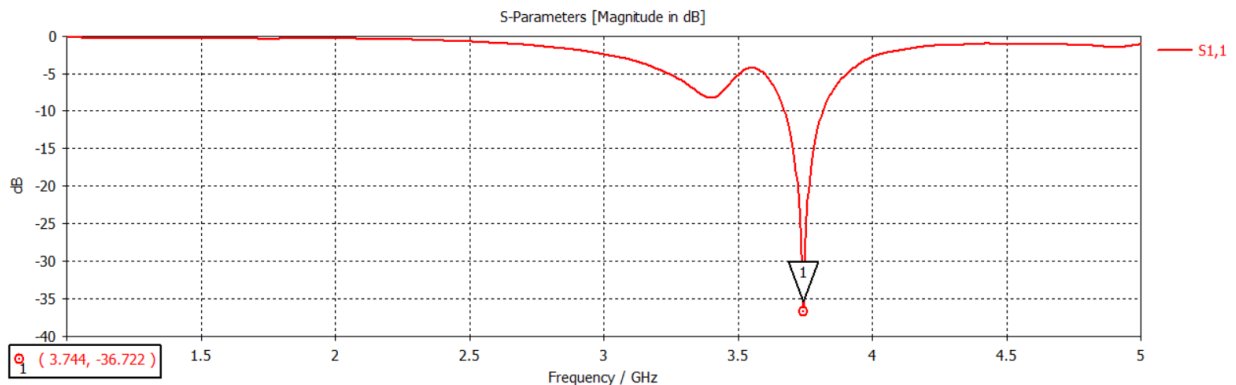


Figure 51. The S₁₁ parameter for the switch OFF

Although the results in the ON state are unacceptable, the OFF state gave acceptable results. This is because in the case of the OFF state the two patches should be separated from each other and that's it. The first patch is designed to work at a certain frequency with acceptable impedance matching, so the first patch alone will not give good results, this means that the design itself needs to be modified and not the switches. However, in the OFF state the values of the switches affect the result because the switch is not perfect of course, but it should not affect the results strongly. On the other hand, the ON state is completely different, and the switch design and the

place where it is put affects the resulting frequency strongly. This can be described with a container resembling the patch, and a water tape resembling the switch. The place of the water tape relative to the container will affect the direction of water motion in the container when the tape is opened, but the tape is closed it will not affect it. Similarly, the place of the switch relative to the patch affects the current distribution in the patch hence changing the resulting frequency. That is why the OFF state is more likely to give better results than the ON state.

The next configuration is using two switches with the same RLC values as in the previous case.

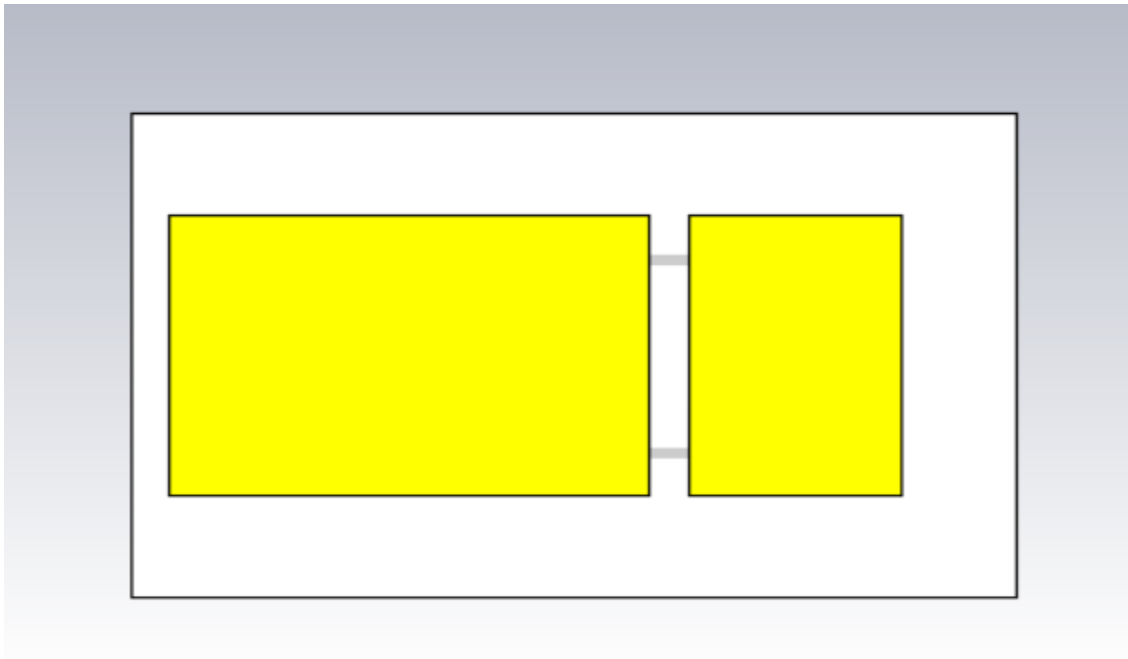


Figure 52. The shape of the configuration with two switches

The S_{11} for this configuration is shown next in figure 53, and 54.

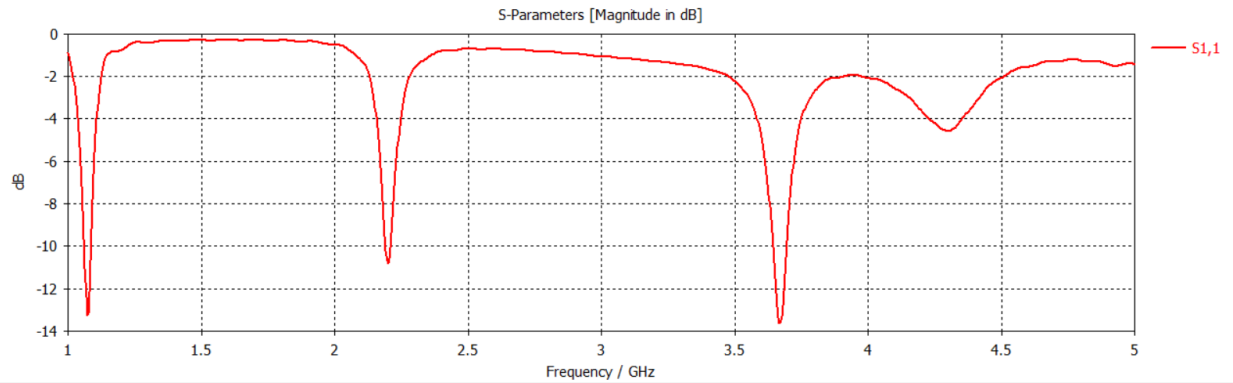


Figure 53. S11 parameter value for using two switch configuration in the ON state

Figure 53 shows better results than the previous case of using only one switch. However, the impedance matching is still unacceptable.

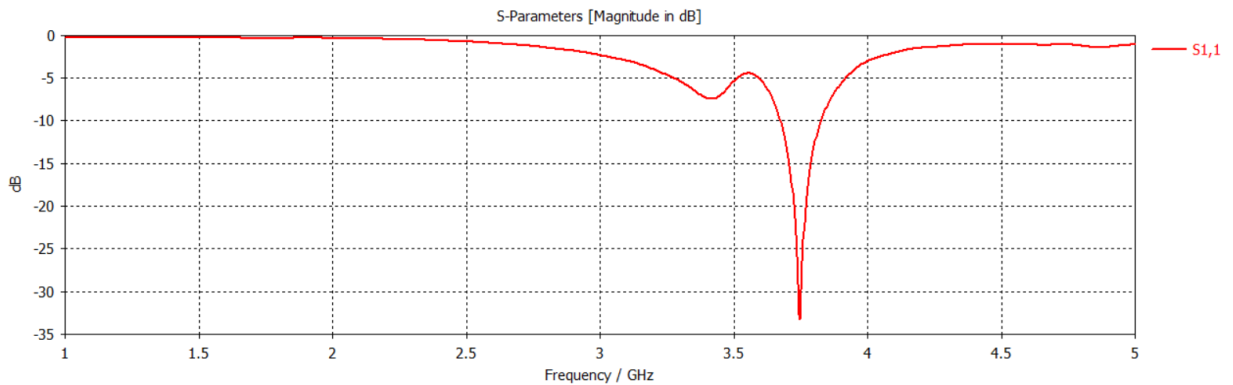


Figure 54. S11 parameter value for using two switch configuration in the OFF state

As mentioned in the OFF state for the previous configuration, the OFF state in this configuration is acceptable as well.

The next configuration is using three switches with the same RLC values as in the previous case. We are increasing the number of switches to see how this affects the resulting frequencies and the S_{11} value.

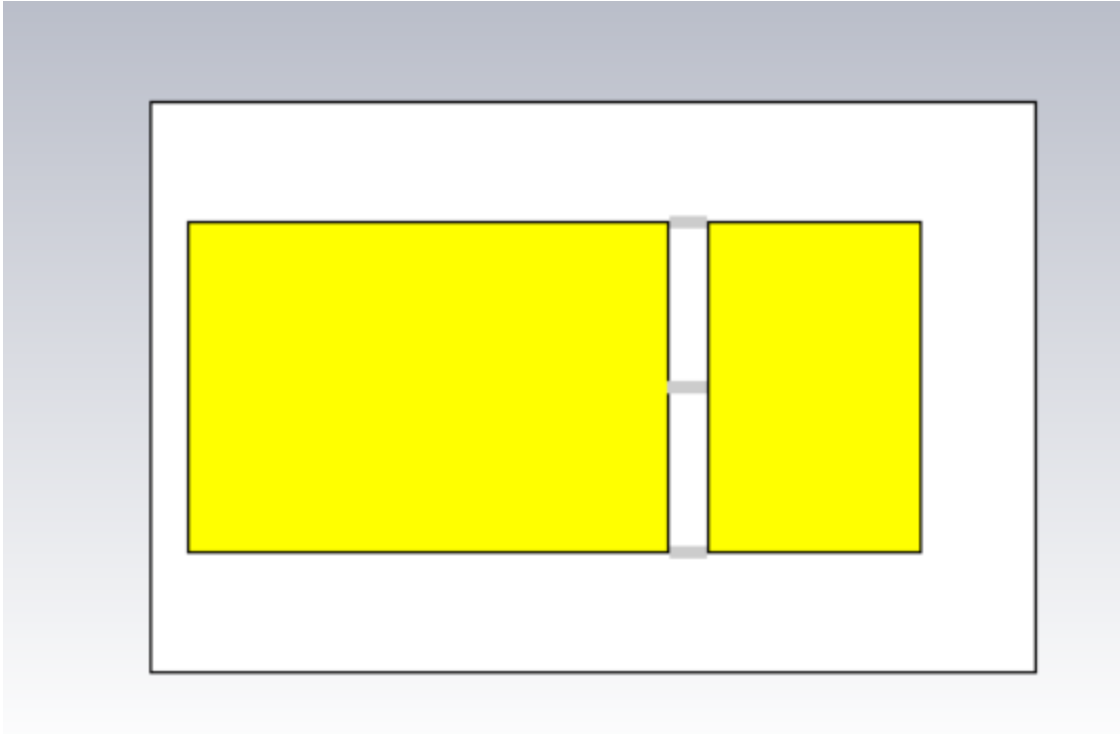


Figure 55. The antenna with three switches

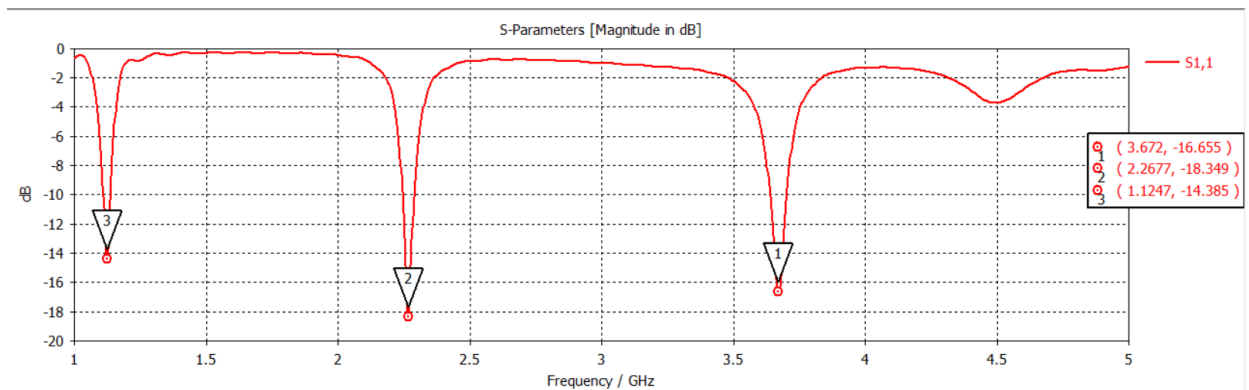


Figure 56. S₁₁ parameter value for using three switch configuration in the ON state

As shown in figure 56, with adding more switches and setting them all ON, the results and impedance matching is better. However, this increases the cost on the device, so it is better if less switches are used to get good results.

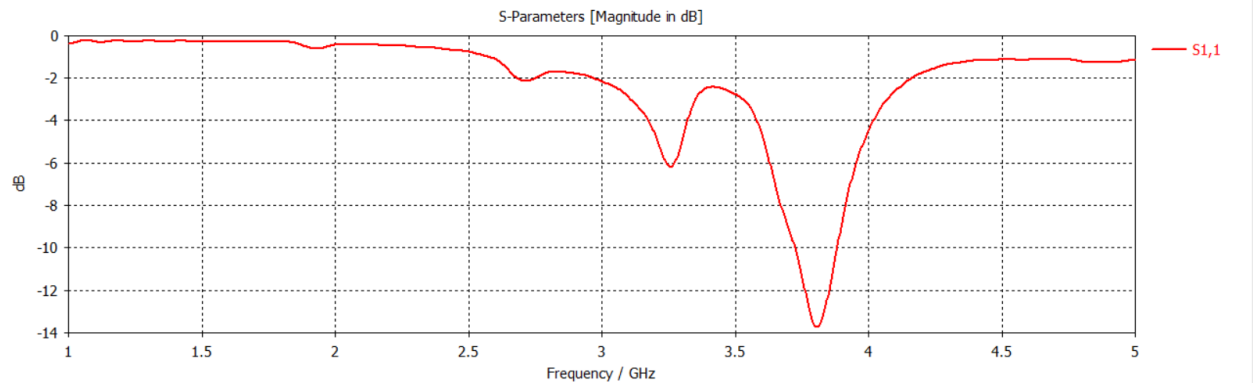


Figure 57. S11 parameter value for using three switch configuration with 2 OFF and 1 ON state

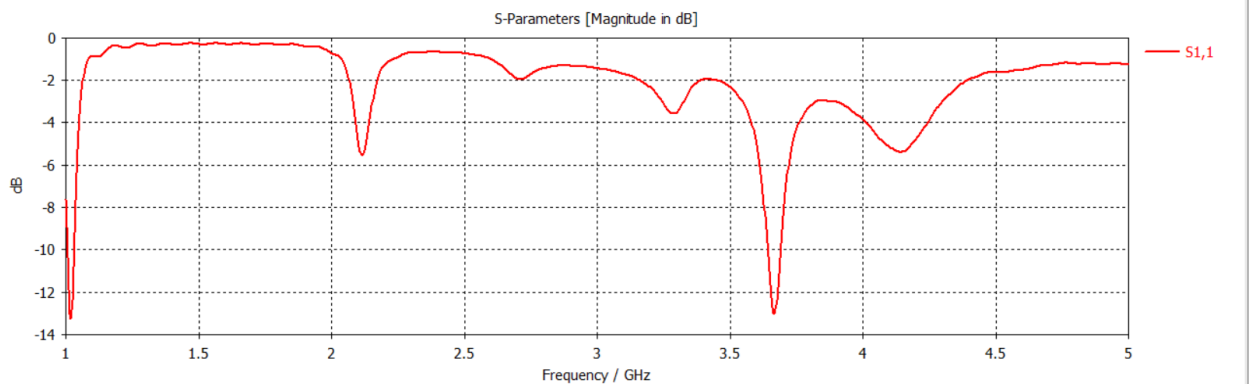


Figure 58. S11 parameter value for using three switch configuration with 2 and 1 ON state

The previous two figures 57, and 58, show other possible configurations for using three switches. One configuration has two switches set ON and the third is set OFF, and the other configuration has two switches set OFF and the third is set ON. The resulting S_{11} shows that the impedance matching is not good in these configurations and hence these states are not useful for this design. This makes the design use more switches without taking advantage of the possible number of

configurations possible, thus increasing the cost with no added value. Hence, two switches are used to make a compromise between good performance and cost of the device.

Now using a more accurate RLC model that has different values according to the targeted frequency, and is given from the MEMS switches simulations. For working at 3 GHz frequency, the values are, $R = 0.328 \Omega$, $L = 0.583 \text{ nH}$ in ON state, and $C = 0.0983 \text{ pF}$ in OFF state. Only two switches were used for these values.

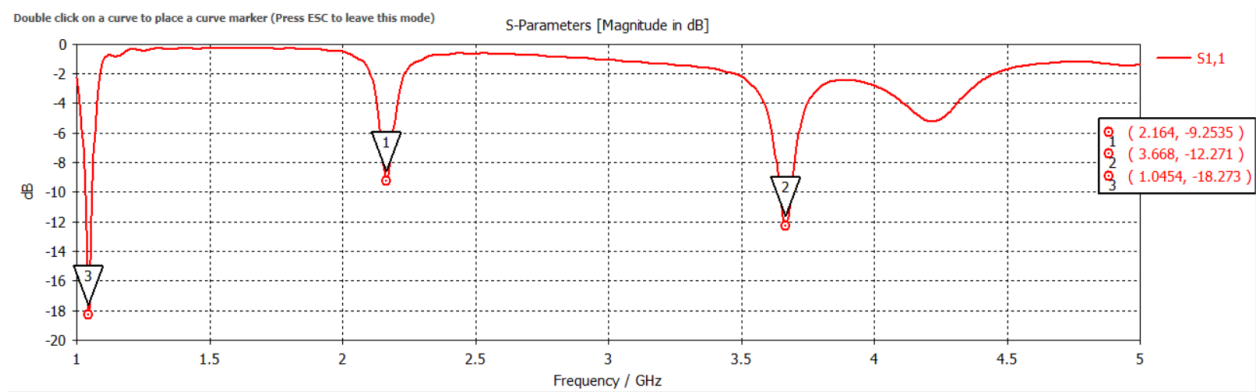


Figure 59. S11 parameter value for using two switches in the ON state

Here in figure 59, the S_{11} is better than using two switches with the previous RLC values. At 1.045 GHz the S_{11} is -18.3 dB, which is not the best value, but close to the acceptable range. While the other two frequencies are low in matching so they can be ignored. So now the frequency resulting in the ON state is 1.045 GHz.

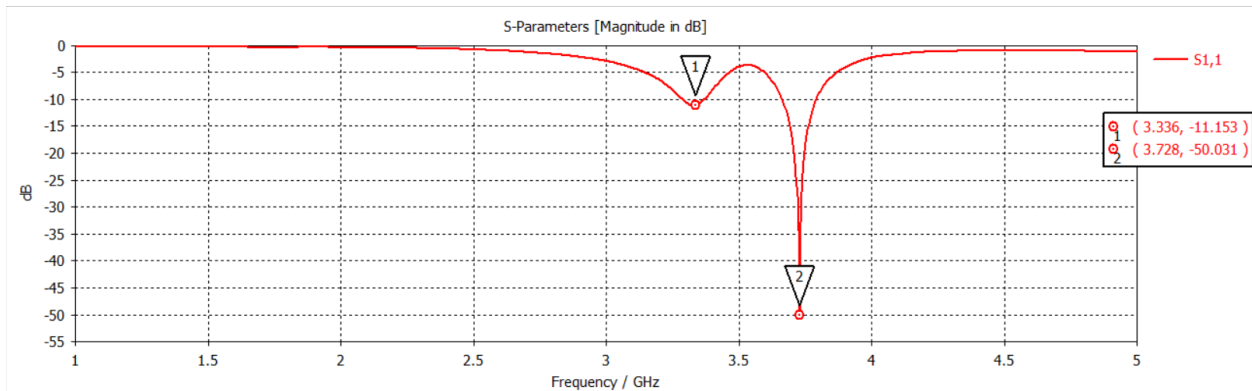


Figure 60. S11 parameter value for using two switches in the OFF state

Now the OFF state has good matching as expected, and the frequency of the antenna in this OFF state is 3.728 GHz.

So, by using these RLC values, the antenna can switch from 3.728 GHz in OFF state to 1.045 GHz in ON state.

Now using a more accurate RLC model that has different values according to the targeted frequency, and is given from the control MEMS switches simulations presented in the MEMS section. For working at 3.2 GHz frequency, the values are, $R = 0.332 \Omega$, $L = 0.621 \text{ nH}$ in ON state, and $C = 0.1049 \text{ pF}$ in OFF state. Only two switches were used for these values.

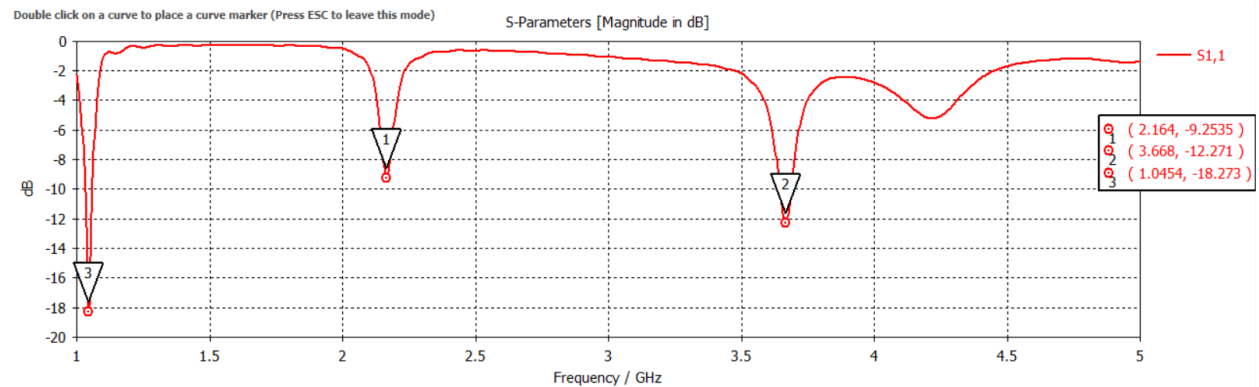


Figure 61. S11 parameter value for using two switches in the ON state

The values are nearly identical to the previous case, so this trial is made to make sure that frequency on which the RLC values are taken will not change the results heavily if the frequencies chosen are close to each other. In this case, the RLC values are taken at 3.2 GHz while in the previous case the values are chosen at 3 GHz.

Using another RLC model given from one meander MEMS switches design simulation presented in the MEMS section. For working at 3 GHz frequency, the values are, $R = 0.568 \Omega$, $L = 0.656$ nH in ON state, and $C = 0.1003$ pF in OFF state. Only two switches were used for these values.

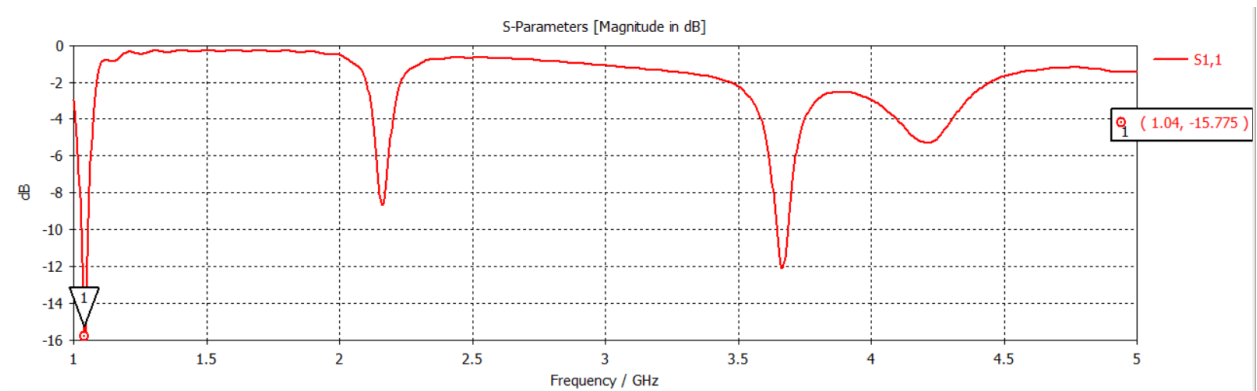


Figure 62. S11 parameter value for using two switches in the ON state

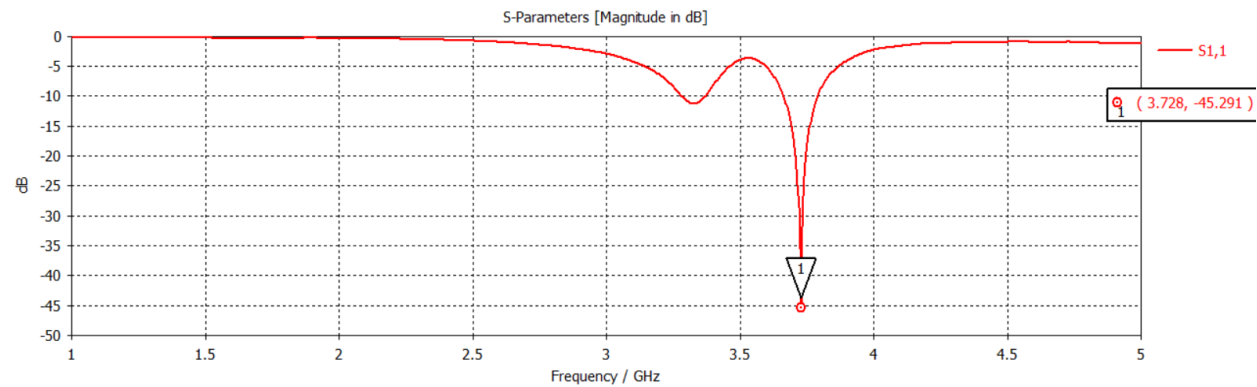


Figure 63. S11 parameter value for using two switches in the OFF state

As seen in figures 62, and 63, the results are similar to the previous cases but with worse S_{11} values in the ON state.

Using another RLC model given from the novel MEMS switches design simulation presented in the MEMS section. For working at 3 GHz frequency, the values are, $R = 0.21 \Omega$, $L = 0.404 \text{ nH}$ in ON state, and $C = 0.0501 \text{ pF}$ in OFF state. Only two switches were used for these values.

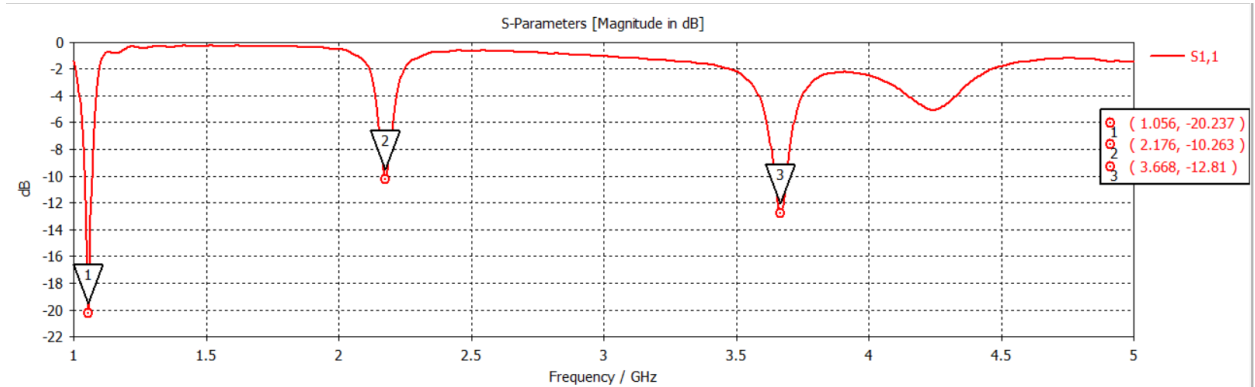


Figure 64. S₁₁ parameter value for using two switches in the ON state

Figure 64 shows that the RLC values used are the best till now in this antenna design. It has a good S₁₁ value at 1.056 GHz which is slightly higher than 20 dB, while the other two frequencies have low impedance matching so they can be ignored.

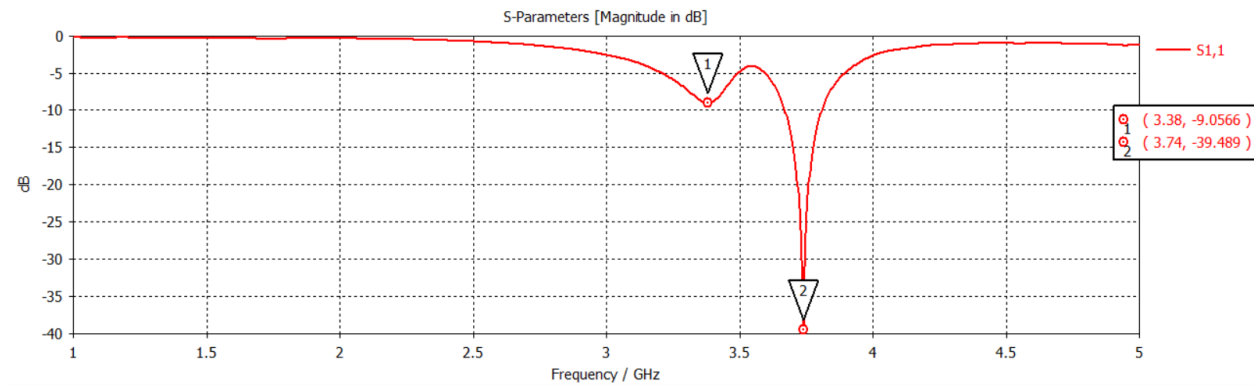


Figure 65. S₁₁ parameter value for using two switches in the OFF state

As previous cases, the OFF state has good results and S₁₁ of nearly 40 dB. Hence, this RLC model makes a good antenna switching from 3.74 GHz at the OFF state to 1.056 GHz at the ON

state. So out of made trials for this antenna, the model used in this case is the best, and the bandwidth values are given in the table 10.

State	Bandwidth (MHz)	Frequency (GHz)
ON	24	1.056
OFF	137	3.74

Table 10. Bandwidth values with using RLC model from the novel MEMS switch design

B. Second design:

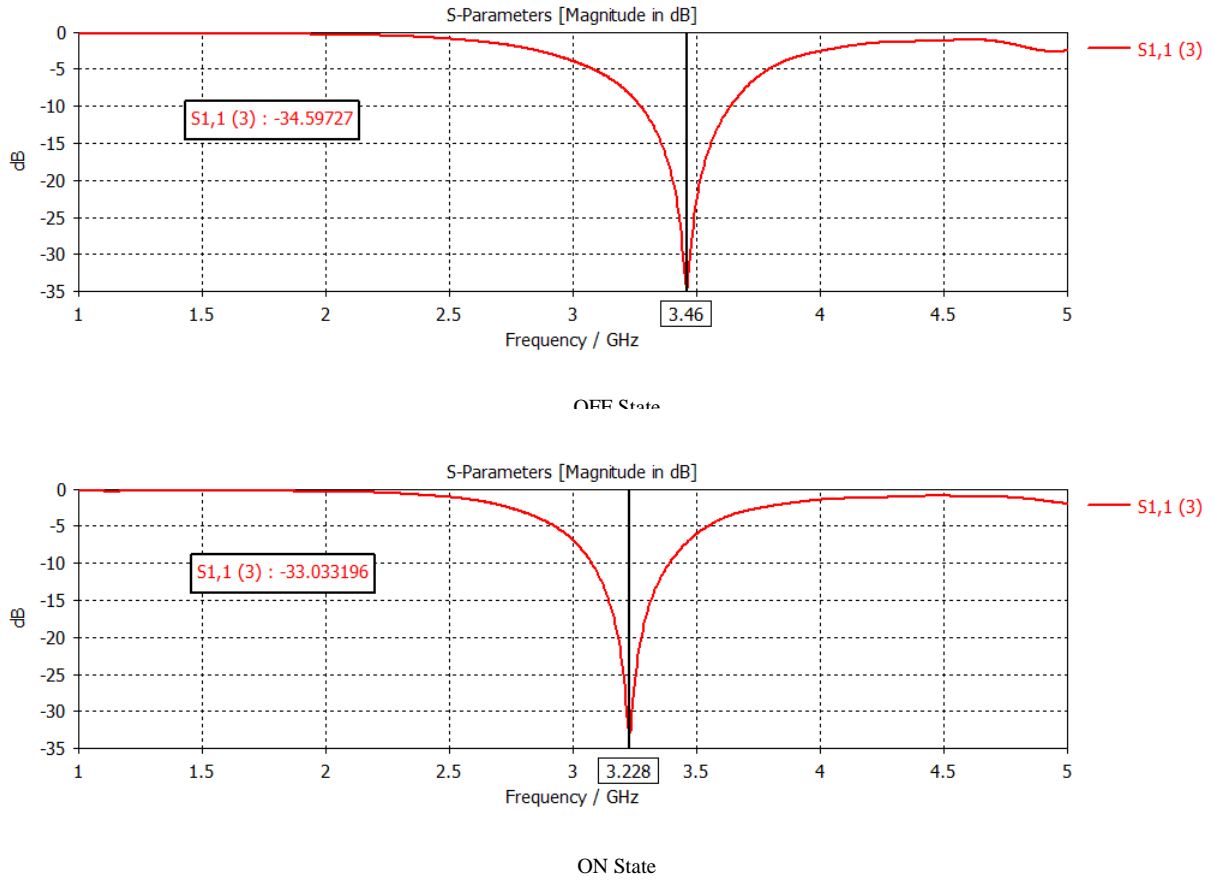


Figure 66. S11 parameter values for the idealized switches' ON/OFF states

State	Bandwidth (MHz)
ON	320
OFF	350

Table 11. The bandwidth based on the switches' state.

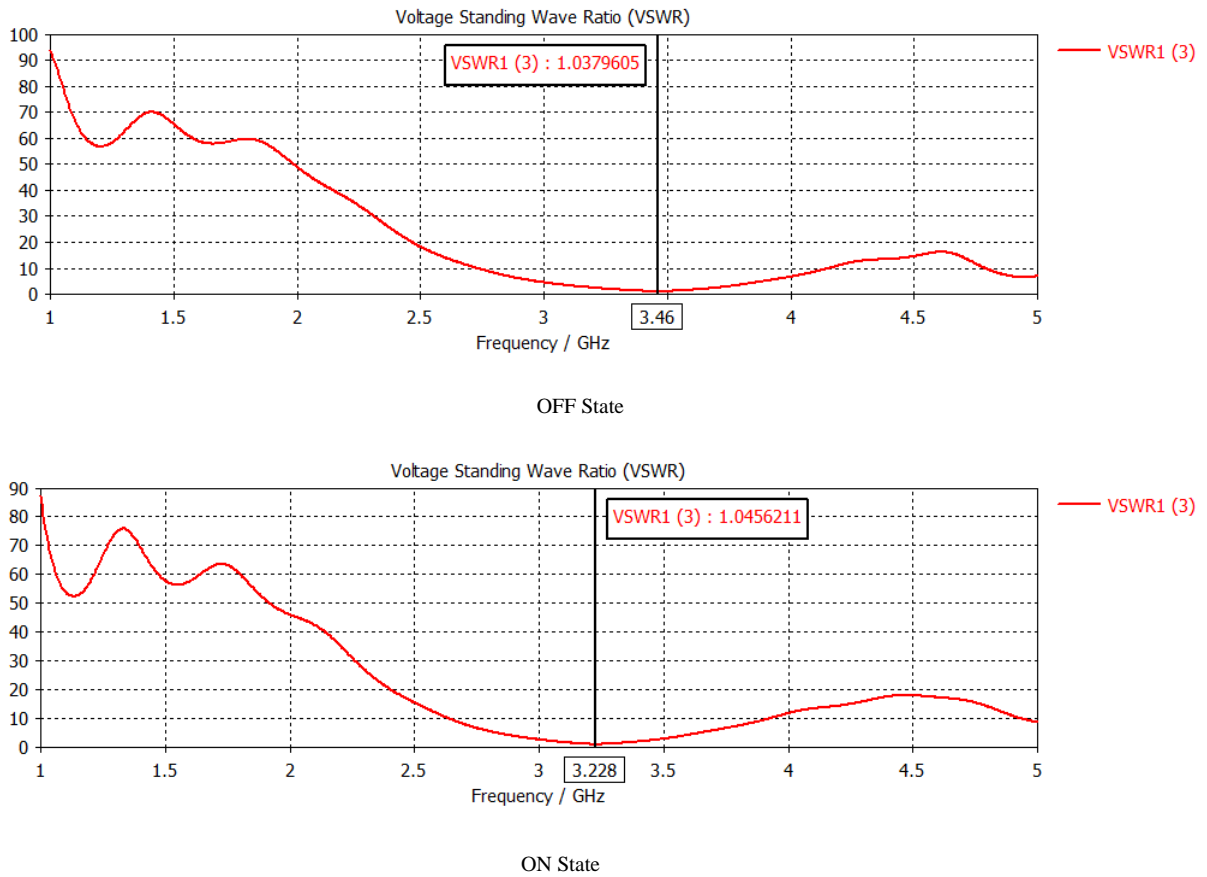


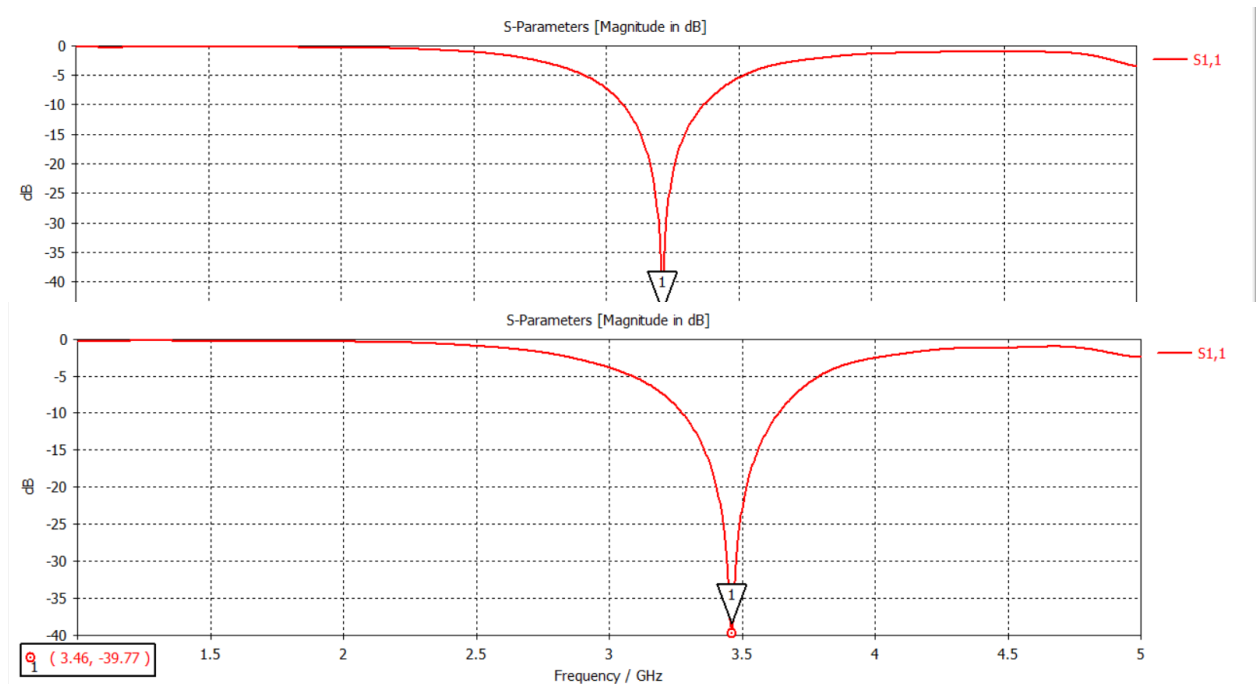
Figure 67. VSWR values for the idealized switches' ON/OFF states

Now using a switch modeled with a generic RLC model, in which when the switch is ON, the values for the RLC circuit are, $R = 0.9 \Omega$, $L = 55 \text{ nH}$, $C = 0$. When the switch is OFF, the values are, $R = 0$, $L = 0$, $C = 2.2 \text{ pF}$. These values are assumed to be constant

with changing the frequency of the antenna. This assumption is made at first for simply testing the antenna. The results are shown in figures 68, and 69.

Figure 68. S11 parameter value for using two switches in the ON state

Figure 69. S11 parameter value for using two switches in the OFF state



This design gives good results in both cases of ON and OFF states. The antenna switches from 3.46 GHz in the OFF state to 3.212 GHz in the ON state, with very good S_{11} value in both cases ($S_{11} < -20$ dB is very good).

Using another RLC model given from one meander MEMS switches design simulation presented in the MEMS section. For working at 3 GHz frequency, the values are, $R =$

0.568 Ω , $L = 0.656$ nH in ON state, and $C = 0.1003$ pF in OFF state. Only two switches were used for these values.

Figure 70 a. S11 parameter value for using two switches in the ON state

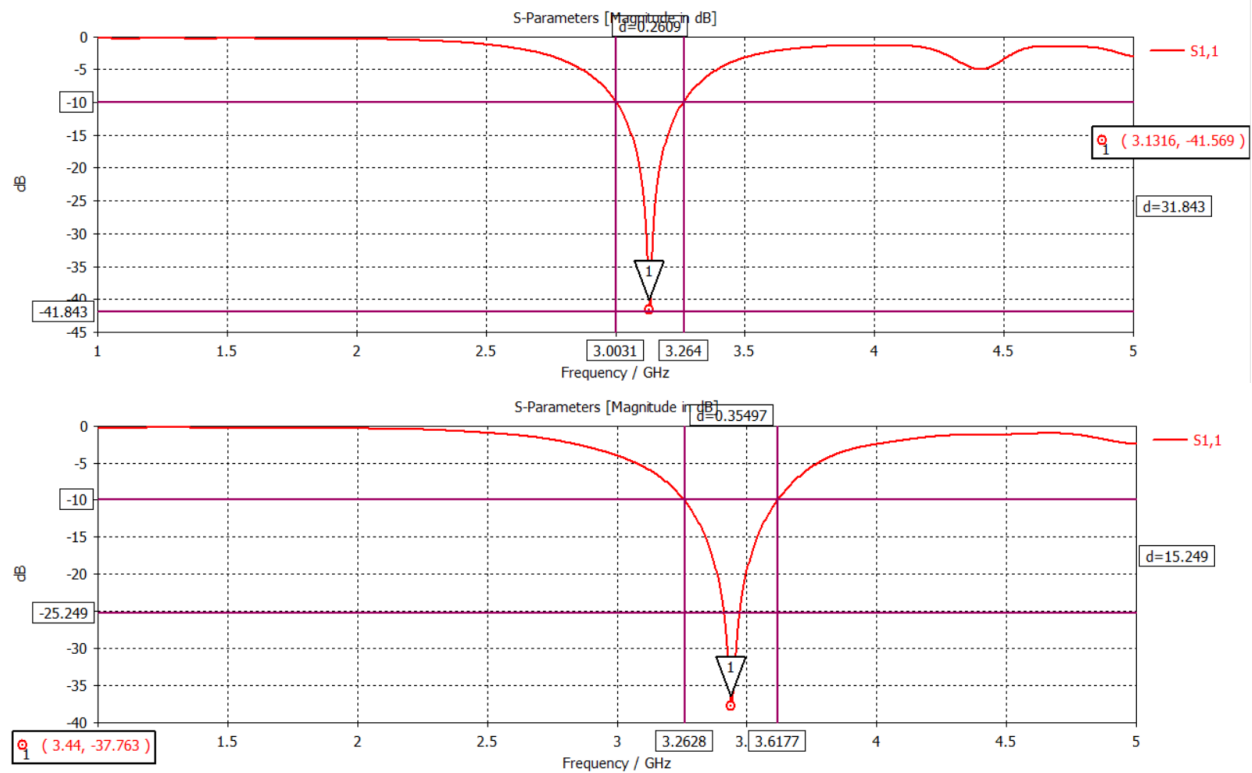


Figure 70 b. S11 parameter value for using two switches in the OFF state

This design gives good results in both cases of ON and OFF states as well. The antenna switches from 3.44 GHz in the OFF state to 3.1316 GHz in the ON state, with very good S_{11} value in both cases. This difference in values from the previous case has an advantage, which is that by changing the switch only, new frequencies are targeted by the antenna. The bandwidth in the ON state is 206 MHz and 355 MHz in the OFF state.

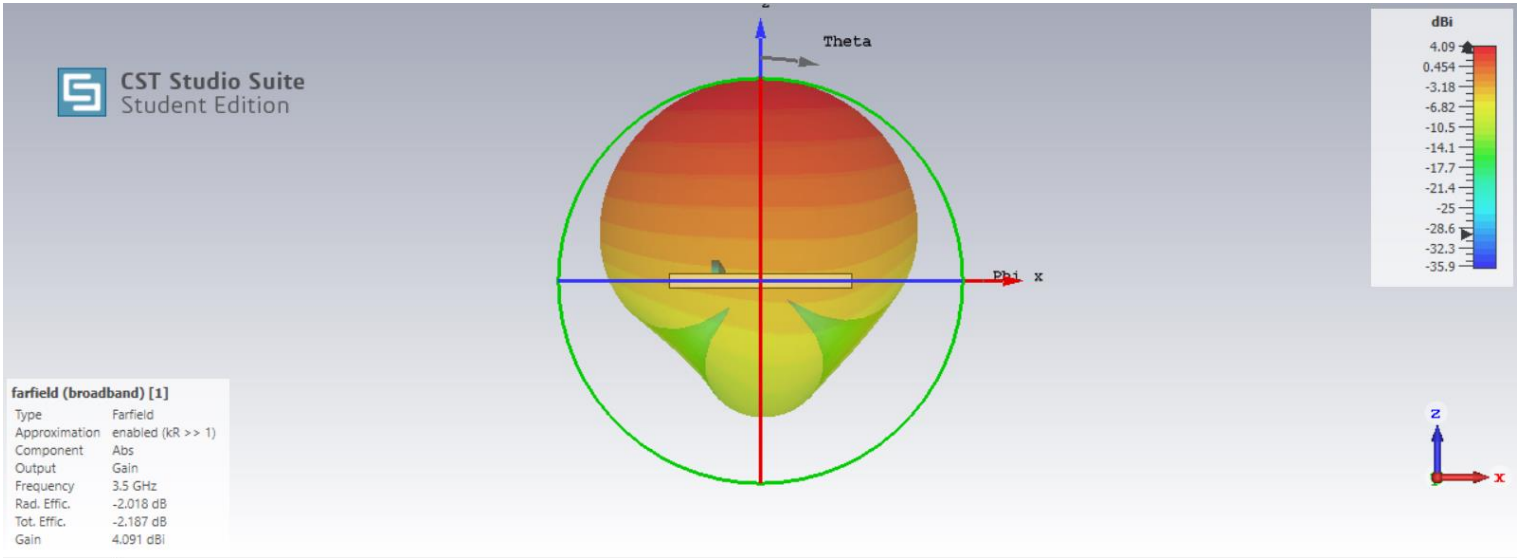


Figure 71 a. Radiation pattern for using two switches in the OFF state

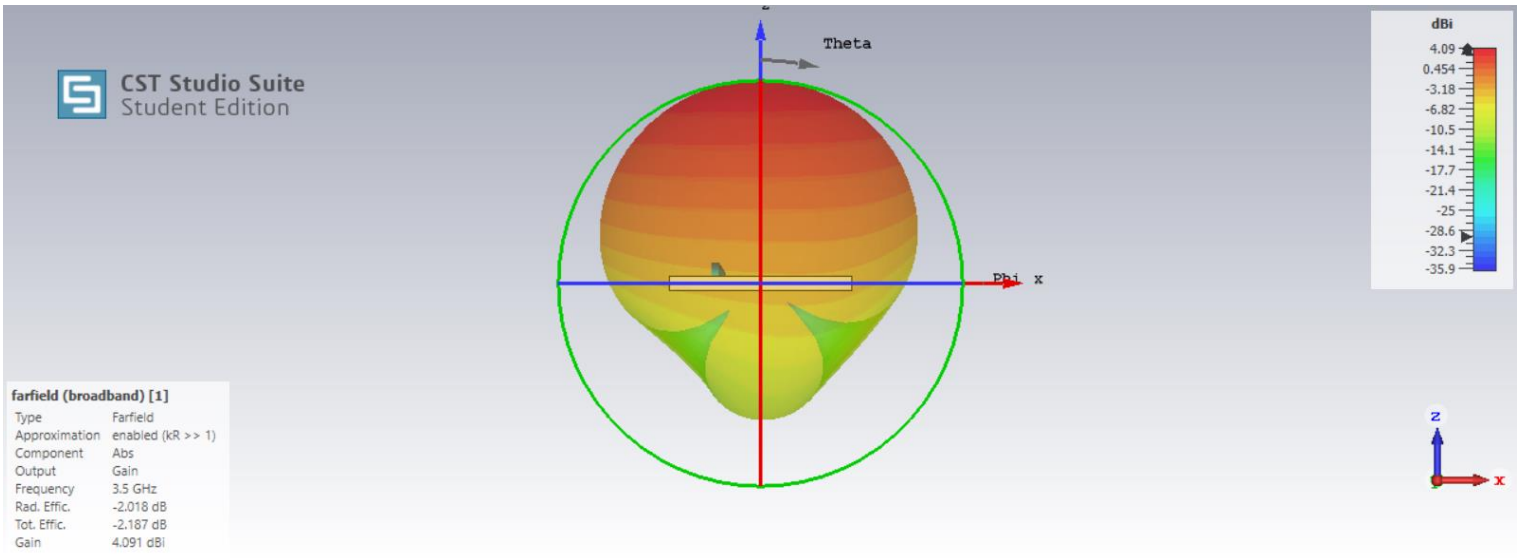


Figure 71 b. Radiation pattern for using two switches in the OFF state

Figures 71 a, and 71 b, show that the state of the switches affect the radiation pattern shape and gain. However, the change is small and acceptable.

Now using RLC model that has different values according to the targeted frequency, and is given from the control MEMS switches simulations presented in the MEMS section. For working at 3.2 GHz frequency, the values are, $R = 0.332 \Omega$, $L = 0.621 \text{ nH}$ in ON state, and $C = 0.1049 \text{ pF}$ in OFF state. Only two switches were used for these values.

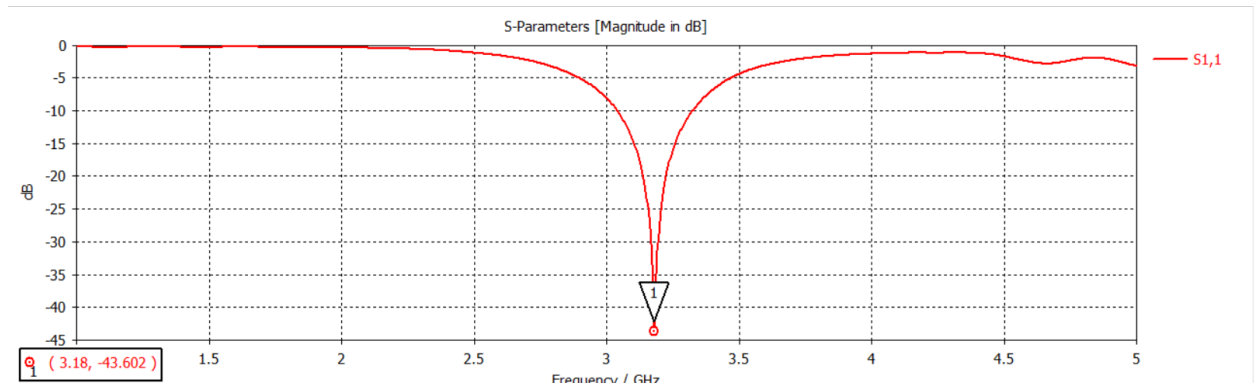


Figure 72. S11 parameter value for using two switches in the ON state

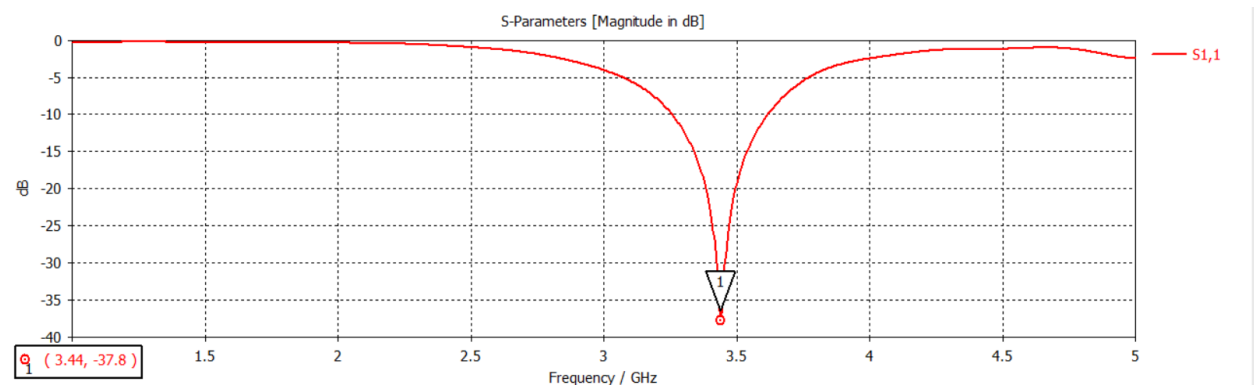


Figure 73. S11 parameter value for using two switches in the OFF state

Again the design gives good results in both cases of ON and OFF states as well. The antenna switches from 3.44 GHz in the OFF state to 3.18 GHz in the ON state with 260 MHz difference. It has very good S_{11} value in both cases as well. This design gives good S_{11} results in both cases of ON and OFF states as well.

Finally, using the RLC model given from the novel MEMS switches design simulation presented in the MEMS section. For working at 3 GHz frequency, the values are, $R = 0.21 \Omega$, $L = 0.404 \text{ nH}$ in ON state, and $C = 0.0501 \text{ pF}$ in OFF state. Only two switches were used for these values.

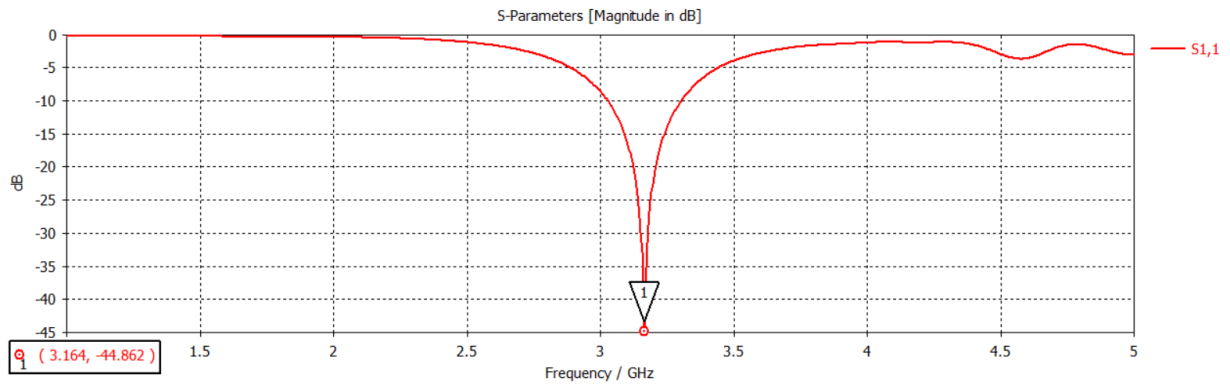


Figure 74. S11 parameter value for using two switches in the ON state

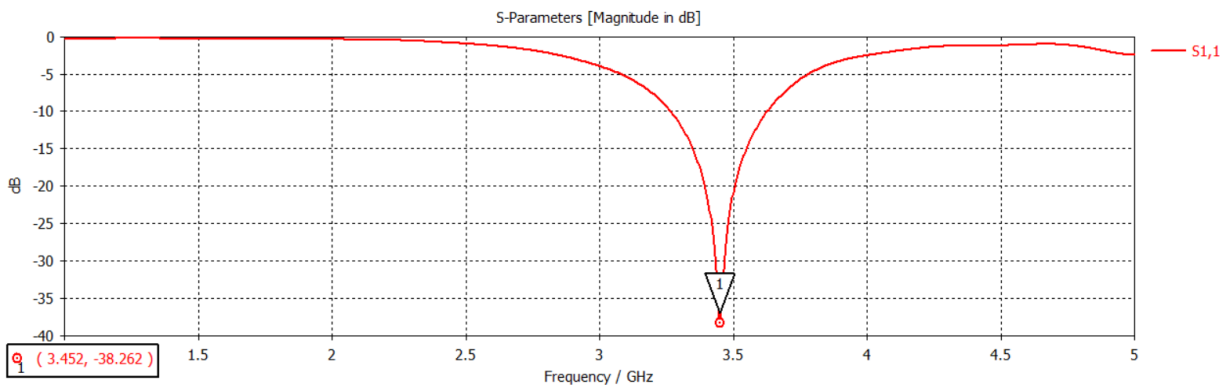


Figure 75. S11 parameter value for using two switches in the OFF state

As with the rest of trials using this antenna design, the design gives good results in both cases of ON and OFF states as well. The antenna switches from 3.452 GHz in the OFF state to 3.164 GHz in the ON state with 288 MHz difference. It has very good S_{11} value in both cases as well. This design gives good S_{11} results in both cases of ON and OFF states as well. These results show that this antenna design can be used with any of the designed MEMS switches and give good performance.

A summary of the obtained results with the MEMS switches' different RLC values is shown in the following table.

Design 2 with generic RLC	
State	Frequency (GHz)
ON	3.212
OFF	3.46

Design 2 with one meander MEMS switch	
State	Frequency (GHz)
ON	3.1316
OFF	3.44

Design 2 with control MEMS switch	
-----------------------------------	--

State	Frequency (GHz)
ON	3.18
OFF	3.44

Design 2 with novel MEMS switch	
State	Frequency (GHz)
ON	3.164
OFF	3.452

Table 11. Summary of the used RLC models with the resulting frequencies

4.3.2 RF MEMS Switches

A. First Design

- **Design Specifications**

The proposed switch consists of a series metal-contact fixed-fixed membrane, suspended over a microstrip line, with two bottom electrodes as shown in fig 76.

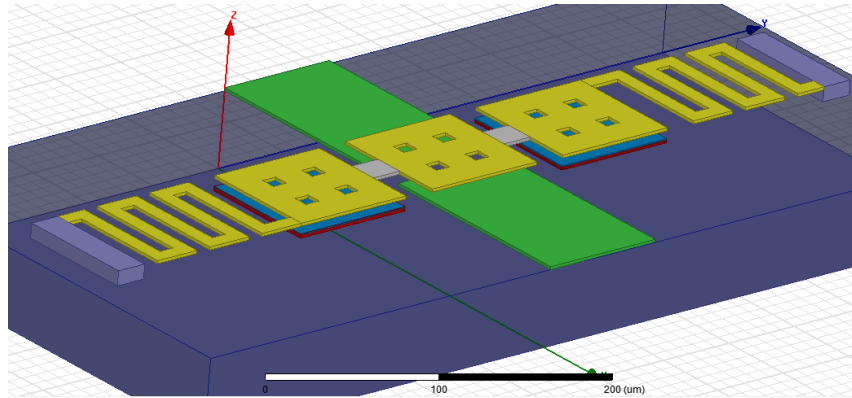


Figure 76 : 3D view of the proposed design on HFSS

The suspended structure consists of two sets of meanders, two areas for pull down, two insulators and contact area. Large areas have holes for better release and to reduce damping. The switch is made entirely of gold metal, except for the insulator pieces; it is silicon dioxide. Another silicon dioxide layer is added on the bottom electrodes to prevent short circuit. This structure is anchored to the substrate from both sides.

The switch is naturally in an off state. The gap in the microstrip line prevents the RF signal from passing through. No voltage bias is applied in this state. To switch to the on state, a voltage bias is applied to the bottom electrode while the switch is grounded. The electrostatic force generated between the bottom and up plates pulls the switch down. This results in the contact area of the switch touching both sides of the signal line, and connecting them. The two insulator pieces prevent the bias voltage from interfering with the signal. When the bias is then removed the switch returns to its original position.

In the off state, the isolation is dependent on the gap in the signal line and the air gap, height of the switch; this results in high isolation. In the on state, the insertion loss relays

mostly on the metal contact. Adding the meanders on both sides significantly reduces the pull-in voltage of the switch.

For a metal-contact switch, the contact part is the most important. Gold metal has clear advantages over other metals. It has excellent conductivity, high chemical resistance to corrosion and contamination. Hence, it is the most commonly used metal for RF MEMS switches. The switch is suspended 1.5 μm over the 20 μm gap in the signal line.

Description	Specifications (in μm)			
	<i>Material</i>	<i>Length</i>	<i>Width</i>	<i>Thickness</i>
Contact	Gold	80	80	2
Bottom & Up Electrodes	Gold	80	80	2
Meanders	Gold	80	8	2

Insulator	SiO ₂	20	20	2
Half signal line	Gold	140	50	1

Table 12: device structure specifications

- **Fabrication of First Design**

The first layer is the bias lines fabricated using 50 nm TiW by plasma sputtering. The geometry and length of these lines are designed to have the needed resistance for proper connection with the whole system. These lines are covered with 0.7 μm of SiO₂ by PECVD at 250°C and patterned using RIE. Secondly, 40nm Cr/70nm Au bilayer is deposited as a seed layer. A negative photoresist (PR) mold is patterned by PR and 1μm Au is electroplated inside that mold. The mold and the seed layer are removed afterwards. Cr serves no more than an adhesion layer for Au fig (1).

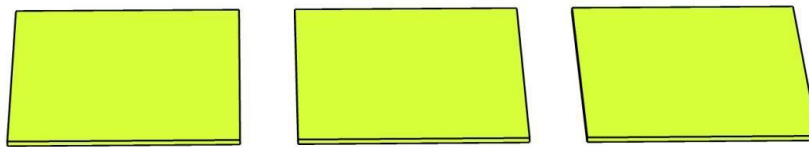


Figure 1. Lower electrodes and signal line

Third, $0.7 \mu\text{m}$ of Si_3N_4 is deposited using PECVD at 140°C and 1.5 mTorr . Ar-diluted SiH_4 and N_2 gases are used as precursors in this process. The low temperature technique is the suitable one not to damage the metal layers fig(77).



Figure 77. Lower electrodes' dielectric layer

Fourth, Spin coated Polyimide is used as the sacrificial layer for the Au structural layer. Initially, it is coated to a thickness of $2.5 \mu\text{m}$; then, it is patterned by RIE in order to etch the polyimide and fully open the anchor holes. This step should be followed by CMP to planarize this layer for one height above structure. Fifth, A $2 \mu\text{m}$ layer of gold is deposited using Electroplating to have the upper structure layer of the electrodes, meanders, and middle part of the switch. A negative photoresist is used to pattern this layer. After this step, holes are etched using RIE that are essential for releasing fig(78).



Figure 78. The upper gold layer

Sixth, $1 \mu\text{m}$ of Si_3N_4 is deposited using the same previous process of PECVD to prevent metal layers' damage. This layer's importance is to insulate between the electrodes and

the middle part that will be connected to the lower signal line fig (79). The last step then is to etch the Polyamide using EKC 265 solution for 5 mins followed by alcohol rinsing and drying. For best results critical point dryer may be used after the release step.



Figure 79. The connecting part

Mask layout has been done using Klayout software (fig 80).

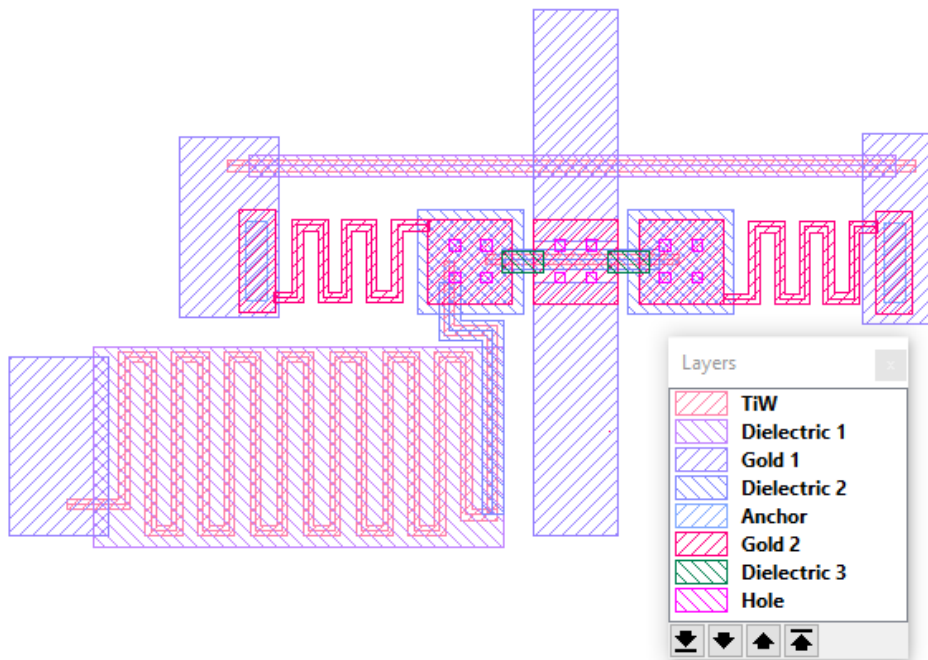


Figure 80. Mask Layout for the First Design

Other Designs

Four other designs have been implemented that are compatible with University of Waterloo's cleanroom (UW-MEMS) fabrication process. These switches do not give the

excellent performance, shown in the previous design, due to limitations of fabrication. However, they have acceptable RF performance and good reliability. In addition, all of the switches are implemented with a CPW signal line. All mechanical simulations are done using Comsol Multiphysics. All electromagnetic simulations are done using HFSS tool.

Following the UW MEMS fabrication process, the substrate is a 0.025” thick Alumina. It also uses gold for all metallic parts and silicon dioxide as a dielectric.

Layer	Thickness	Description
First Gold	1 μm	CPW lines & Bottom Electrode
Dielectric	0.7 μm	Shielding Bottom Electrode
Second Gold	2 μm	Suspended structure

Table 13. Layers thickness for fabrication

B. Second Design

The proposed design is a series metal-contact electrostatically actuated switch. It consists of a suspended cantilever above the gap in the signal line and the bottom electrode, as shown in figure 81.

The cantilever is $2.5\ \mu\text{m}$ above the signal line, with a $1\ \mu\text{m}$ dimple at the free end. The square holes have a side length of $10\ \mu\text{m}$ and spacing of $20\ \mu\text{m}$. For the CPW lines, the signal line, gap and the ground lines have widths of $80\ \mu\text{m}$ and $100\ \mu\text{m}$ respectively. In addition, adding a rectangular hole, $40\ \mu\text{m} * 20\ \mu\text{m}$, noticeably reduces the actuation voltage.

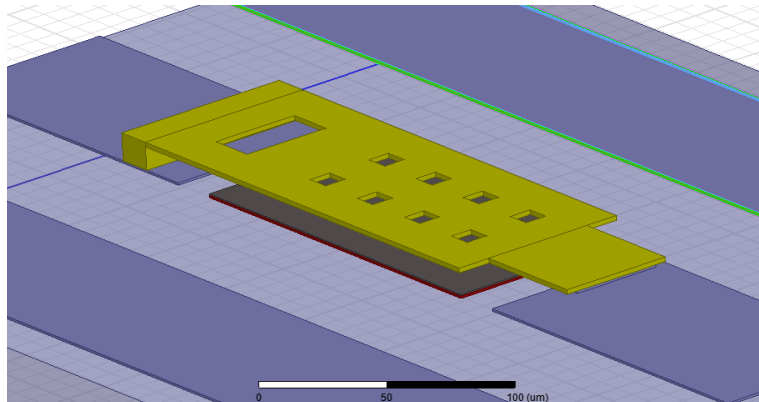


Figure 81. 3D view of the second design on HFSS

In normal position, the switch is in OFF state. When a bias voltage is applied between the cantilever and the bottom electrode, it is pulled down and the gap is closed, ON state. The contact happens at the dimple area, hence reducing the actuation voltage.

C. Third Design

The proposed design is a shunt capacitive electrostatically actuated switch. It consists of a suspended membrane above the signal line, and anchored from both sides on the grounds, as shown in figure 82.

The switch is $2.5\ \mu\text{m}$ above the signal line and supported by two meanders. The square holes have a side length of $10\ \mu\text{m}$ and spacing of $20\ \mu\text{m}$. For the CPW lines, the signal line, CPW gap and the ground lines have widths of $100\ \mu\text{m}$ and $100\ \mu\text{m}$, respectively. Supporting meanders have a width of $15\ \mu\text{m}$ and a length of $80\ \mu\text{m}$.

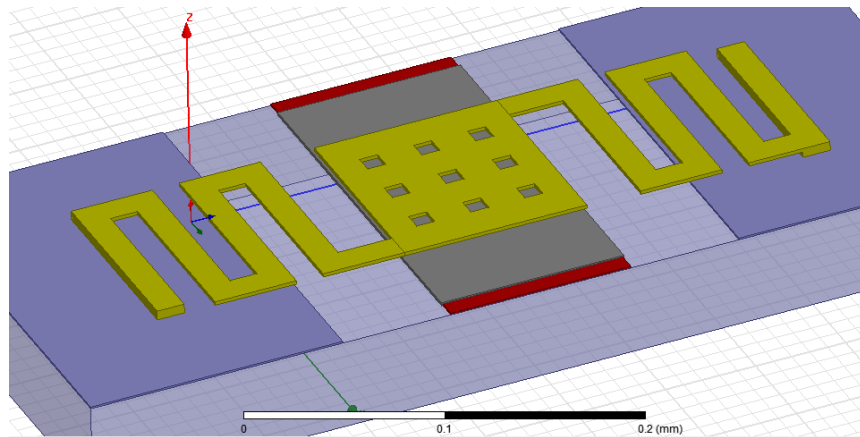


Figure 82 3D View of the second design on HFSS

In normal position, the switch is in ON state. The signal passes under the bridge without interference. When a bias voltage is applied between the bridge and the signal line, it is pulled down and the gap is closed, OFF state. The switch is stopped by the dielectric to prevent short circuit. This results in high capacitance that connects the signal to the ground on both sides, hence no signal passes through.

D. Fourth Design

The proposed design is a series metal-contact electrostatically actuated switch. It consists of a suspended cantilever above the gap in the signal line and the bottom electrode, as shown in figure 83.

The cantilever is $2.5\ \mu\text{m}$ above the signal line, with a $1\ \mu\text{m}$ dimple at the free end. The square holes have a side length of $10\ \mu\text{m}$ and spacing of $20\ \mu\text{m}$. For the CPW lines, the signal line, gap and the ground lines have widths of $80\ \mu\text{m}$ and $100\ \mu\text{m}$ respectively. Supporting meanders have a width of $15\ \mu\text{m}$ and a length of $80\ \mu\text{m}$.

In normal position, the switch is in OFF state. When a bias voltage is applied between the cantilever and the bottom electrode, it is pulled down and the gap is closed, ON state.

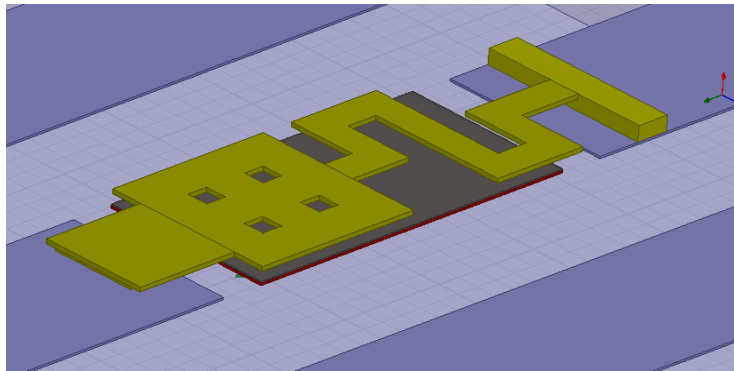


Figure 83. 3D view of the fourth design on HFSS

The contact happens at the dimple area, hence reducing the actuation voltage. The addition of the meander support introduces a significant reduction in the actuation voltage.

E. Fifth Design

The proposed design is a shunt capacitive electrostatically actuated switch. It consists of a suspended membrane above the signal line, and anchored from both sides to the ground, as shown in figure 84.

The switch is $2.5\ \mu\text{m}$ above the signal line and supported by two meanders. The square holes have a side length of $10\ \mu\text{m}$ and spacing of $20\ \mu\text{m}$. For the CPW lines, the signal line, CPW gap and the ground lines have widths of $100\ \mu\text{m}$, $80\ \mu\text{m}$ and $100\ \mu\text{m}$, respectively. The membrane has an additional step down, of $1\ \mu\text{m}$, to help reduce the actuation voltage. Each of the four supporting legs has a width of $15\ \mu\text{m}$ and a length of $85\ \mu\text{m}$.

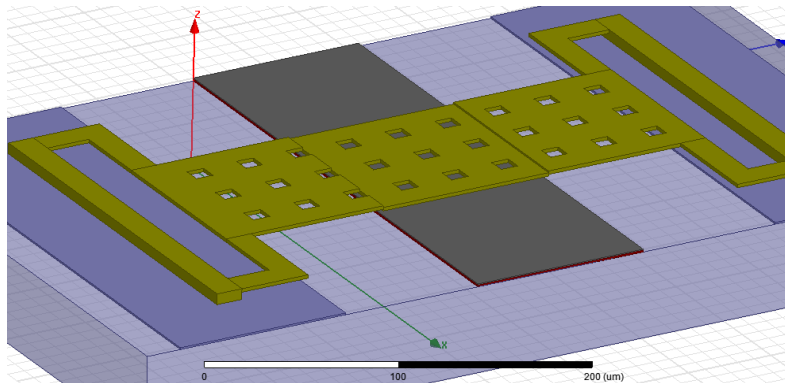


Figure 84. 3D view of the Fifth design on HFSS

In normal position, the switch is in ON state. The signal passes under the bridge without interference. When a bias voltage is applied between the bridge and the signal line, it is pulled down and the gap is closed, OFF state. The switch is stopped by the dielectric to prevent short circuit. This results in high capacitance that connects the signal to the ground on both sides, hence no signal passes through.

F. Fabrication

All of the designs follow the UWMEMS handbook. The fabrication process is explained here.

The UW MEMS microfabrication process employs only seven masks, and it starts with a 0.025” thick Alumina substrate polished on both sides with a relative permittivity of 9.9 and loss tangent of 0.0001 at 1MHz. The seven masks used for the entire fabrication are electron-beam-write chromium masks that are produced from nine layout layers, which are detailed in table 1.

<i>Layer Name</i>	<i>Material Thickness</i>	<i>Layer Order</i>	<i>Layer Description</i>	<i>Comments</i>
“TiW”	50 nm	1	Resistive Voltage Biasing	Resistive Layer
“D1” & “D1HOLE”	0.7 μ m	2 & 3	Dielectric	0.7 μ m SiO ₂ to cover the bias lines
“G1”	1 μ m	4	Conductive Layer	40nm evaporated Cr + 70nm evaporated Au + 0.9 μ m electroplated Au

“D2”	0.7μm	5	Dielectric	50nm TiW + 0.7μm SiO ₂
“A” & “D”	2.5μm	6 & 7	Sacrificial Layer	2.5μm Anchor and 1μm Dimple openings
“G2” & “G2R”	2μm	8 & 9	Conductive Layer	70nm sputtered Au + 1.9μm electroplated Au

Table 14: Specifications of the Fabrication Layers

Layer #1: Titanium Tungsten Bias Lines

After the RCA cleaning of the wafer, the 50 nm TiW layer is sputtered and patterned using the layer “**TiW**”.

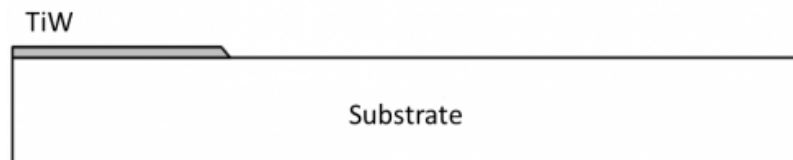


Figure 85. After patterning using Layer “TiW”

Layers #2 and #3: First Dielectric

A 0.7 μm SiO_2 is deposited at 250°C by plasma enhanced chemical vapor deposition (PECVD) and patterned using reactive ion etching (RIE). RIE is then used to strip away the etch-mask photoresist. The pattern is formed using a single mask based on the layout layers “D1” and “D1HOLE” combined.

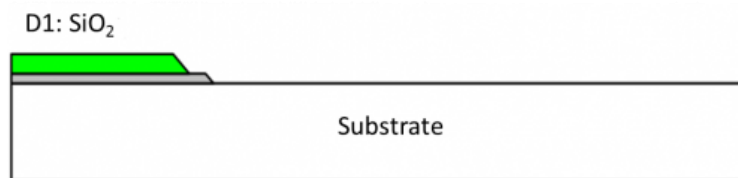


Figure 86 After patterning using Layers “D1” & “D1HOLE”

Layer #4: First Gold

An evaporated 40nm Cr/70nm Au bilayer is deposited as a seed layer. A negative photoresist (PR) mold is patterned by photolithography using layer “G1” and 1 μm Au is electroplated inside that mold. The mold and the seed layer are removed afterwards. Cr serves no more than an adhesion layer for Au.

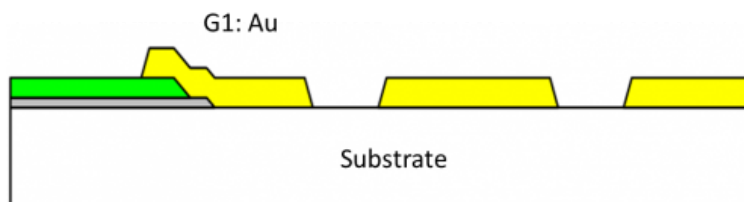


Figure 87. After patterning using Layer “G1”

Layer #5: Second Dielectric

A 30nm of TiW is sputtered followed by the deposition of 0.7 μ m SiO₂ PECVD at 250°C. The SiO₂ and TiW layers are then dry etched in RIE in order to pattern them using the “D2” layer. TiW layer serves as an adhesion layer between SiO₂ and Au.

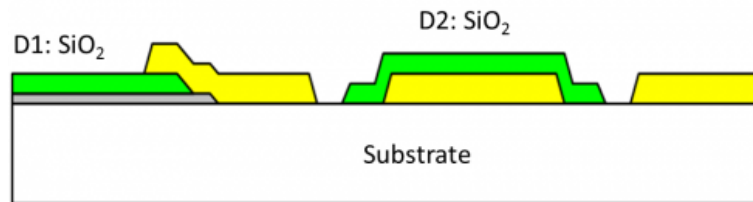


Figure 88. After patterning using Layer “D2”

Layer #6: Anchor Openings

Spin coated Polyimide is used as the sacrificial layer for the Au structural layer in UW-MEMS. Initially, it is coated to a thickness of 2.5 μ m; then, it is patterned by the “A” layer in RIE in order to etch the polyimide and fully open the anchor holes.

Layer #7: Dimple Openings

Similar to anchor patterning, the dimple openings are performed in polyimide using an RIE etching step using the pattern of “D” layer.

Layers #8 and #9: Second Gold

The second Au layer consists of the sputtered 70nm Au seed layer and an electroplated Au layer. The total thickness of Au is set to be 2 μ m, and it is used as the structural layer

for all the MEMS devices. A negative PR mold is used to pattern this layer based on the layout layers “G2” and “G2R” combined appropriately.

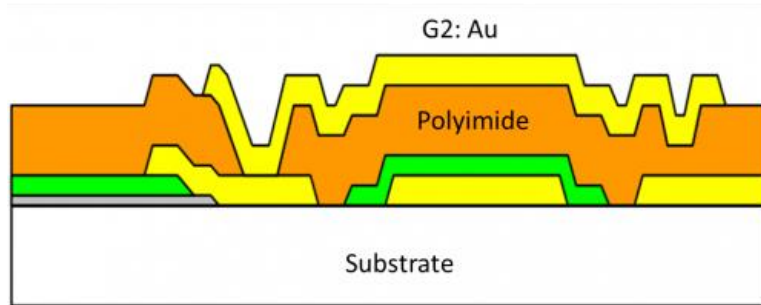


Figure 89. After patterning using Layers “G2” and “G2R”

Final Release Step

Before releasing the devices, the wafers are diced into individual dies according to the dicing lines in the layout. The sacrificial layer is then removed in O₂ plasma dry etching in RIE. At this stage, the microfabrication of UW-MEMS devices is complete and the samples are packaged for shipping to the customers.

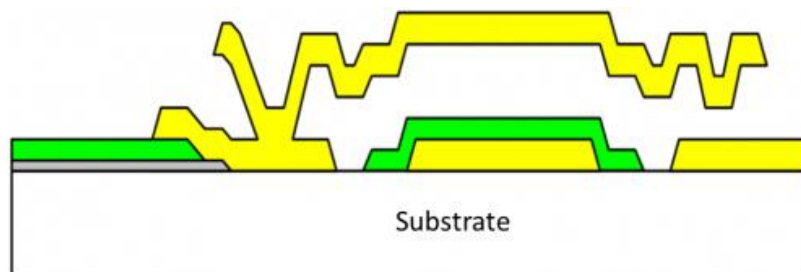


Figure 90. After releasing the device by stripping away all polyimide

G. Masks Layout

Mask layout for each of the designs has been done for fabrication using Klayout software.









Layers	
	TiW
	D1
	G1
	D2
	Anchor
	Dimple
	G2
	Hole

Figure 91. Layers used in Klayout

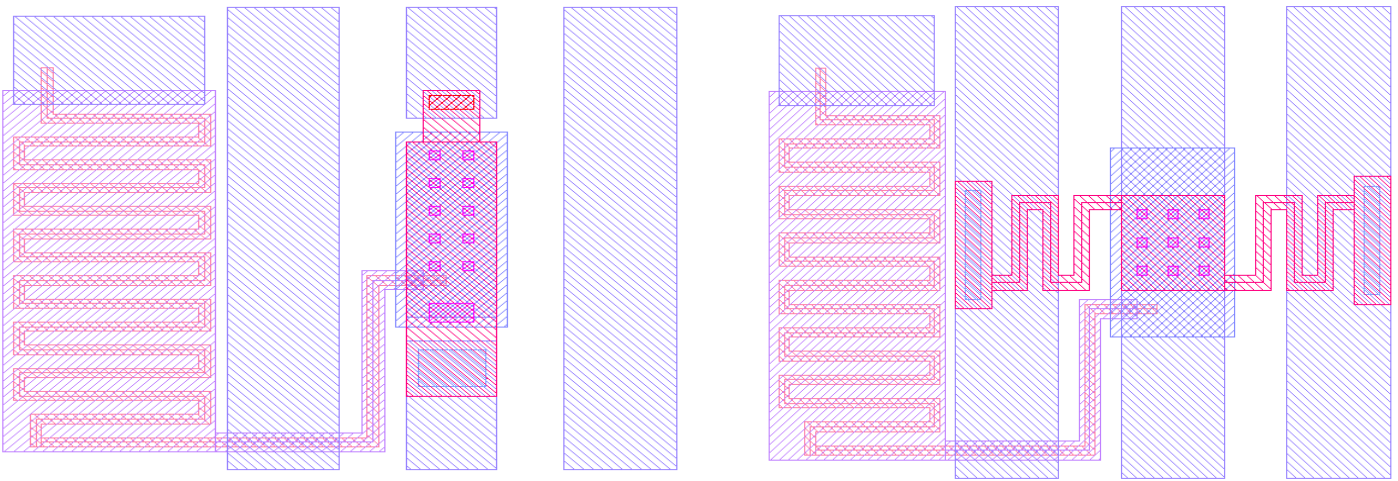


Figure 92. Mask Layout for the Second design, the Third design

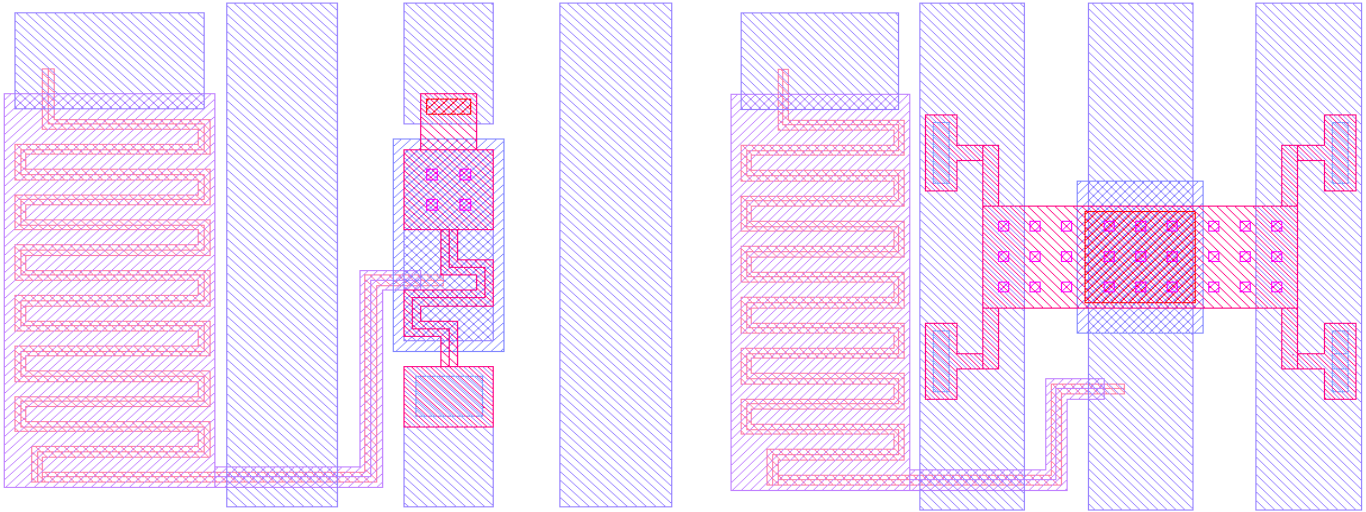


Figure 93 Mask Layout for the Fourth design, the Fifth design

4.3.2.3 Discussion

The proposed four switches are designed following the UWMEMS fabrication process. They were eventually integrated into one chip for fabrication (figure). The designs show relatively high actuation voltage. In terms of the RF performance, the contact switches have much better isolation and insertion loss than the capacitive switches. However, as expected, the capacitive designs delivered very good performance at very high frequencies.

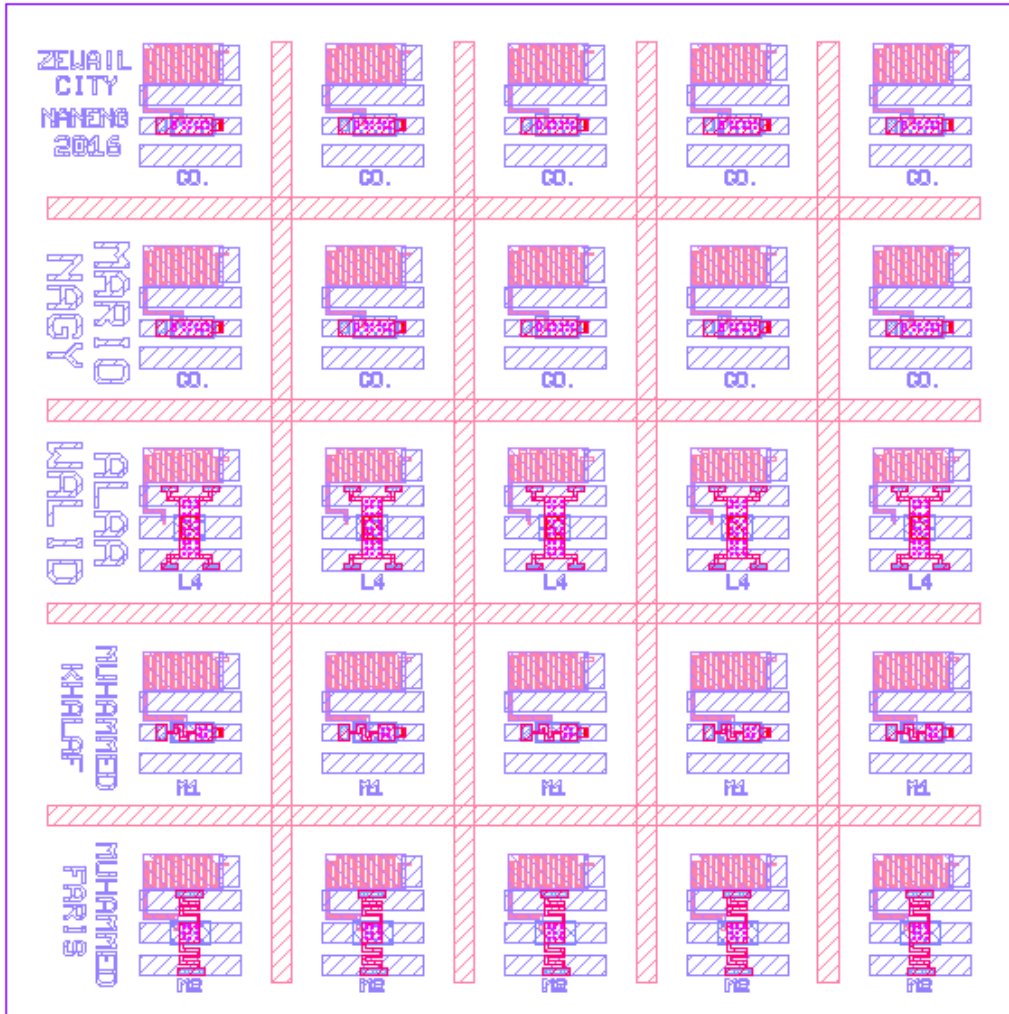


Figure 94: The entire chip including all four designs ready for fabrication

4.3.2.4 RF MEMS Switches Simulation

To fully characterize an RF MEMS switch, it needs to be modeled mechanically and electromagnetically. In this section, we will show the simulation and results obtained by the proposed designs. The mechanical simulation of the switch is done using COMSOL Multiphysics FEM tool. The RF performance is modeled using HFSS tool.

A. First Design

- **Mechanical Modeling**

The bridge is suspended $1.5\ \mu\text{m}$ above the electrode and fixed from both ends. To switch on, a voltage difference is applied between the switch and the electrodes resulting in a downward deflection.

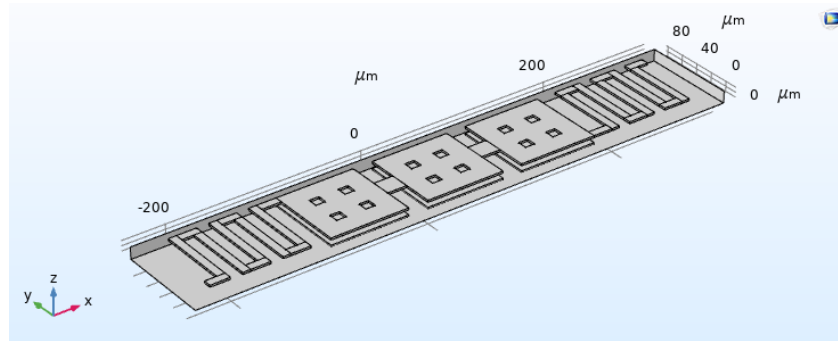


Figure 95: 3D view of the mechanical simulation on Comsol Multiphysics

Stress distribution across the structure is shown in figure 96. A maximum stress level is observed to be $6.6\ \text{MN}/\text{m}^2$, which is way below the max stress value for gold ($100\ \text{MN}/\text{m}^2$). The vertical displacement of the switch is shown in figure 97. A voltage sweep is done to achieve pull-in and cover the $1.5\ \mu\text{m}$ gap.

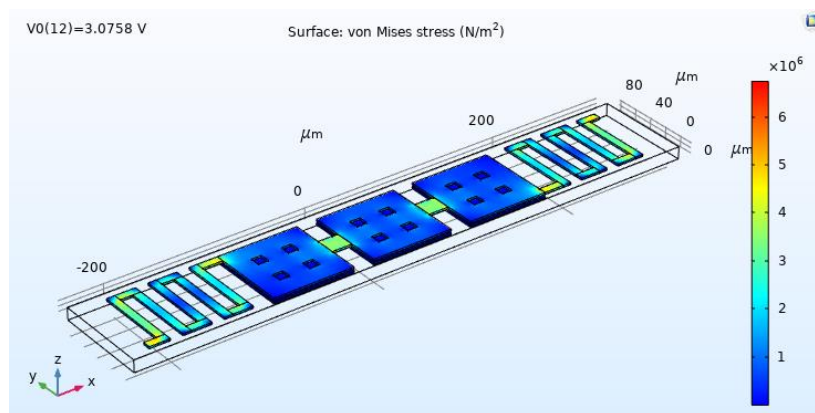


Figure 96: Distribution of stresses over the whole structure

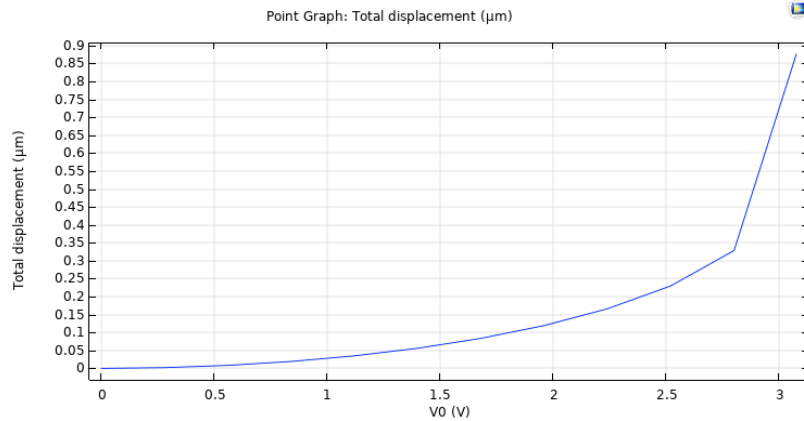


Figure 97: Vertical displacement of the contact of the switch vs the applied voltage

As shown in figure 98, the switch reaches the pull-in state when voltage of 3.1 V is applied. Also, the switching time is 64 μs.

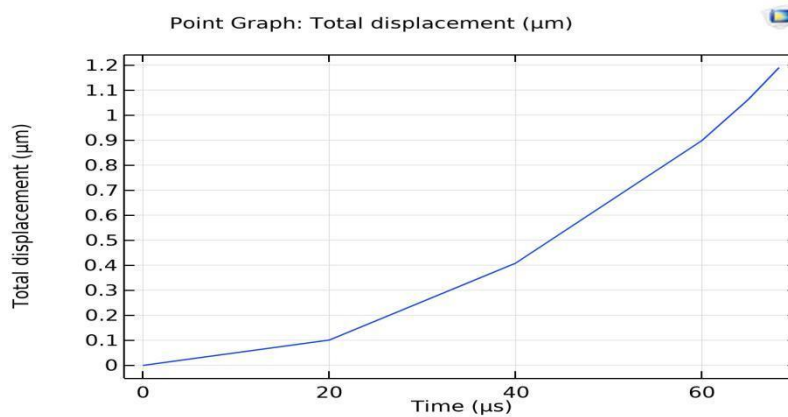


Figure 98: Switching Time for the First Design

- **Electromagnetic Modeling**

The switch is suspended over the microstrip line with a 20μm gap. The switch, at a 1.5 μm height, is anchored at each side of the signal line. The substrate used is FR4 epoxy dielectric, with a thickness of 50 μm and ϵ_r of 4.4.

The switch is simulated in two positions. In OFF state, the bridge is suspended above the signal line; here, we measure the isolation from the s-parameters as S21. In ON state, the bridge is down and contacts the two separate parts of the signal line; here, we measure the insertion loss from the s-parameters as S21. We are interested in the frequency range of 0.01-10 GHz.

As shown in the figures, the switch achieves an insertion loss of -0.012 dB and an isolation of 34.4 dB at 3 GHz.

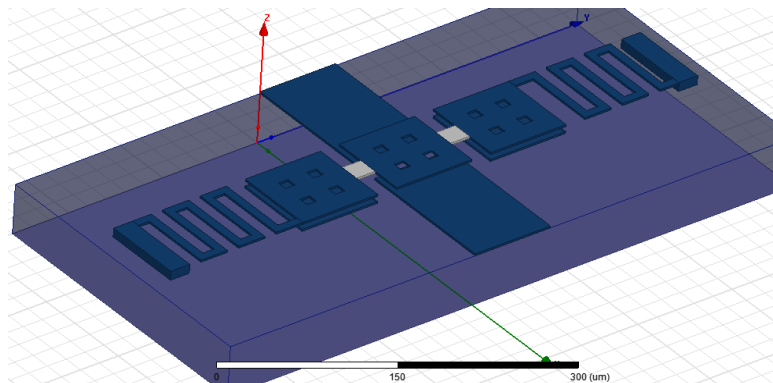


Figure 99: 3D view of the electromagnetic simulation on HFSS

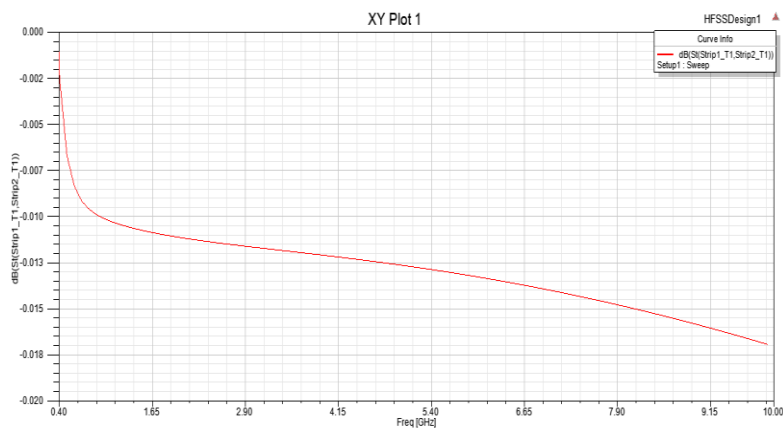


Figure 100: Insertion loss (S21) from 0.4 to 10 GHz on HFSS

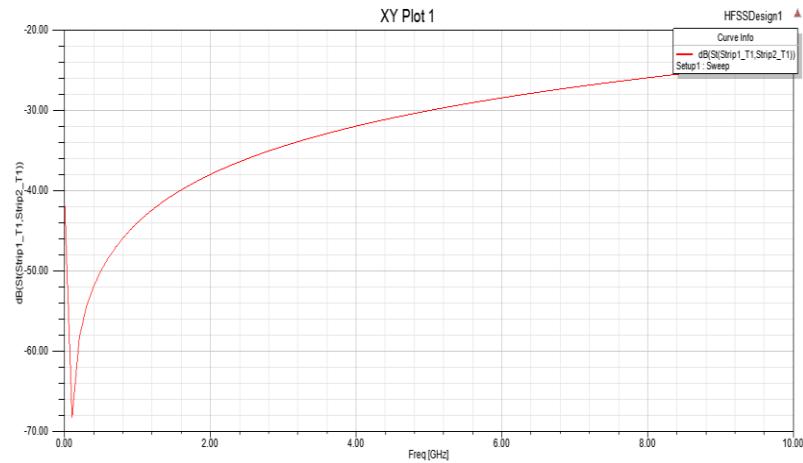


Figure 101. solution (S21) from 0.01 to 10 GHz on HFSS

The proposed switch shows a very low actuation voltage of 3.1 V. Compared to the typical switches, which require tens of volts, this actuation voltage is excellent for portable devices and mobile phones. This also removes the need for a voltage-up convertor, reducing the circuit complexity and the footprint on the wafer. The RF performance of the switch is excellent for low frequency ranges, sub 6 GHz, which makes it suitable for reconfigurable antennas and IOT applications. For frequencies less than 5 GHz, the insertion loss is less than -0.013 dB and the isolation is more than 30 dB.

In terms of fabrication, although most of the switch is easily fabricated, the insulator pieces introduced a challenge with standard fabrication techniques. Furthermore, we worked on a few other designs that are fully compatible with known fabrication processes and can be fabricated.

B. Second Design

- **Mechanical modeling**

Design of the cantilever is shown in figure. In terms of stress distribution, the maximum stress is 12.5 MN/m², as shown in figure. For the actuation voltage, the cantilever achieves pull-in at 20.8 V, as shown in figure. The switching time is 30 μ s.

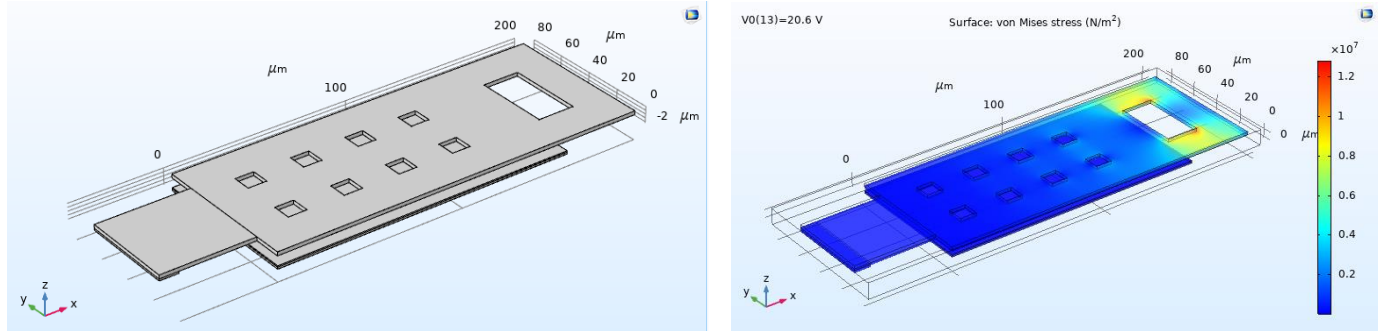


Figure102. 3D view of the cantilever on Comsol, Distribution of stresses over the cantilever

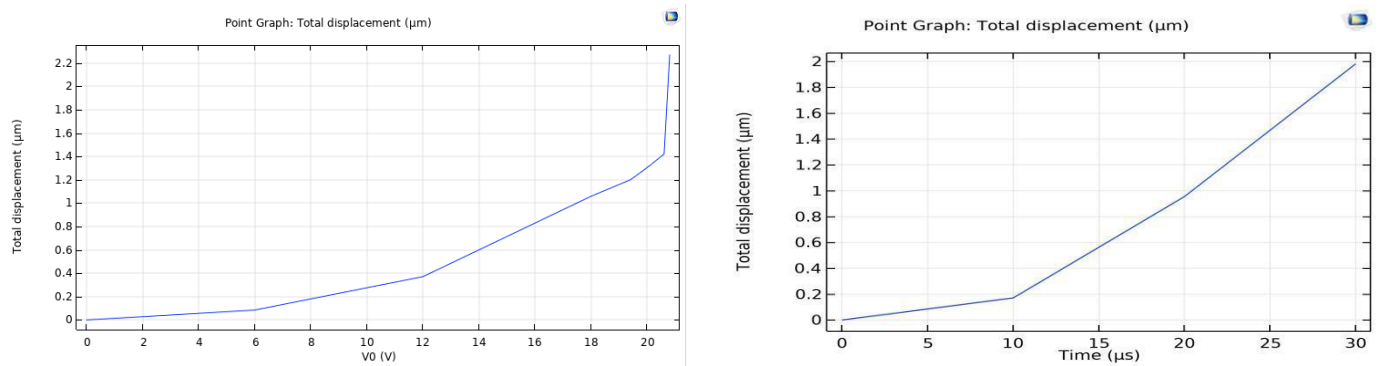
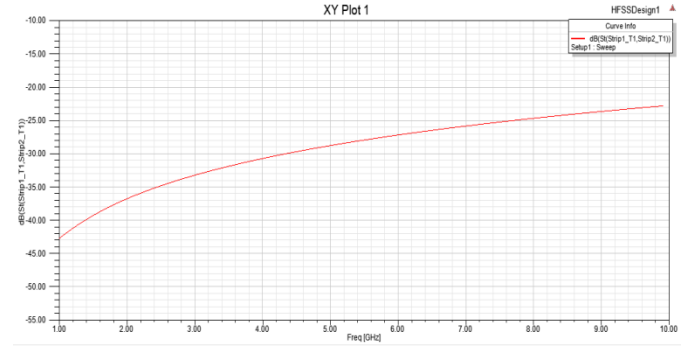
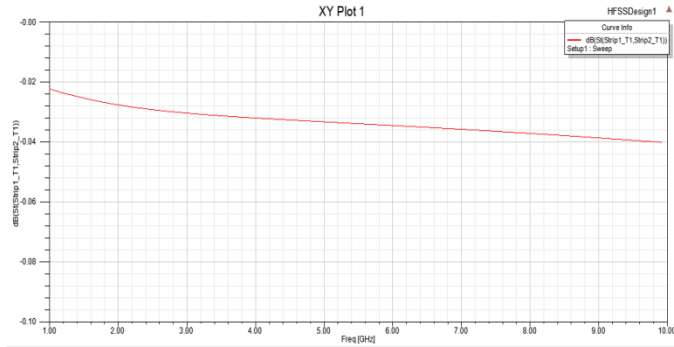


Figure 103. Vertical displacement of the dimple vs the applied voltage, Switching Time for the second Design

- **Electromagnetic modeling**

RF performance of the switch, in ON and OFF states, is shown in figures. The switch achieves an insertion loss of -0.03 dB and an isolation of 33 dB at 3 GHz.



Insertion loss (S21) from 1 to 10

GHz on HFSS Insolation (S21) from 1 to 10 GHz on HFSS

C. Third Design

- **Mechanical modeling**

Mechanical modeling of the cantilever is shown in figure 105.

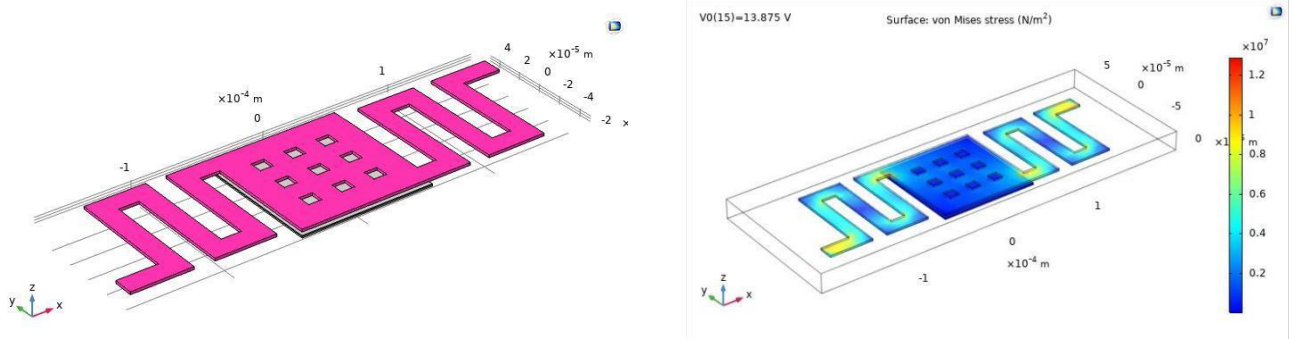


Figure105. 3D view of the cantilever on Comsol, Distribution of stresses

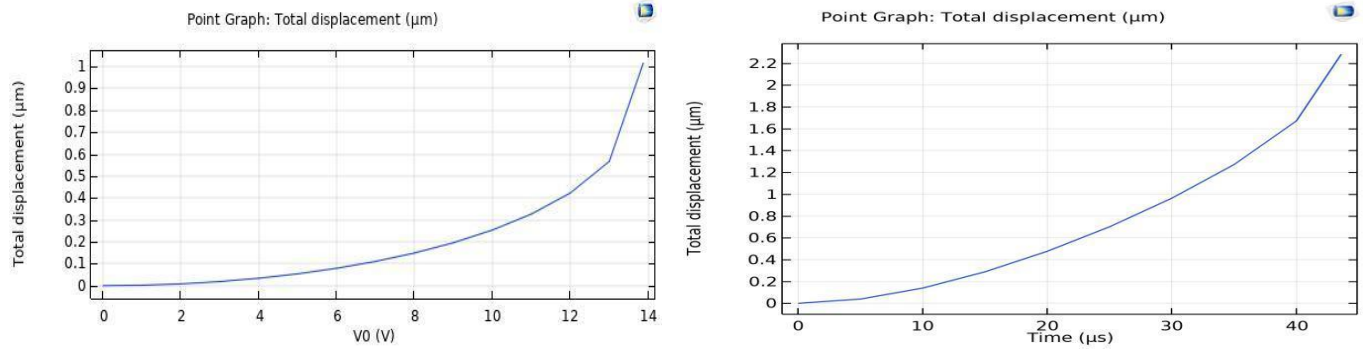


Figure 106: Vertical displacement of the dimple vs the applied voltage and Switching time

In terms of stress distribution, the maximum stress is 12.7 MN/m², as shown in figure. This is a safe value from any mechanical failure. For the actuation voltage, the cantilever achieves pull-in at 13.9 V, as shown in figure. The switching time is 43.5 μs as shown in figure.

- **Electromagnetic modeling**

RF performance of the switch, in ON and OFF states, is shown in figures. Since it is a capacitive switch, it gives better RF performance at high frequencies. The switch achieves an insertion loss of -0.45 dB and an isolation of 35.8 dB at 44 GHz. It is clearly shown that this switch can work efficiently at very high frequency; however, it results in a very high insertion loss.

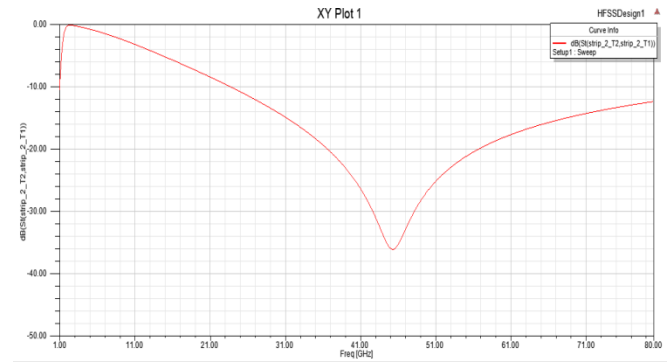
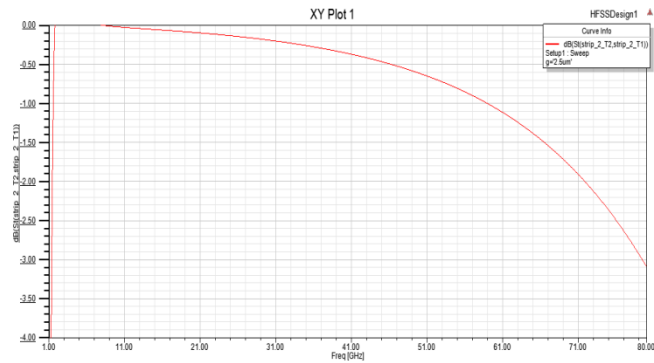


Figure 107. Insertion loss (S21) from 1 to 80 GHz on HFSS, Isolation (S21) from 1 to 80 GHz on HFSS

D. Fourth Design

- **Mechanical modeling**

Mechanical modeling of the cantilever is shown in figure 108.

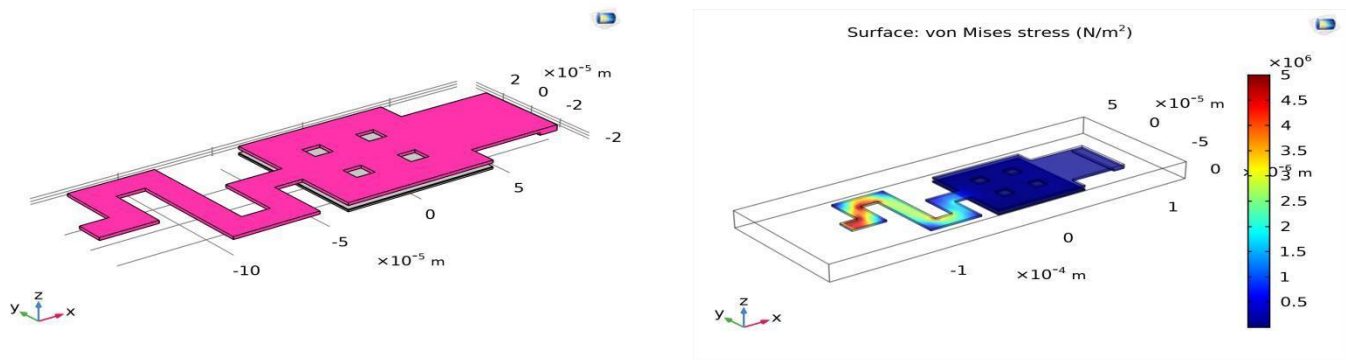


Figure 108 3D view of the cantilever on Comsol, Distribution of stresses over the cantilever

In terms of stress distribution, the maximum stress is 5 MN/m², as shown in figure. This is a safe value from any mechanical failure. For the actuation voltage, the cantilever achieves pull-in at 6 V, as shown in figure. The switching time is 100 μ s as shown in figure.

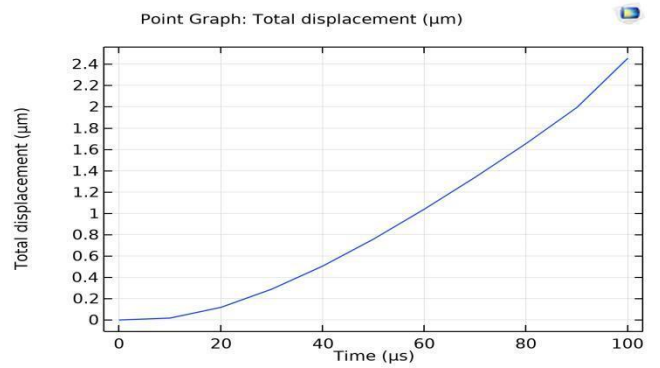
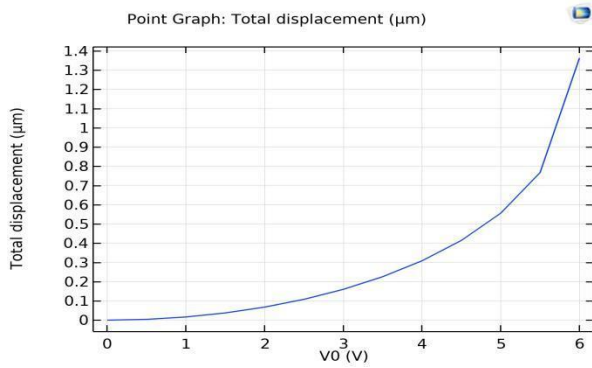


Figure 109. Vertical displacement of the dimple vs the applied voltage, Switching time of the Fourth Design

- **Electromagnetic modeling**

RF performance of the switch, in ON and OFF states, is shown in figures.

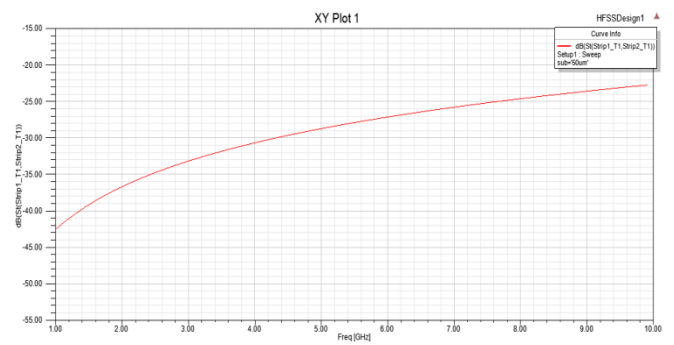
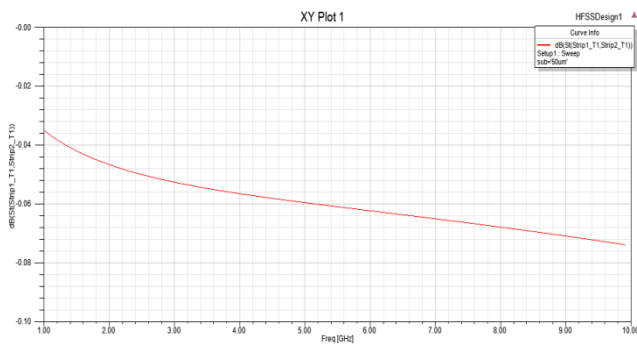


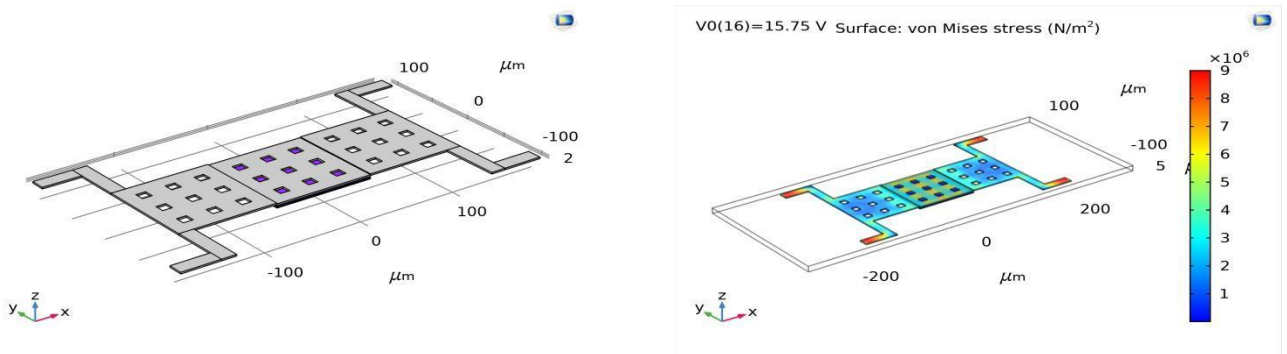
Figure 110. Insertion loss (S21) from 1 to 10 GHz on HFSS, Isolation (S21) from 1 to 10 GHz on HFSS

The switch achieves an insertion loss of -0.052 dB and an isolation of 33.8 dB at 3 GHz. It is clearly shown that this switch can work efficiently at very high frequency; however, it results in a very high insertion loss.

E. Fifth Design

- **Mechanical modeling**

Mechanical modeling of the switch is shown in figure 111.



3D Figure 111. view of the cantilever on Comsol, Distribution of stresses over the cantilever

In terms of stress distribution, the maximum stress is 9 MN/m², as shown in figure. This is a safe value from any mechanical failure. For the actuation voltage, the cantilever

achieves pull-in at 15.8 V, as shown in figure. The switching time is 21 μs as shown in figure.

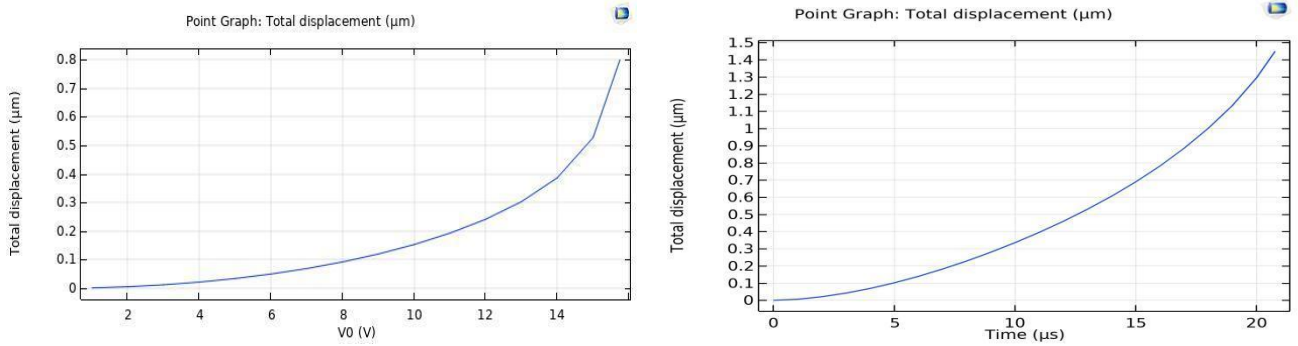


Figure 112. Vertical displacement of the dimple vs the applied voltage, Switching time of the Fifth Design

- **Electromagnetic modelling**

RF performance of the switch, in ON and OFF states, is shown in figures.

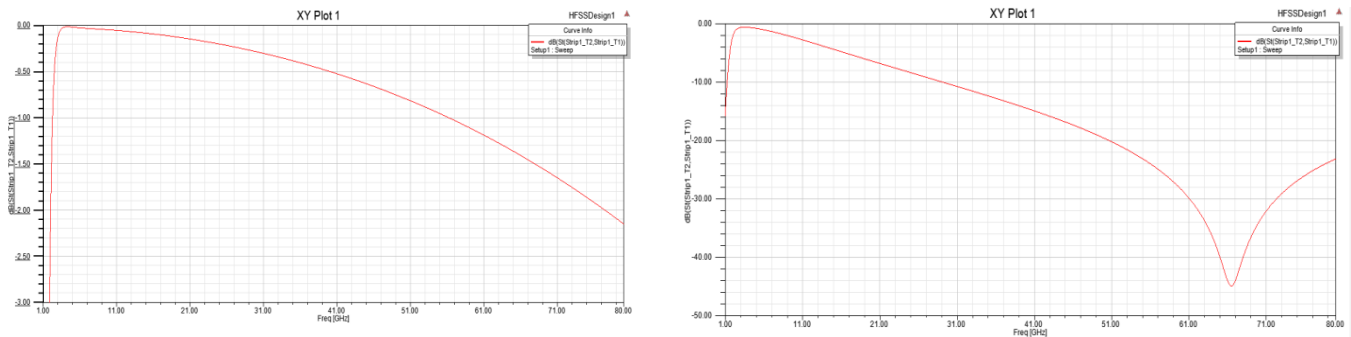


Figure 113. Insertion loss (S21) from 1 to 80 GHz on HFSS, Isolation (S21) from 1 to 80 GHz on HFSS

The switch achieves an insertion loss of -1.4 dB and an isolation of 45 dB at 67 GHz. It is clearly shown that this switch can work efficiently at very high frequency; however, it results in a very high insertion loss.

Chapter 5

Cost Analysis

As we are empowering the IoT applications on a large base, the impact of our product is going to hit different aspects of life on different levels including social, commercial, and environmental levels. Regarding social impact, as our daily life has become more dependent on different technologies and applications starting from health to entertainment, our product will have a great impact on the performance of these applications that drive human welfare. The commercial impact is going to be affected as our RF MEMS antenna is going to make the same product used in more applications easily, so this design can compete with the available technology. The impact on the environmental level is very significant as we are working on minimizing the hardware used within systems and consequently the burdens of disposal will be decreased.

Chapter 6

Conclusion and Future work

In conclusion, we have designed a reconfigurable antenna based on RF MEMS switches mainly for IoT applications, which operates at the midband 5G. Specifically, the frequencies of interest are 1-2 GHz and 3-4 GHz with bandwidth of about 300 MHz. Five RF MEMS switches are designed and simulated, with four of them to be fabricated at University of Waterloo RF MEMS cleanroom. Each switch is designed with different concept and technique to reach the specific specifications, meanders, fixed-fixed, and fixed-free. As a result, the final resulting switches can serve the low and high frequencies. Moreover, we designed a reconfigurable antenna that will be based on these designed switches to switch between the 1 and 3.3 GHz in one design, and between 3.4 to 3.6 GHz frequency of operation in the second design.

In the future, further research should be done on the other specifications of the RF MEMS switch such as reliability and materials selection. In addition, working on other actuation techniques may be beneficial and significant. Regarding the antenna, it is suggested to work on broadening the bandwidth as needed in several applications. Moreover, characterizing the influence of the real RF MEMS switch on the antenna will be of great importance to prove its concept and idea.

References

- [1] *Home*. Physics LibreTexts. (2020, September 8). <https://phys.libretexts.org/>.
- [2] Bevelacqua, P. (n.d.). *Welcome to Antenna-Theory.com!* The Antenna Theory Website. <https://www.antenna-theory.com/>.
- [3] Parchin, N.O.; Al-Yasir, Y.; Abdulkhaleq, A.M.; Elfergani, I.; Rayit, A.; Noras, J.M.; Rodriguez, J.; Abd-Alhameed, R.A. Frequency reconfigurable antenna array for mm-Wave 5G mobile handsets. In Proceedings of the 9th International Conference on Broadband Communications, Networks, and Systems, Faro, Portugal, 19–20 September 2018.
- [4] Chen, S.-Y.; Chu, Q.-X.; Shinohara, N. A bandwidth reconfigurable planar antenna for WLAN/WiMAX applications. In Proceedings of the Asia-Pacific Microwave Conference (APMC), New Delhi, India, 5–9 December 2016.
- [5] Tu, Yuxiang, et al. "A Survey on Reconfigurable Microstrip Filter–Antenna Integration: Recent Developments and Challenges." *Electronics* 9.8 (2020): 1249.
- [6] G. M. Rebeiz, *RF MEMS: Theory, Design and Technology*. 2003.
- [7] M. L. Ya, "Comprehensive Study on RF-MEMS Switches Used for 5G Scenario," IEEE, 2019.
- [8] Chowdhury, Sazzadur & Ahmadi, Majid & Miller, William. (2006). Pull-In Voltage Study of Electrostatically Actuated Fixed-Fixed Beams Using a VLSI On-Chip

Interconnect Capacitance Model. *Microelectromechanical Systems, Journal of.* 15. 639 - 651. 10.1109/JMEMS.2005.863784.

[9] *The Basics of Electromagnetic Forces: Products Information: MABUCHI MOTOR CO., LTD.* MABUCHI MOTOR. (n.d.). <https://www.mabuchi-motor.com/product/knowledge/structure/electromagnetic-forces.html>.

[10] Potekhina, A.; Wang, C. Review of Electrothermal Actuators and Applications. *Actuators* **2019**, 8, 69. <https://doi.org/10.3390/act8040069>